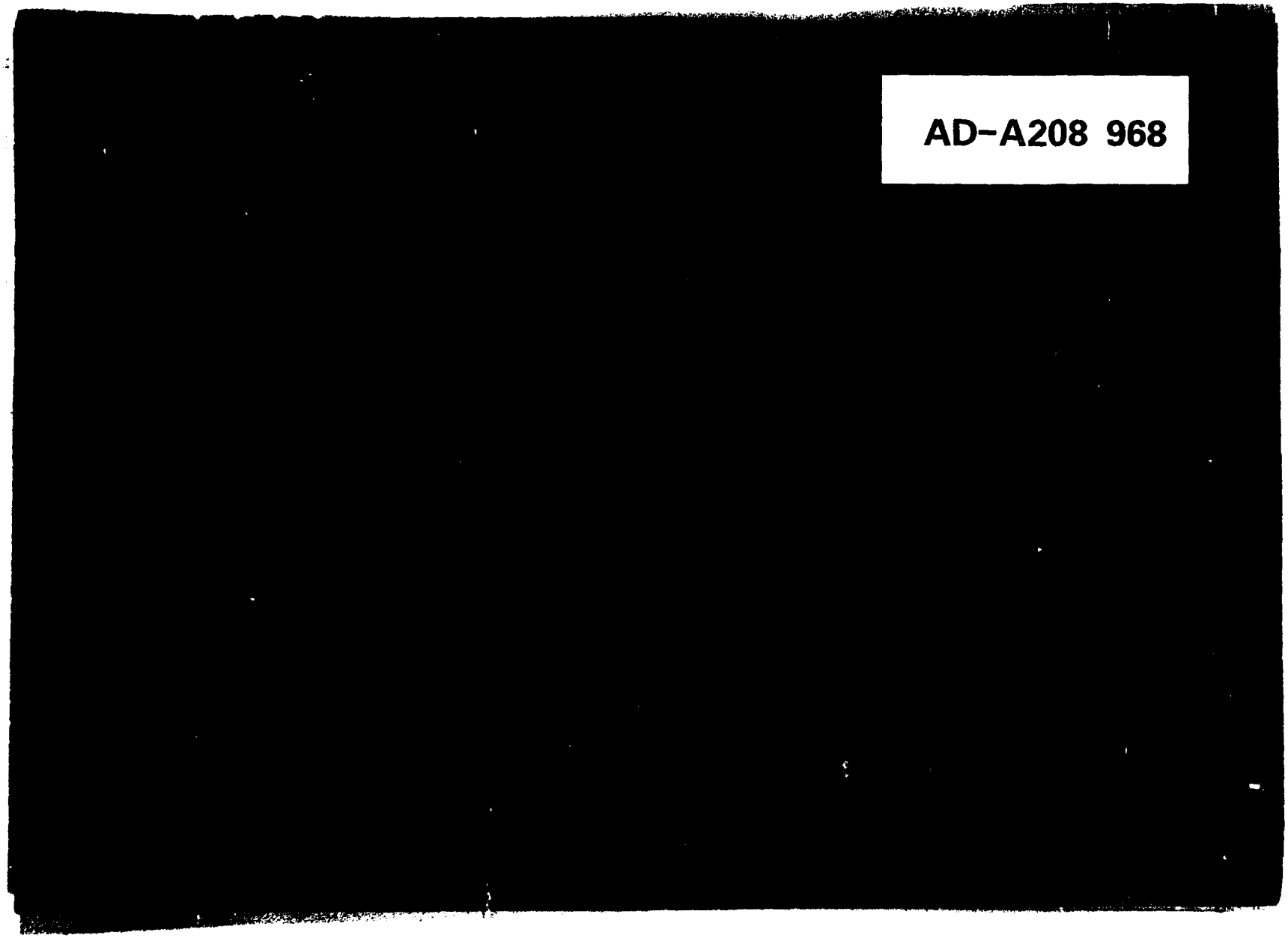
AD-A208 968

(4)

AD

TRANSITION AND TURBULENCE STRUCTURE IN THE BOUNDARY LAYERS OF AN OSCILLATING AIRFOIL

Final Technical Report
by

DE RUYCK J., HAZARIKA B., HIRSCH CH

January 1985 - December 1988

VUB report STR-16

United States Army

RESEARCH & STANDARDISATION GROUP (Europe)

London, England

Contract number DAJA45-85-C-0039

Contractor : Vrije Universiteit Brussel
Dept. of Fluid Mechanics

Dept. of Fluid Mechanics
Vrije Universiteit Brussel
Pleinlaan 2, 1050 Brussels
Belgium

Approved for public release, distribution unlimited

UNCLASSIFIED

SECURITY CLASSIFICATION OF THIS PAGE

REPORT DOCUMENTATION PAGE

1a. REPORT SECURITY CLASSIFICATION Unclassified	1b. RESTRICTIVE MARKINGS
2a. SECURITY CLASSIFICATION AUTHORITY	3. DISTRIBUTION/AVAILABILITY OF REPORT Approved for public release Distribution unlimited
2b. DECLASSIFICATION/DOWNGRADING SCHEDULE	
4. PERFORMING ORGANIZATION REPORT NUMBER(S) VUB-STR-16	5. MONITORING ORGANIZATION REPORT NUMBER(S)
6a. NAME OF PERFORMING ORGANIZATION Vrije Universiteit Brussel Dept. of Fluid Mechanics 6b. OFFICE SYMBOL (If applicable) VUB-STRO	7a. NAME OF MONITORING ORGANIZATION European Office for Aerospace Research and Development
6c. ADDRESS (City, State and ZIP Code) Pleinlaan 2 1050 BRUSSELS BELGIUM	7b. ADDRESS (City, State and ZIP Code) Marylebone Road LONDON ENGLAND
8a. NAME OF FUNDING/SPONSORING ORGANIZATION US Army Research and Standardisation Group (E) 8b. OFFICE SYMBOL (If applicable) USARSG	9. PROCUREMENT INSTRUMENT IDENTIFICATION NUMBER DAJA45-85-C-0039
8c. ADDRESS (City, State and ZIP Code)	10. SOURCE OF FUNDING NOS. PROGRAM ELEMENT NO. / PROJECT NO. / TASK NO. / WORK UNIT NO.
11. TITLE (Include Security Classification) Transition and Turbulence structure in the ..	
12. PERSONAL AUTHOR(S) De Ruyck J., Hazarika B., Hirsch Ch.	
13a. TYPE OF REPORT final 13b. TIME COVERED FROM 85-1-1 TO 89-12-31	14. DATE OF REPORT (Yr., Mo., Day) 89-12-31 15. PAGE COUNT
16. SUPPLEMENTARY NOTATION	

17. COSATI CODES			18. SUBJECT TERMS (Continue on reverse if necessary and identify by block number)
FIELD	GROUP	SUB. GR.	
01 01	20 04		Unsteady Aero Dynamic stall High angle of attack Separation Rotorcraft Transition

19. ABSTRACT

The objectives of this investigation were to identify: (i) the conditions under which a sinusoidally oscillating NACA 0012 airfoil operates with a leading edge separation bubble; (ii) the conditions under which it operates with leading edge stall; (iii) to conduct complete boundary layer and near wake survey in the presence of the leading edge separation bubble and (iv) to investigate the flow near the trailing edge and in the near wake while the airfoil was undergoing leading edge stall.

20. DISTRIBUTION/AVAILABILITY OF ABSTRACT UNCLASSIFIED/UNLIMITED ☒ SAME AS RPT. ☒ DTIC USERS ☐	21. ABSTRACT SECURITY CLASSIFICATION Unclassified
22a. NAME OF RESPONSIBLE INDIVIDUAL Hirsch Ch.	22b. TELEPHONE NUMBER (Include Area Code) 32-2-641.23.91 22c. OFFICE SYMBOL STRO

DD FORM 1473, 83 APR EDITION OF 1 JAN 73 IS OBSOLETE.

Unclassified

SECURITY CLASSIFICATION OF THIS PAGE

The airfoil oscillates about an axis at 25% chord from the leading edge, with a nominal reduced frequency of 0.3 and Reynolds number of 300,000. The experiments were made at 4 to 14, 5 to 15, 6 to 16 and 8 to 18 degrees angle of attack . It was found that the most probable cause of leading edge stall was due to the leading edge separation bubble burst and it occured soon after static stall limit was exceeded. The leading edge stall is not due to the rapid upstream movement of the trailing edge separation.

The velocity vectors and the Reynolds stress tensors were measured using a slanted rotating single sensor hot-wire. The complete suction side boundary layer profile and the near wake was surveyed at 5 to 15 degrees oscillation where no interaction is observed between the leading edge and the trailing edge flows.

In addition experiments were made at 8 to 18 degrees, at full stall condition. The flow near the trailing edge and in the near wake was surveyed to study the effect of leading edge stall and leading edge vortex on the flow in this region which was not investigated previously.

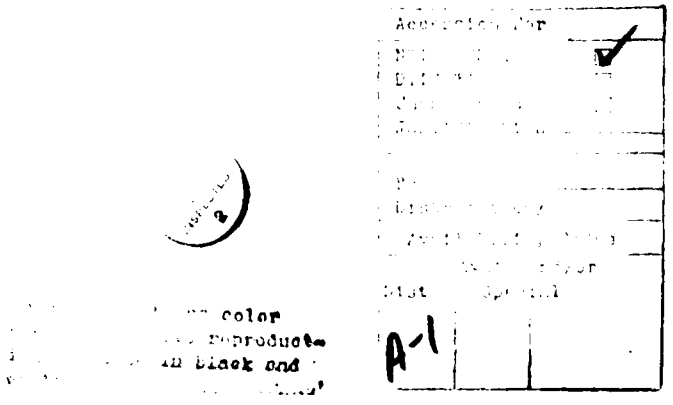

ABSTRACT

The objectives of this investigation were to identify: (i) the conditions under which a sinusoidally oscillating NACA 0012 airfoil operates with a leading edge separation bubble; (ii) the conditions under which it operates with leading edge stall; (iii) to conduct complete boundary layer and near wake survey in the presence of the leading edge separation bubble and (iv) to investigate the flow near the trailing edge and in the near wake while the airfoil was undergoing leading edge stall.

The airfoil oscillates about an axis at 25% chord from the leading edge, with a nominal reduced frequency of 0.3 and Reynolds number of 300,000. The experiments were made at 4 to 14, 5 to 15, 6 to 16 and 8 to 18 degrees angle of attack . It was found that the most probable cause of leading edge stall was due to the leading edge separation bubble burst and it occured soon after static stall limit was exceeded. The leading edge stall is not due to the rapid upstream movement of the trailing edge separation.

The velocity vectors and the Reynolds stress tensors were measured using a slanted rotating single sensor hot-wire. The complete suction side boundary layer profile and the near wake was surveyed at 5 to 15 degrees oscillation where no interaction is observed between the leading edge and the trailing edge flows.

In addition experiments were made at 8 to 18 degrees, at full stall condition. The flow near the trailing edge and in the near wake was surveyed to study the effect of leading edge stall and leading edge vortex on the flow in this region which was not investigated previously.

1. INTRODUCTION

Rapid advances in the capacity of computers and the development of numerical methods to solve the full Navier-Stokes equations have pushed the computation of unsteady flows far ahead of the existing experimental data, with which the computed results could be validated. Most of the previous experiments on unsteady flow past airfoils were either of a qualitative nature (flow-visualization) or were aimed at finding the overall effect of the flow at the boundary (pressure coefficient, pitching moment coefficient, normal force coefficient etc. on airfoils).

Extensive measurements of mean velocity vectors and Reynolds stress tensors in the 2-dimensional unsteady boundary layer over an oscillating airfoil and in the wake behind the airfoil were carried out by De Ruyck and Hirsch [1-6], using a slanted single sensor hot-wire. The method has been quite successful in mapping the flow in the investigated region, giving a clear picture of the flow, including flow reversal and vortex formation. These experiments were conducted using an NACA 0012 airfoil with a tripping wire to promote transition of the boundary layer.

The present experiments are the extensions of the measurements conducted by De Ruyck and Hirsch [1-6]. The present experiments were conducted without the tripping wire, to take a closer look at the formation of the leading edge separation bubble and the events leading to the turbulent separation downstream of the bubble. The measurements near the trailing edge and in the wake of the airfoil were conducted with and without the tripping wires. These experiments were expected to throw new light on the Unsteady Kutta Condition for airfoil operating under stalled condition.

These experiments will contribute to the data base needed for the validation of solutions of the Navier-Stokes equations for unsteady flows and turbulence modelling for these cases.

2.PREVIOUS WORK

Most of the previous works closely related to the unsteady flow over pitching airfoil has been reviewed by De Ruyck and Hirsch [3]. A number of excellent reviews were published by various authors on the subject of unsteady flows. McCroskey [7] carried out an extensive review of the published research on unsteady flows. The investigations closely related to the present experiments are reviewed here.

2.1 Unsteady Flow Over Airfoils and Separation Bubble

Martin et al [8] studied the dynamic stall behaviour of a pitching NACA 0012 airfoil section by correlating surface pressure signals, signals from hot wires in close vicinity of the surface and smoke flow visualization data. The presence of a separation bubble ahead of the turbulent separation was noted but the interaction between these two could not be determined. Enough evidences was not collected to determine how it leads to the leading edge stall. The formation and shedding of a leading edge vortex was also reported.

McCroskey et al [9] carried out experimental investigations on several airfoil shapes in sinusoidal pitch oscillations. The type of stall was reported to be dependent on the leading edge shape of the airfoil. The mechanism of the leading edge stall of NASA 0012 airfoil was reported to be due to the sudden breakdown of the flow downstream of the separation bubble rather than bubble bursting.

Hydrogen bubble flow visualization for laminar flow past an oscillating airfoil, reported by McAlister and Carr [10] showed large hysterisis effect on the onset of reverse flow. McCroskey et al [11], McCroskey and Pucci [12] investigated the dynamic stall behaviour of several airfoil shapes in sinusoidal pitching . Large hysteresis effect was observed in the fluid dynamic forces and moments, when airfoils oscillate around its static stall limit. It was concluded from these measurements that behaviour of airfoils at stall onset and during light stall seemed to be strongly dependent on the shape of the wing section. During deep dynamic stall a vortex like structure forms near the leading edge suction surface and rolls over the suction surface and the flow over the suction surface completely breaks down. This vortex creates unusually large lift, moment and drag coefficients. McAlister and Carr [10] produced well defined pictures of this phenomena from their flow visualization experiments.

Bass et al [13] conducted hydrogen bubble flow visualization in the reduced frequency range of 0.5 to 10 and at various mean angle of attack and pitch amplitude. In the reduced frequency range 0.55 to 0.81, on the forward half of an NACA 16-012 airfoil a separation bubble was observed. This separation bubble, under certain test conditions, extended over a large portion 25% to 40% of the chord of the airfoil.

McCroskey et al [9,11] concluded that separation bubble burst causing leading edge stall is observed in the profiles with sharp leading edge. This mechanism is caused by the inability of the separation bubble to reattach and spreading downstream to bring about complete breakdown of the flow over the suction surface. In case of sections with rounded leading edge like NACA 0012, the separation bubble grows in size at higher angle incidence. As the angle of incidence increases a sudden breakdown of the boundary layer occurs downstream of the turbulent reattachment point. This turbulent separation point rapidly progresses upstream and immediately leads to leading edge stall.

A complete boundary layer survey for distribution of mean velocity and Reynolds stress tensor over an oscillating airfoil was reported by DeRuyck and Hirsch [3,4,5,6]. The airfoil used was a 0.6 m chord and 0.94 m span uncambered NACA 0012 section with tripping wires at 0.1C. Experiments were conducted at reduced frequencies 0.48 and 0.3 and the Reynolds numbers were 178,000 and 300,000. The amplitude of the pitching oscillations was fixed at 5 degrees and mean angles of incidence were varied between 10 to 15 degrees. In case of separated flows, the reported Reynolds stresses measured were considerably higher than those for a flat plate. Formation of two leading edge vortices were reported and a close similarity with computed results of Mehta [14] was noted although Mehta's calculations were carried out for lower Reynolds number.

The effect of oscillating free-stream on a separation bubble formed over a Wortmann airfoil was examined by Brendel and Mueller [15]. At a Reynolds number of 100,000 the separation bubble extended from 33% to 62% of the chord, both in steady as well as in the unsteady flow. However it was found that the separated region becomes thinner due to the unsteadiness in the flow, the proximity of the separated shear layer to the wall has a large effect on the stability of the flow downstream of the reattachment.

A review of turbulent flow reattachment was published by Eaton and Johnston [16]. Need of more research on this subject was pointed out by the authors.

Serpa, Lessmann and Hagist [17] studied the flow in a two-dimensional

separated and reattached bubble formed over a curved surface. Significant surface pressure variation was observed ahead of the mean separation point accompanied by large pressure fluctuation. Large fluctuations in the surface pressure were also observed near the mean reattachment point. The displacement, momentum and energy thicknesses show an increase through the separation bubble. The displacement thickness peaks near the reattachment point but the momentum and energy thicknesses form a plateau near the middle of the separation bubble.

The characteristics of a turbulent separating flow created over a flat plate by imposing an external adverse pressure gradient was reported by Simpson, Chew and Shivaprasad [18,19] and Shiloh, Shivaprasad and Simpson [20]. Effects of periodic free-stream unsteadiness on this separation layer was later reported by Simpson, Chew and Shivaprasad [21], which has relevance to the trailing edge separation in an unsteady flow.

2.2 Unsteady Kutta - Condition and the Wake

Satyanarayana and Davis [22] carried out wall static pressure measurements near the trailing edge of an oscillating NACA 64A010 airfoil operating at various fiequencies and in unstalled condition. It was concluded from these experiments that application of the Kutta-Joukowsky condition on the flow over an unstalled sinusoidally oscillating airfoil is valid below the reduced frequency of 0.6. At higher reduced frequency the steady Kutta condition predicts lower pressure differencial and this error increases with frequency.

The unsteady Kutta condition for high reduced frequency, periodic disturbances, sudden change in airfoil incidence and sharp edged gust were investigated by Basu and Hancock [23] for inviscid flow condition. They pointed out that each individual case needs its own consistent unsteady Kutta condition. A general numerical model was outlined using the Geising and Maskell trailing edge condition [23], which can be described as follows. In case of a steady flow past a lifting airfoil with sharp trailing edge the pressure difference between the surfaces at the stagnation point becomes zero. This in effect makes the stagnation streamline to leave the airfoil along the bisector of the wedge angle. However, in case of unsteady flows, the steady Kutta condition would predict the pressures not to approach the same value, due to the rate of change of circulation associated with the lifting airfoil. This would leave the flow with a non-physical behaviour and the Geising and Maskell trailing edge condition states that the

stagnation streamline at the trailing edge will be tangential to the pressure surface for positive (anticlockwise) shed vorticity and to the sucttion surface in the opposite case.

Bass et al [14] from their hydrogen bubble flow visualization reported that unsteady Kutta condition was violated for many incidences when trailing edge separation occurs. The violation was due to the reverse flow on the suction surface near the trailing edge. It was also reported [14] that introducing a phase lag into the circulation function provides better agreement between theory and experiment.

Poling and Telionis [24] experimentally investigated the unsteady Kutta condition for a NACA 0012 airfoil using LDA and concluded that the condition proposed by Geising and Maskell is valid for high reduced frequencies. The flow visualization carried out by Poling and Telionis [25] at the trailing edge of a pitching airfoil also supports the Geising and Maskell trailing edge condition provided the rate of change of circulation (of the bound vortex) is far from zero. It was reported that there is indication of violation of the condition of zero loading at the trailing edge, however this condition does not extend beyond 3% chord downstream of the trailing edge [24].

Ho and Chen [26,27] reported measurements carried out near the trailing edge of a pitching airfoil over a reduced frequency range of 0 to 1 using x-wires. Except for the time mean streamwise velocity profiles no other profile attained self similarity within the measurement distance of 1 chord length downstream from the trailing edge. At reduced frequency of less than 0.51 and angle of attack less than 7.5 degrees, the unsteady Kutta condition was found to be valid.

Measurements reported by DeRuyck and Hirsch [1,2] in the wake of a pitching NACA 0012 airfoil were made at the Reynolds number of 300,000, at various reduced frequencies between 0 to 1.2 and at various amplitude of oscillations. The boundary layer on the airfoil was tripped with tripping wires fixed at 10% chord. The test cases extended to a lightly stalled case. The influence of oscillation was found to be important only at high amplitudes. At high frequency large values of turbulence were observed close to the trailing edge. A strong phase shift in the turbulent responses were also reported.

In summary the general picture which emerges is that:-

(i) The mean and the turbulent quantities measured in the flowfield of an

oscillating airfoil are not yet complete for validation of analytical methods.
(ii) The extent and duration of the leading edge separation bubble is not yet fully investigated.
(iii) The extent of trailing edge separation and the effect of the leading edge separation bubble on the trailing edge separation under the influence of unsteadiness is not yet known.
(iv) The effect of separation bubble on unsteady Kutta condition,
(v) the effect of leading edge stall on the unsteady Kutta condition and
(vi) the effect of deep dynamic stall on the wake parameters require further investigation.

The aim of the present investigation is to collect data so that some of the gaps in the knowledge mentioned above can be examined.

3. PRESENT CONTRIBUTION

The present experiments were conducted on the airfoil of De Ruyck and Hirsch [1-6]. On this airfoil wake experiments were made with a fixed probe, and boundary layer experiments with a probe mounted on the airfoil (figure 3.1). These set-ups did not provide investigations close to the leading edge and around the trailing edge, although these areas are of primary interest.

The present experiments were conducted by adding two end plates on which a probe can be mounted, allowing experiments anywhere around the airfoil (figure 3.2). An important consequence of these end-plates is to minimize the effect of aspect ratio and of tipvortices. A large number of chordwise stations were clustered near the leading edge to study the separation bubble and near the trailing edge to investigate the trailing edge separation.

3.1 Separation Bubble and Leading Edge Stall

In a first step a fixed hot wire was mounted close to the wall (1.5 mm) at different chordwise locations and at angles of attack oscillating between 4 to 14, 5 to 15, 6 to 16 and 8 to 18 degrees. Static pressure taps were added in the leading edge stations. The obtained hot wire and pressure signals were used to identify the conditions under which a separation bubble and leading edge stall occur. Leading edge bubbles were observed at 4 to 14 and 5 to 15 degrees, which burst at higher angles of attack.

For the 5 to 15 degrees test case, boundary layer profiles were measured (1mm to 7 mm from the wall). Due to the very small size of the boundary layer, these experiments were conducted with a single, non-rotating wire. Returning flows could be detected from the hot wire signals.

3.2 Boundary Layer and Wake

For the same 5 to 15 degrees test case, the measurement of the velocity vector and the Reynolds stresses has been performed over the whole boundary lyer and near wake, with emphasis on leading edge and very near wake. Slight trailing edge separations are observed.

In addition to the boundary layer experiments of De Ruyck and Hirsch [4,5,6], the experiments were conducted in the very near wake with the airfoil in deep periodic separation (8 to 18 degrees). This experiment is

seen as a complement of the 8 to 18 degrees investigation (with tripping wire) discussed in [4,5,6]. No significant difference was observed except when the airfoil is deeply stalled. During deep stall the flow at the trailing edge is found to be separated over a larger portion of the chord in [4,5,6] and there appears to be a phase lag in the flow near the trailing edge. The tip clearance in [4,5,6] was less than 5% chord and the tip vortices were expected to be much weaker than that of a free 1.56 aspect ratio airfoil. The blockage effect due to the model with the end-plates is discussed in section 5.3.

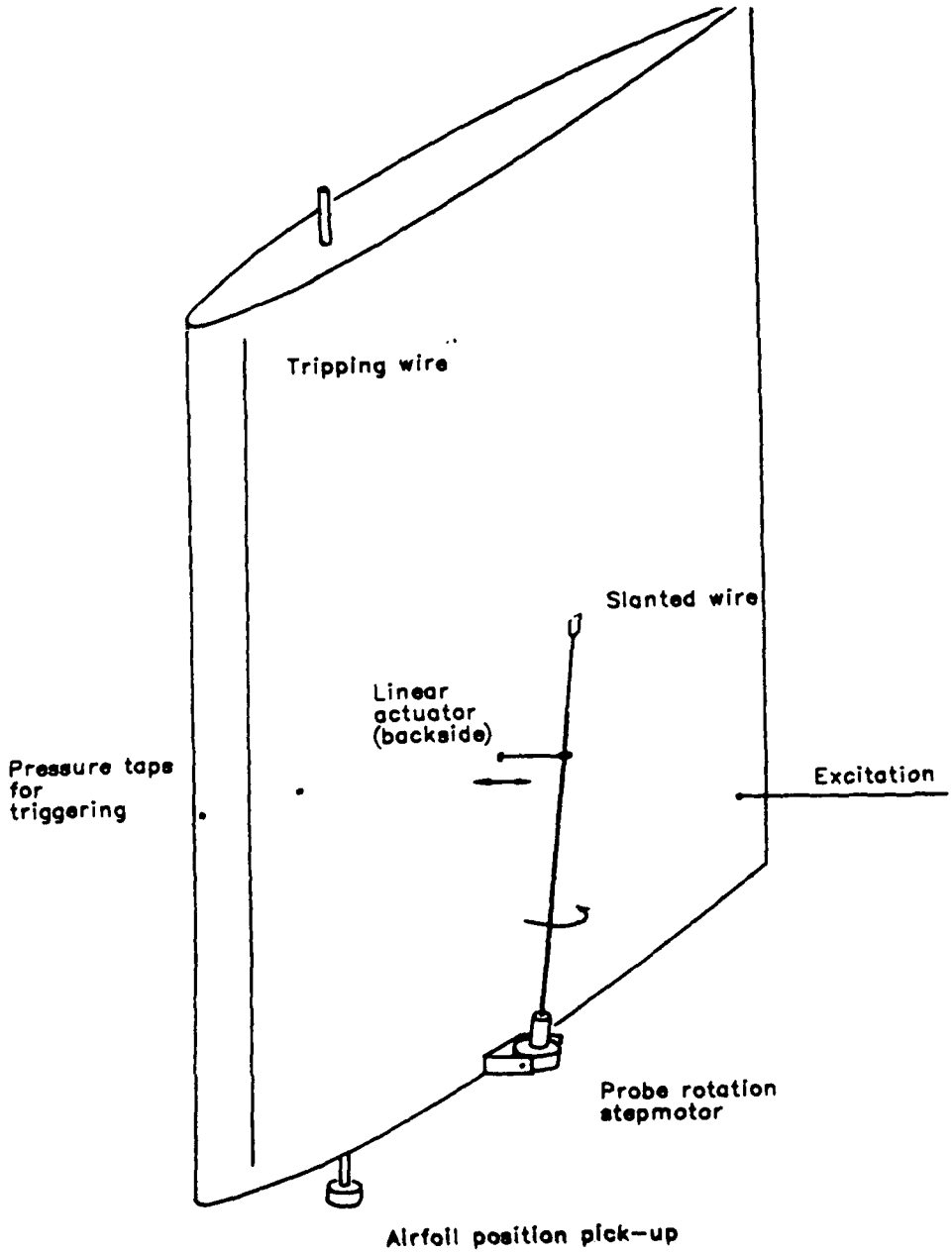

Figure 3.1 : Experimental set up for the early experiments of De Ruyck and Hirsch [1-6]

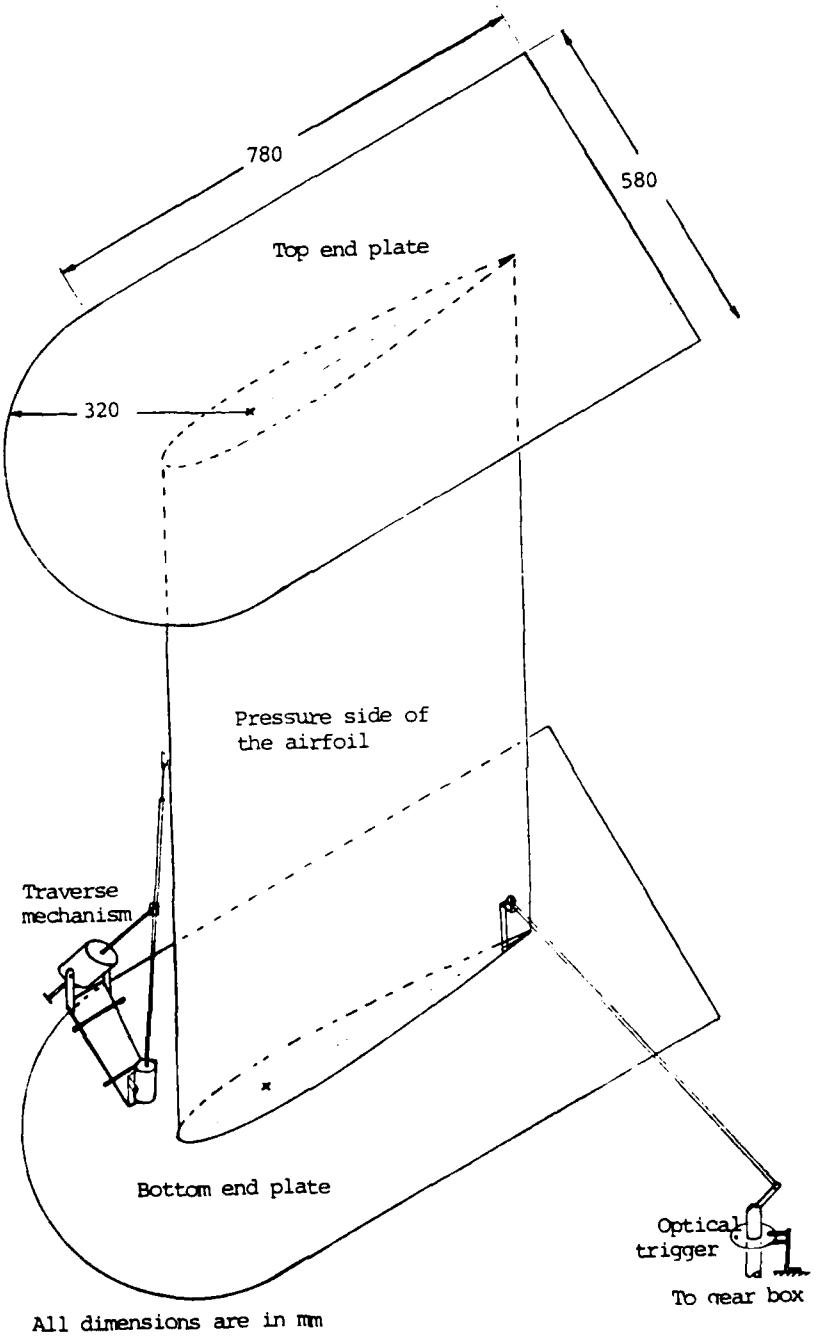

Figure 3.2 : Present experimental set-up

4. EXPERIMENTAL SETUP

4.1 Wind Tunnel, Airfoil and the Oscillating Mechanism.

The experiments were conducted in an open-circuit blow-down wind tunnel in the Department of Fluid Mechanics of VUB, Brussels. The cross section of the test-section is 1m x 2m, and the tests were conducted at the nominal wind speed of 11.32 m/s and the free stream turbulence intensity less than 0.2 %.

The test model consisted of an airfoil and two end plates (figure 3.2). It was oscillated by an asynchronuous motor driving a crank and connecting rod through a reduction gear box. The period of oscillation was accurately measured and found to be 0.542 seconds. The airfoil is a NACA 0012 airfoil section with 60.4 cm chord and 94 cm span. The lower end plate served as a platform to mount the traverse mechanism. The relevant dimensions and the arrangement of the model and the oscillating mechanism are shown in Figure 4.1. The reduced frequency and the Reynolds number based on the chord of the airfoil and the nominal wind speed were 0.309 and 300,000 respectively.

The profile shape near the leading edge was accurately measured close to the mid span. The largest deviation of the profile from the standard NACA 0012 profile was found to be less than 0.01% chord. The result of the measurements are given in Appendix 1.

4.2 Traverse Mechanism.

The mechanism to traverse and rotate the slanted single sensor hot-wire is shown schematically in Figure 4.1. The mechanism was designed for lightness, stiffness and low disturbance. The bulk of the volume was kept away from the region of investigation and as close to the clamping position as possible. The step motor Z rotates the probe about its axis and takes 48 steps to complete a full revolution. The step motor Y, which changes the distance of the sensor from the airfoil surface, moves the linear actuator by 0.0254 mm in each step. The linear motion of the sensor from the airfoil surface (along an arc, to be exact) depends on the distance of the sensor from pivot point A, retainer clamping position (of sleeve C) on the probe support, and inclination of the probe support with the span of the airfoil. The resolution on the sensor position from the wall was 0.08 mm or less for one step. The rotation of the probe and the distance of the sensor from the airfoil surface during the experiments were controlled by the acquisition system (Macintosh Computer). The chordwise position was changed manually by

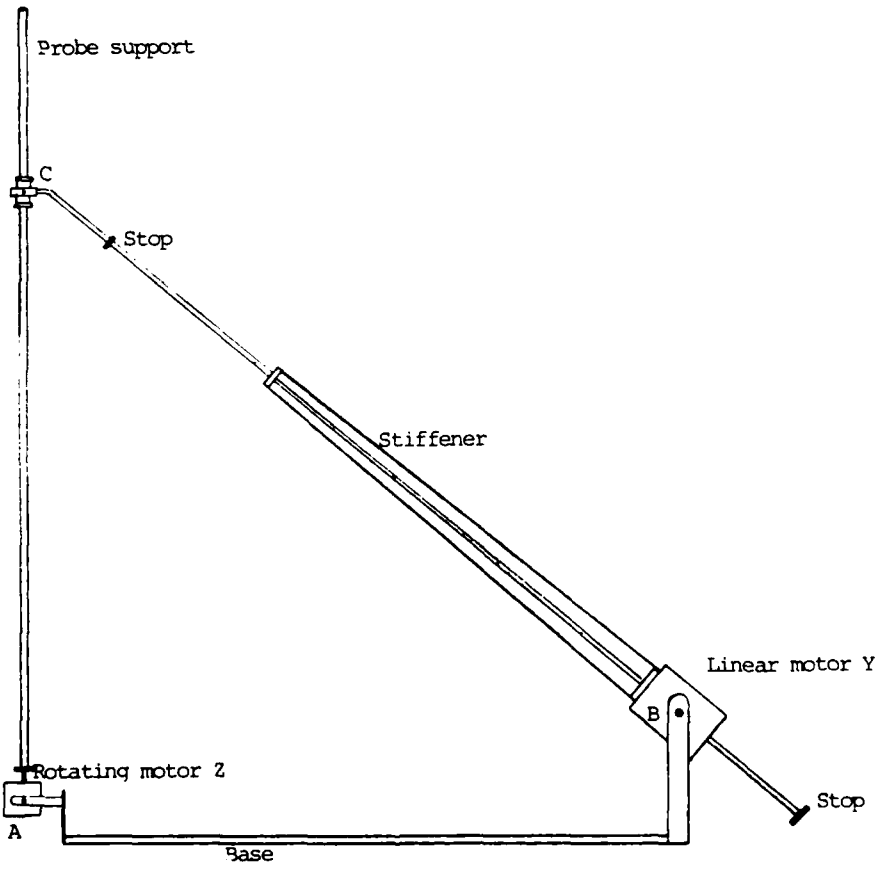

Figure 4.1 : traverse mechanism

moving the base of the traverse mechanism.

4.3 Probes, Transducers and Anemometer.

A 45° slanted single sensor hot-wire was used for all the velocity and turbulence measurements. The particular type of sensor used was DANTEC gold plated hot-wire type 55P02. The 1.25 mm long sensor had 0.005 mm diameter. The probe was connected to a DANTEC constant temperature anemometer (CTA). The output of the CTA was given a known constant offset, so that an optimum level of sensitivity of the digital converter (TEK 2430A Oscilloscope) could be utilized, before digitizing.

The periodic sampling was triggered by a pressure transducer for the cases where a sharp change of wall pressure signal was available (during test cases when leading edge stall occurs). The triggering of the periodic sampling was accomplished by an optical device when pressure signal was erratic or insufficient. The stations used for the leading edge investigations are listed in appendix 2, where (p) indicates the stations where pressure taps were drilled and 8 cm long 1 mm diameter stainless steel tubes were installed to be connected to the pressure transducer. The pressure taps were drilled 24 mm away (spanwise) from the traverse position. The hot-wire was always positioned with the plane of the prongs perpendicular to the airfoil surface.

4.4 Controllers and Acquisition System.

The arrangement of the data acquisition system is shown schematically in Figure 4.2. A PC (Apple-Macintosh Plus) acts as the principal controller to coordinate the actions of the step motor controller and the TEK 2430A Digital Oscilloscope.

The PC asks the step motor controller to place the probe in a certain position (rotational as well as linear). When the action is completed, the computer sets the oscilloscope in the required acquisition mode and starts the acquisition of 100 hot wire and pressure transduces periodic signals (542 samples/cycle). At the end of the acquisition the computer collects the data, performs a periodic averaging and stores the periodic averages and their r.m.s. values on disc (in volt). The reference values needed for fouling and temperature corrections of the hot-wire sensor (section 5.2) are saved as values averaged over 64 acquisition cycles.

For the leading edge bubble measurements, the original time signals are

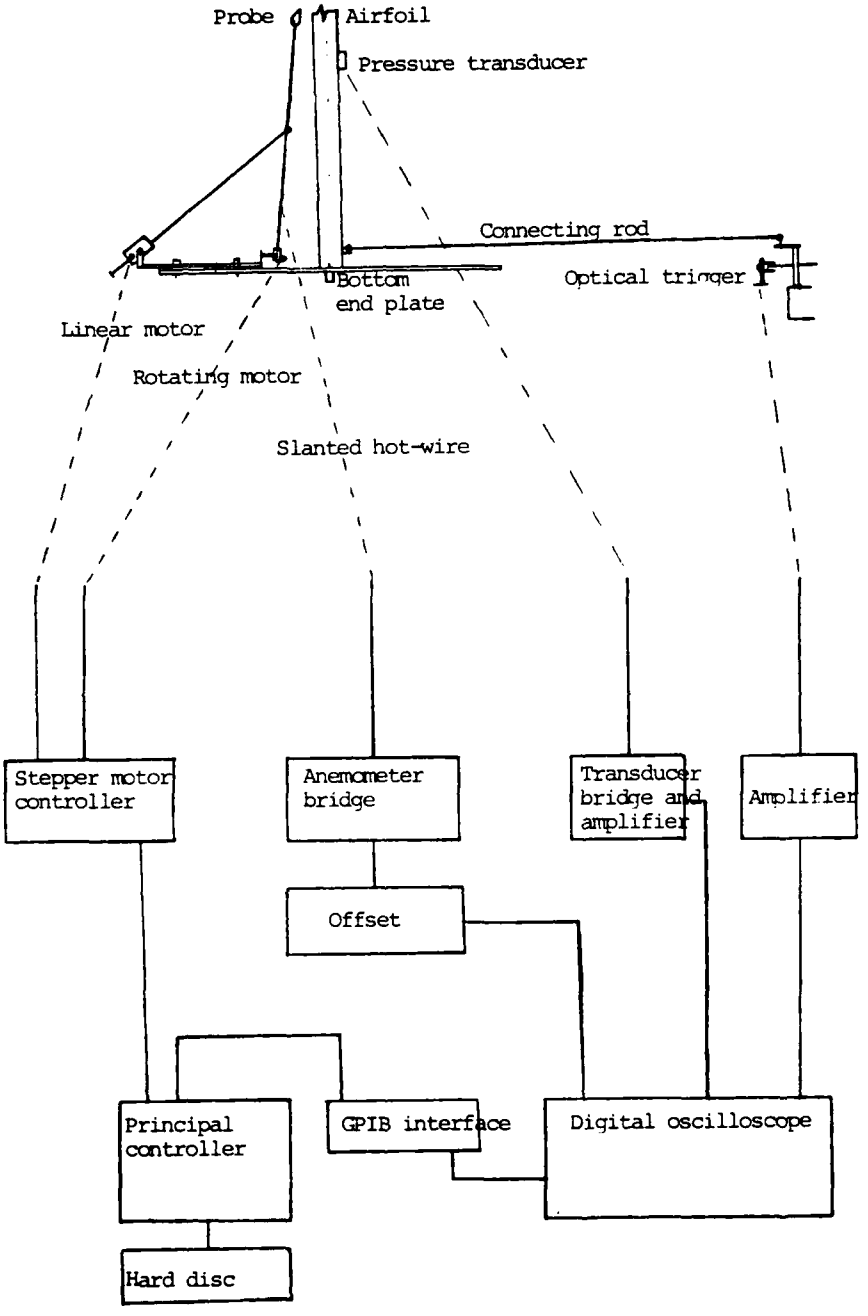

Figure 4.2 : Data acquisition

saved, without periodic averaging. The volume of data to be analysed were relatively small.

The final data processing was carried out on an Apollo work-station, where the mean and r.m.s. voltages are tranformed into velocities, from which two mean velocity components and four non-zero Reynolds stresses are computed. The techniques used to obtain these data are given in section 5.1 and section 5.2.

5. MEASUREMENT TECHNIQUE

5.1 Detection of Separation Bubble and Leading Edge Stall

Since the separation bubble exists in a very thin region close to the solid surface and the effect of unsteady flow is to make it thinner [15], the rotating single slanted hot-wire technique could not be used to investigate the separation bubble. A combined analysis of pressure signals and fixed hot-wire signals was used to identify the duration for which a station was in the separation region. The signals contain 542 data points per period, and are ensemble averaged over 100 periods.

Figure 5.1 shows a sample of ensemble averaged traces, with the corresponding rms values over approximately 2 cycles of oscillation. These rms values of pressure and hot wire signal are used to detect the transition and the high turbulence areas. Since the normal velocities are very small that close to the wall, the averaged single wire signal can be used to estimate the velocity. Although the flow direction cannot be determined without ambiguity, these signals allow to determine the reversed flow areas and the data on figure 5.1 can be interpreted as follows.

The period between A and B is a significantly laminar flow period with fluctuations in the hot-wire signal less than the resolution of the digital oscilloscope setting. The fluctuation in the pressure in this region is due to drift in the amplifier used. At time B, the transition to turbulence crosses the measuring station, while moving upstream. In reality the transition is already upstream of it at time B, since the wire is 1.5 mm away from the wall. Indeed, slightly ahaed of B, a dip in the mean wall pressure signal (pt,m) is observed, with a small peak in the pressure rms (pt,f). From all the experiments, these dips appear to correspond with the passage of a transition or separation point. From B to C, the transition point moves further upstream, the boundary layer is growing (decreasing velocity, increasing turbulence). At point C there is an important drop in the ensemble averaged hot-wire output to point D, accompanied by: (i) slight increase in the rms value of hot-wire signal, (ii) a large reduction in the ensemble averaged pressure signal and most important of all (iii) sudden increase in the rms value of the pressure signal fluctuation. The application of the high turbulence correction of De Ruyck [6] yields a velocity quite close to zero at point D. The increase in the output between point C and D indicates flow reversal (as will appear from the overall

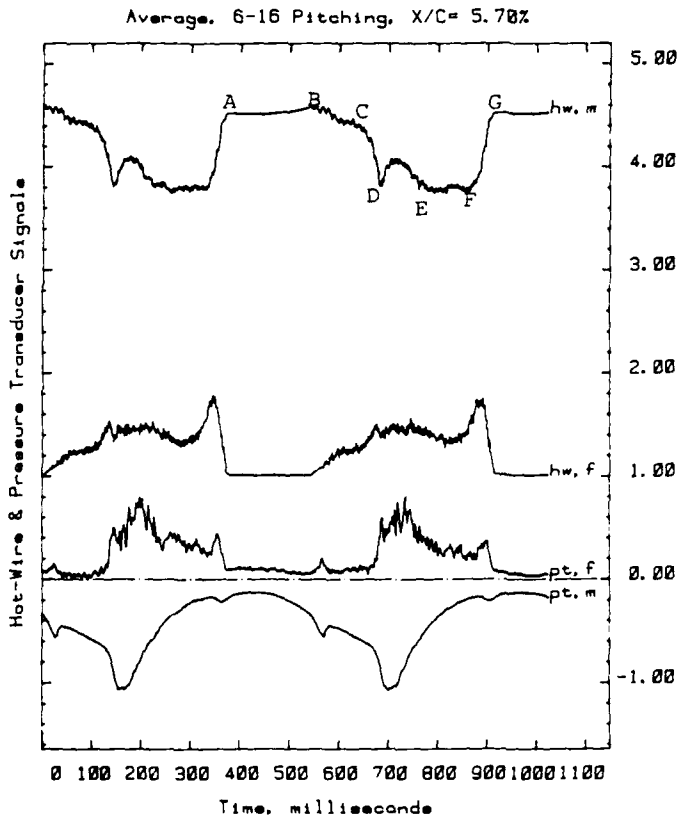

Figure 5.1 Sample of Fixed Hot-Wire and Pressure Transducer Signal

hw,m : ensemble average of hot-wire output

hw,f : rms value of hot-wire output, multiplied by 2 and shifted upwards by 1 volt

pt,m : ensemble average of pressure transducer output

pt,f : rms value of pressure transducer output, multiplied by 10

results,the flow is completely separated in the leading edge region, from D to F). During this period rms values of hot-wire and pressure transducer signal fluctuations remain high and the average value of pressure transducer signal remain small. During the period between E and F, after correcting for high turbulence the mean velocity was found to be negligibly small (same order of magnitude as the turbulence, smaller than the turbulence in some cases). During this period the rms values of pressure transducer signal was about the half of the peak value.

The increase in the rms values between F and G is attributed to the cycle to cycle variation, since the reattachment time was observed not to be perfectly periodic (from the oscilloscope). Since the rate of change of velocity is large at this time, about 10% to 50% of the measured turbulence is due to the cycle to cycle variation of events. At other times this effect is negligible.

Figure 5.2 shows clearly the detection of a separation bubble at 5 to 15 degrees angle of attack, at 3.5% chord from the leading edge. The traaces are taken at different distances from the wall. At the distance 1 mm from the surface of the airfoil, during the period A to B a laminar flow is observed. The output of hot-wire suddenly reduces during the period from B to C accompnied by an increase in the rms value. After turbulence correction, the velocity at C yields a value close to zero. This indicates that the separation point has crossed the position of the sensor and moved upstream of it. The sensor remains in the separated region from C to D where the backflow velocity first increases then falls to the near zero velocity value. Between D and E the velocity sharply increases and rms value reduces to zero, indicating that the separation point has moved downstream of the sensor. The output at 1.5 mm from the surface is similar to that at 1 mm in many respect. A laminar portion from F to G, sharp drop during G to H and a sharp increase in velocity between I to J. However, between H and I the flow is turbulent and the velocity is near zero, during this time the sensor is in the free shear layer formed on the top of the reverse flow region. At 2.5 mm away from the surface only a slight reduction in the mean velocity along with increase in turbulence was observed near the point L. This indicates that the sensor during this time was at the outer edge of the shear layer. A near perfect sinusoidal variation of the output is observed at the position 3.5 mm away from the airfoil surface, slight turbulence which appears near M is probably caused by the cycle to cycle variation of the separation. In conclusion, the two

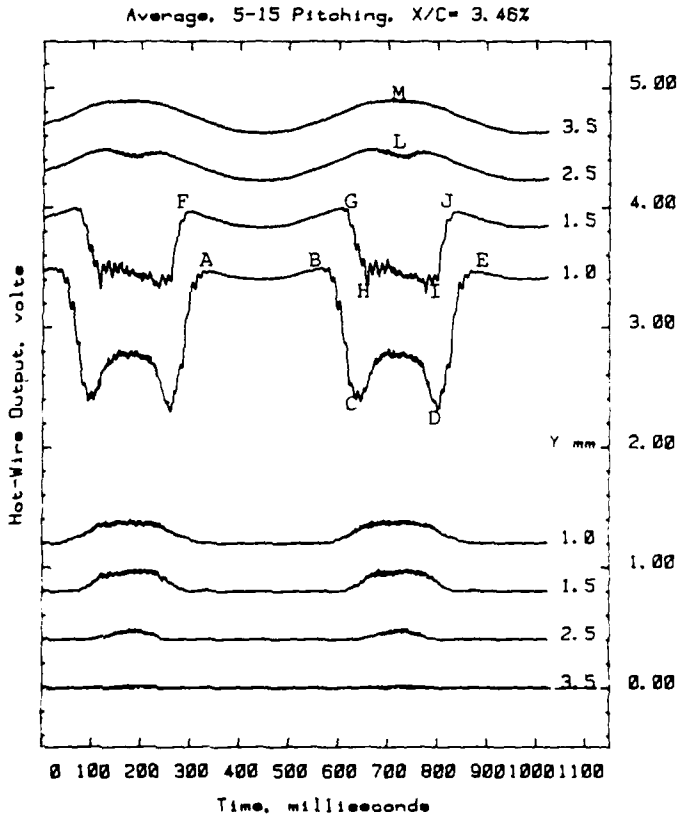

Figure 5.2 Sample of Fixed Hot-Wire Output at Various Transverse Positions
The four upper curves are ensemble average, the lower curves represent rms values.
The outer curve is in the correct position, the other figures are shifted towards each other by 0.4 volts each.

dips in the lowest signal correspond to flow reversals, revealing the presence of the bubble with a thickness of approximately 1.5 mm.

Figure 5.3 shows the variation of velocity and turbulence calculated by the method described above, against phase angle for 5-15 degrees oscillation (phase angle zero coincides with the mean angle of incidence at increasing incidence). These are the quantities measured at a constant height 1.5 mm (0.25% chord) from the airfoil surface but at different chordwise positions. The mean velocity variation at 1.94% chord from the airfoil shows a sinusoidal variation with very small turbulence (of the order of the uncertainty involved, see section 5.3), indicating that neither separation nor turbulence ever invades this position. The variation of velocity and turbulence at 3.46% chord indicates that for more than half the time of oscillation the sensor is in the laminar flow region. A part of the time near the maximum angle of incidence the sensor is in the shear layer above the reverse flow region indicated by low velocity and high turbulence. At the next two stations (4.24% and 5.03% chord) the flow is affected by the separation bubble for a longer duration, with flow reversal for a short duration at 4.24% chord. The velocity variation at the two consecutive positions (6.61% and 8.15% chord) shows a laminar portion followed by a turbulent portion with a dip in the middle of the turbulent portion. The turbulent portion indicates that the transition to turbulence takes place upstream of the considered station (due to the separation bubble in this particular case), and the dips indicate that the position was in the free shear layer near the reattachment point, this is also indicated by a sudden rise in the turbulence. As will become clear from the overall data (see section 6.1), this low velocity corresponds with a tendency of the bubble to burst, and the increase in bubble size reduces the velocity at this location. The curves upto 15.4% chord show a laminar flow during the time around the phase angle 300 degrees, though the duration of the laminar portion reduces as the sensor is moved downstream. Downstream of 15.4% chord no laminar portion could be found.

In some cases, a strong high frequency oscillation in the ensemble averaged velocity can be observed. All these oscillations observed in the mean velocity curves are perfectly periodic, otherwise they would disappear by the ensemble averaging. Hence, they do not correspond with turbulence and they do not contribute to the turbulence as can be seen in the laminar portions in the curves at 12.8% chord in figure 5.3. These oscillations are due to vibrations of the sensor (and/or the wall) and the oscillations period is 12 milliseconds. This is found to correspond with the vibrations

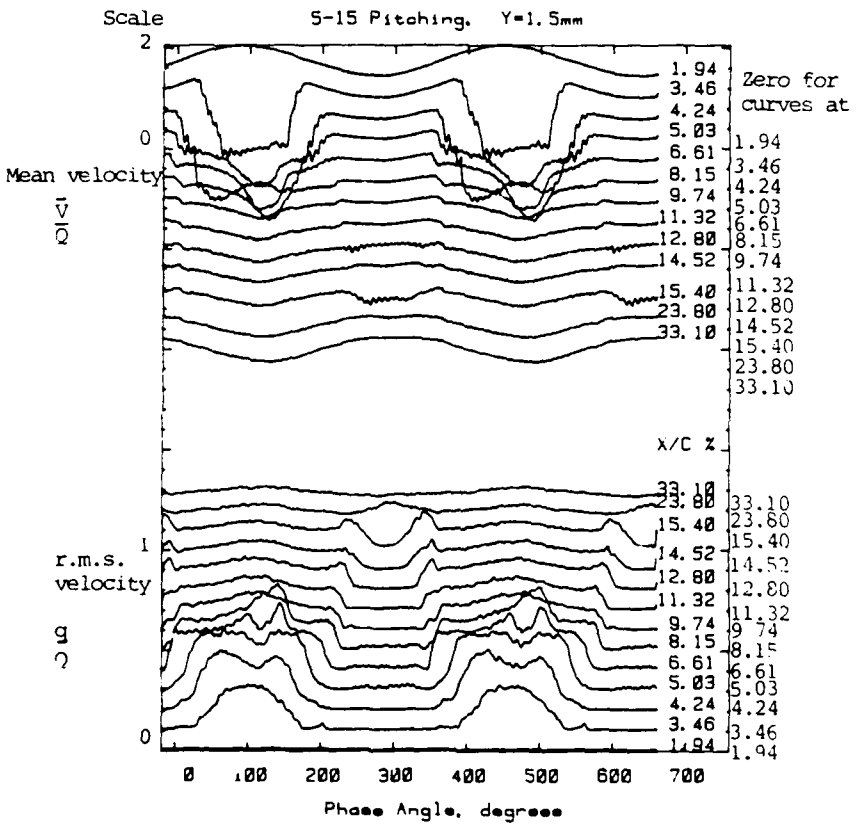

Figure 5.3 Sample of Velocity and Turbulence Intensity Calculated from Fixed Hot-Wire Output

caused by the gear box and they change the location of the wire inside the boundary layer, giving rise to changes in local velocities. According to the thickness of the boundary layer and the amplitude of the observed vibrations, the amplitude of the vibration is estimated at 0.1 mm, which cannot be avoided with the present construction. The oscillations become evident only during the time when there is sharp velocity gradient in the transverse direction, as in the free shear layer close to the separation point (figure 5.3, in the part with sudden variation at 3.46%,4.24% and 5.03% chord) or in the laminar boundary layer (the laminar part in the curve at 15.4% chord).

A clearer picture emerges from these curves if represented as isovelocity lines and isoturbulence lines in a space-phase angle(or time) domain. These results are presented in that manner in the next section for detection of the separation bubble and the leading edge stall (figures 6.1 to 6.4). For comparison with boundary layer measurements these data are also presented as velocity vectors parallel to the airfoil surface (true only in the close proximity of the surface) and isoturbulence lines at various angles of incidence (e and d, respectively in figures 6.5 to 6.20).

5.2 Measurements in the Boundary Layer and Near Wake

The hot-wire technique used for the measurements is described in reference [3] and is reproduced in Appendix 3. Ensemble averages were made with 542 samples per period and 100 periods and 48 rotational positions. The low number of periods is compensated by the high amount of samples per periods which allows some local time averaging. The ensemble averaging is done in real time, reducing considerably the required amount of mass storage.

Since a complete boundary layer survey requires up to about 40 hours, it was necessary to correct the results for any change in the hot-wire output due to temperature change and fouling of the sensor. This was done by measuring reference hot wire voltages at all the transverse (normal to the chord and the span of the airfoil) positions before, during and after the experiments (all automatic). Calibrations before and after each experiment in general indicated no wire fouling and only temperature corrections were made according to the changes in reference voltages (data taken with foul sensor are rejected along with the probe). The difference was proportionately distributed over 48 angular positions. For the narrow range

of temperature encountered during an experiment (18°C-26°C over the year, about 2°C during one experiment), and for a constant velocity, a simple linear temperature correction could be used.

The final calculations were performed off-line in an Apollo work-station. The 542 samples were reduced to 181 by conditional averaging to reduce scatter, without reducing relevant events. For the deep stalled case 8 to 18 degrees, 8 point smoothing on the time signals was applied before processing of the data, as described in the appendix.

5.3 Accuracy

The resolution in the chordwise position was 0.5 mm (0.08% chord). The resolution in the transverse position was better than 0.08 mm (0.013% chord). However, the amplitude of vibration of the probe was found to be 0.1 mm by using a piezo-electric accelerometer fixed near the tip of the probe holder. Therefore, the uncertainty in the transverse position is 0.1 mm (0.016% chord).

The freestream velocity in the test section with the model at zero angle of incidence and without the model was measured using a pitot tube before starting the experiments at different chordwise distances. Sufficiently away from the model, the differences between these measurements and the nominal speed were less than 1% of the nominal speed.

The resolution on the output voltage was 8 millivolts, with an 8-bit accuracy. When converted to velocity this amounts to about 1.3% of the nominal wind speed. Therefore, this will be the maximum resolution in the the mean velocity and in the turbulence for the techniques described in section 5.1. There was no linearization error involved because the data were ensemble averaged after they were converted to velocity.

After correcting for temperature variations the error due to calibration was made less than 1%. The drift due to fouling was kept below this level by rejecting data and sensor if any sudden change in the reference reading was observed.

Scatter on the results for unstalled conditions were in general very small (less than 1% on all the results). In stalled conditions, important scatter is observed, in particular on the turbulent shear stress. In this region the random error in velocity varies between 1% and 5%, scatter on normal stress profiles varies between 2% to 10% and for the turbulent shear

stress the maximum scatter exceeds 15%.

The systematic error for the measurements of the stresses in high turbulent conditions (above 10%) is increased by linearizations during the processing of the data. These errors are estimated at 5 to 10%, and to 1 to 2% in unstalled conditions.

At reattachment, slight cycle to cycle changes are observed. Due to the strong velocity changes at reattachment, the error introduced in the corresponding turbulence quantities due to the cycle to cycle variation is quite important (more then 50% increase in turbulence). At present no way is found to correct the data for this problem.

6. RESULTS AND DISCUSSION

All the measurements were performed at the nominal freestream velocity of 11.32 m/s and at a period of oscillation of 0.542 second. The Reynolds number based on chord was 300,000 and the reduced frequency was 0.309. In the figures of this section the velocity vectors and turbulence intensities are presented as fractions of nominal velocity and the Reynolds shear stresses with negative sign as fractions of nominal dynamic pressure. The distances are scaled equally and are presented as fraction of the chord.

6.1 Leading Edge Measurements

The results of the fixed wire data are shown on figures 6.1 to 6.4. Velocities and turbulence intensities are plotted as isolines in a chordwise distance-phase angle domain. Two series of results are shown : results at a fixed distance of 1.5 mm from the wall and increasing angles af incidence (figures 6.1 and 6.2) and results at a fixed incidence 5 to 15 degrees and different distances from the wall (figures 6.3 and 6.4). In all cases, eventual flow reversals have been detected and considered in the representation of the data. The dark colors indicate the smallest velocities and strongest turbulence. Returned flow areas are left blank for contrast, indicating the bubble area. The laminar regions correspond with the yellow areas in the turbulence plots.

The events that occur on a plane parallel to the airfoil surface at 1.5 mm and 4 to 14 degree oscillation are shown in figures 6.1a and 6.2a. At 4% chord a very low speed area (below 0.1 of the outer speed) and a small reversed flow area (white area) were observed for a part of the oscillating period when the angle of incidence was above 10 degrees (6.1a). Peak values of turbulence (>25%) were observed at 5% chord around maximum incidence (6.2a) which is just downstream of the low speed area (6.1a). As will be observed below, a larger reversed flow area is present closer to the wall (the separation bubble) and the dark area in figure 6.1a represents the duration and the extent of the shear layer above that separation bubble. Experiments at closer distances are necessary, preferably with sensors on the surface, to determine the exact separation and reattachment positions. It can be argued that the separation bubble extends from about 2% to 5% chord at the maximum incidence in this case. The turbulence reaches a maximum around or just before the reattachment point and above the bubble. This is in accordance with observations in [16]. The pressure rms values

reach a maximum inside the separated area (figure 5.1,[17,28]). Downstream of the separation bubble, on this plane, the velocity increases up to 9% chord due to the recovering boundary layer. Downstream of this position (9% chord) the velocity gradually reduces indicating decelerating flow and boundary layer growth. After the lowest angle of attack (indicating a mild phase lag of about 10°) the transition occurs much more downstream, at positions up to 20% distance from the leading edge, and nothing indicates the presence of separation bubbles. A high turbulence (>15%) appears in the transition area around 15% chord at 9 degrees incidence.

Figures 6.1 b and 6.2 b show the events at 5-15 degree oscillation, in many respect these figures are similar to the ones at 4-14 degree with one striking difference - a sudden enlargement of the low velocity region downstream of the bubble immediately after the maximum incidence (6.1 b). This indicates the onset of a bubble burst which can trigger the leading edge separation as is clear from 6.1c and 6.1d. In figure 6.2 b turbulence peaks are observed at the same time and place. It is also an onset of asymmetry in the non-stalled results where in general no significant phase lag is observed near leading edge. The burst onset clearly occurs at decreasing angle of attack and it is probable that it would burst completely if the angle of attack was kept above 14 to 15 degrees, which is around the static stall angle. The laminar region in this case extends to about 15% chord distance at the lowest angle of incidence, in this case also the appearance of the high turbulence area near 15% chord was noticed around 9 degree incidence (6.2 b).

At higher angles of attack (6 to 16 and 8 to 18 degrees), a reversed flow region extending to all the measurement stations appears (figures 6.1 c and 6.1 d). This phenomenon appears near the 5% chord immediately after the airfoil crosses 16 degrees incidence. For 6-16 degree oscillation (6.1 c), the reverse flow is not seen upstream of 5% chord at 1.5 mm from the surface (some black isolines are found), but it is clear that nearer to the airfoil the reverse flow region will be found even upstream of 2% chord. The reversed flow region then rapidly spreads in both upstream and downstream directions from 5% chord position. For these two oscillations (6-16 and 8-18), less experimental stations are available. In particular no stations are available between 2 and 5% chord distance from leading edge, and no details are available in this area. From the figures 6.1 a and 6.1 b, it can be assumed that measurements at all the stations shown in appendix 2

should reveal the presence of a bubble around 4% chord, which bursts into leading edge separation. Hence, the leading edge separation is not due to interactions with the trailing edge separation, in contradiction to observations from [9,11]. It can be seen that the slopes of the lines dividing the reverse flow from the forward flow region are positive downstream of 5% chord (6.1c,d). The dividing lines on the left side of the figures downstream of 5% chord is the reattachment line. Therefore, the reattachment point rapidly moves downstream as phase angle increases and cause leading edge separation. Only a negative slope of this line will indicate rapid movement upstream of a downstream separation point, which was not the case.

At 6-16 degrees oscillation the low velocity region near 5% chord never disappeared (6.1 c), at 8-18 degrees oscillation a low velocity region appears at 7% chord at around 17 degrees in the decreasing incidence stroke (6.1 d). As the incidence reduces below 11 degrees the separation point rapidly moves downstream from leading towards trailing edge. The high turbulence areas (>25%) in these two cases appear in the separated region (6.2 d) and during the reattachment (6.2 c, 6.2 d). The portion of the leading edge that remains laminar again becomes largest slightly after the minimum incidence. The laminar portion reduces to 13% chord for 6-16 degrees (6.2 c) and to 10% for 8-18% degrees (6.2 d). The high turbulence (>15%) areas around 15% chord are again evident around 9 degrees incidence.

The figures 6.3 and 6.4 show the results of measurements at various distances from the airfoil surface at 5-15 degrees oscillation. At 1 mm distance (6.3 a) more than 2% of the chord (ahead of 3% up to 5%) shows a reversed flow. At 1.5 mm distance the region appears as a low forward velocity region (6.3 b) but at 2.5 mm only a sharp velocity gradient is observed (6.3 c). When looking at the turbulence intensity plot (6.4) high turbulence intensity (>25%) is more extended at 1.5 mm (6.4 b) than in the rest of the plots. As highest turbulence occurs in the free shear layer above the separation bubble it is reasonable to assume that the maximum thickness of the separation bubble is about 1.5 mm. A high turbulence intensity (>15%) and relatively low velocity (20% of the outer velocity) region is seen at 8 degree incidence near 13% chord for measurements at 1 mm from the surface (6.3 a, 6.4 b). For measurement at 1.5 mm (6.1 b, 6.2 b, 6.3 b and 6.4 b) these high turbulence intensity and low velocity are detected near 15% chord and at 2.5 mm it was not detected up to the distance

of 16% chord.

The highest turbulence intensity encountered at 4-14 degrees and 5-15 degrees incidence cases were 36% of the nominal velocity. If the value of the turvulence intensity is expressed as a fraction of the highest velocity encountered for the particular case, this value reduces to less than 20% and is comparable to the values reviewed in reference [16]. As discussed earlier, the high values observed for the cases with complete flow reversal (more than 45% of the nominal velocity) are partly due to the contribution of cycle to cycle variations at reattachment.

In conclusion it seems that the leading edge stall is triggered by the burst of the leading edge bubble, after which the complete flow pattern is changed. When periodic stall is present, the separation starts not at the leading edge, but at about 4% chord distance from it, with rapid propagation in both directions. The reattachment occurs through a rapid downstream motion of the separation point. In the absence of separation bubble, the location of the area of transition to turbulence varies considerably with incidence. The use of sensors on the surface can indicate the the exact location and the movement of the transition point. The present results are further analysed below, in conjunction with experiments over the whole airfoil.

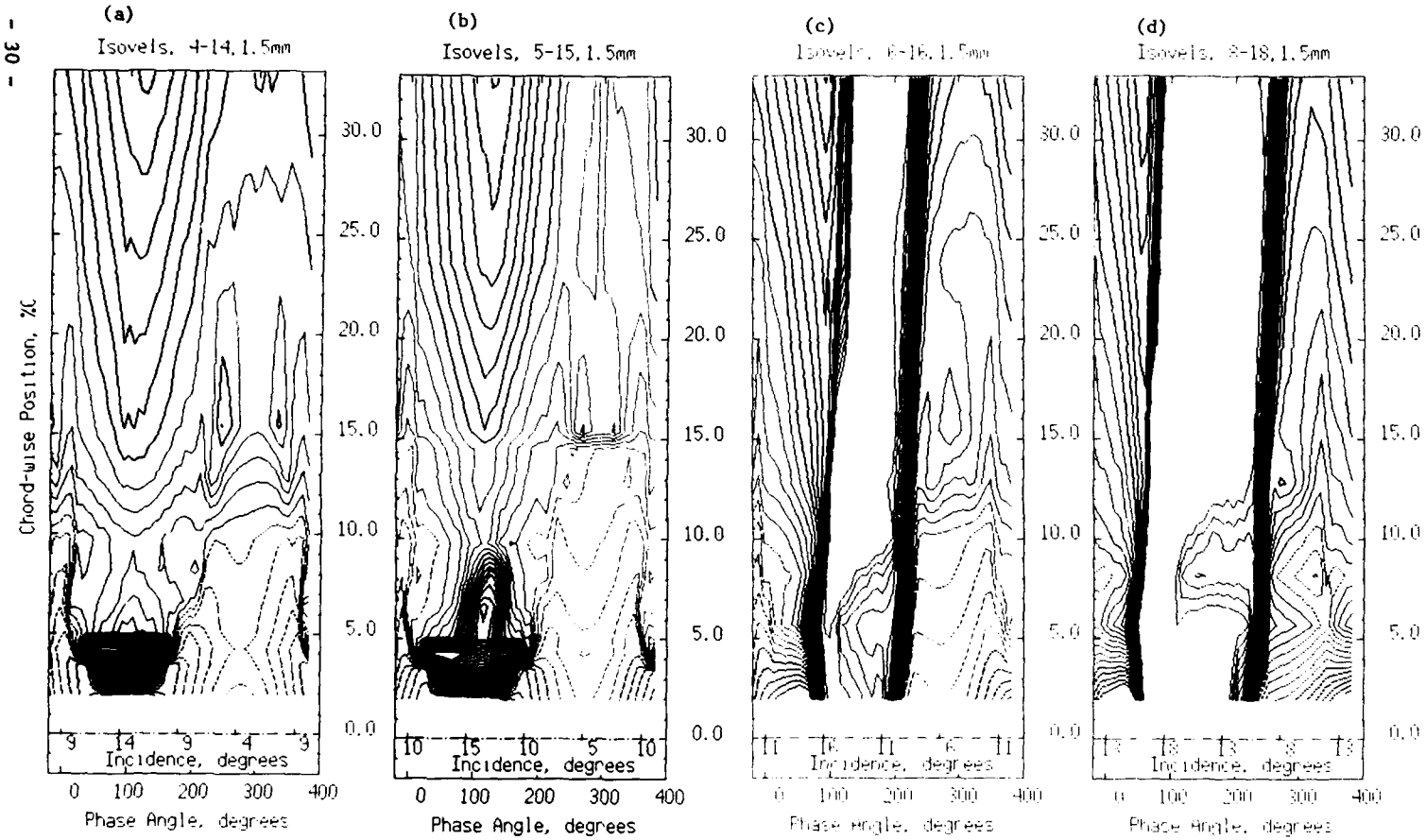

Figure 6.1 : Isovelocity Lines in space-time domain at 1.5 mm distance from the wall, at incidences of 4-14, 5-15, 6-16 and 8-18°.
Color code: black 0-.29 ; navy blue .3-.59; blue .6-.88; red .89-1.17; orange 1.18-1.46; green 1.47-1.76; yellow 1.77-2.05

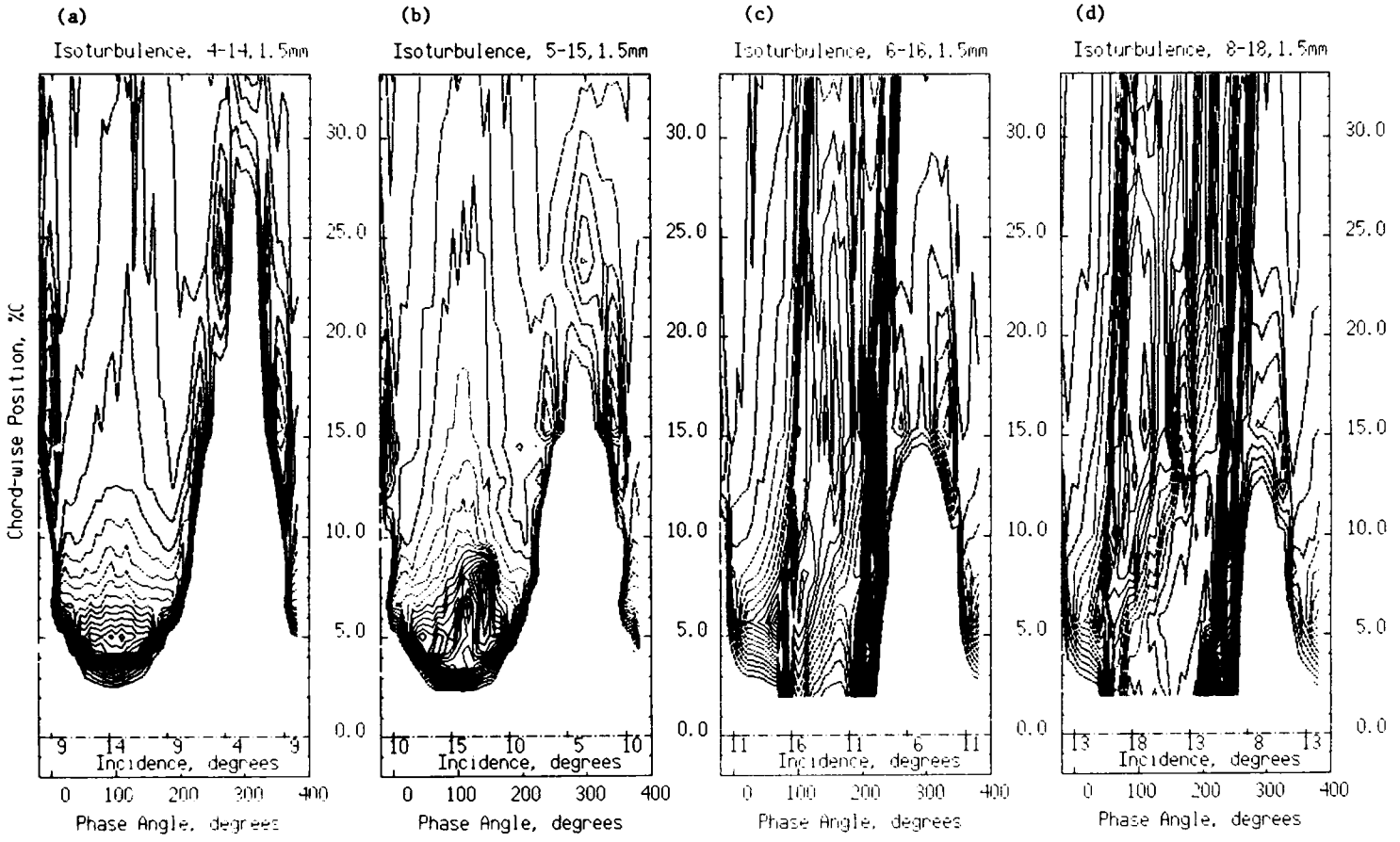

Figure 6.2 : Isoturbulence Lines in space-time domain at 1.5 mm distance from the wall, at incidences of 4-14, 5-15, 6-16 and 8-18°.
Color code: yellow .01-.07; green .08-.14 ; orange .15-.21;
red .22-.28; blue .29-.35 ; navy blue .36-.42; black .43-.49

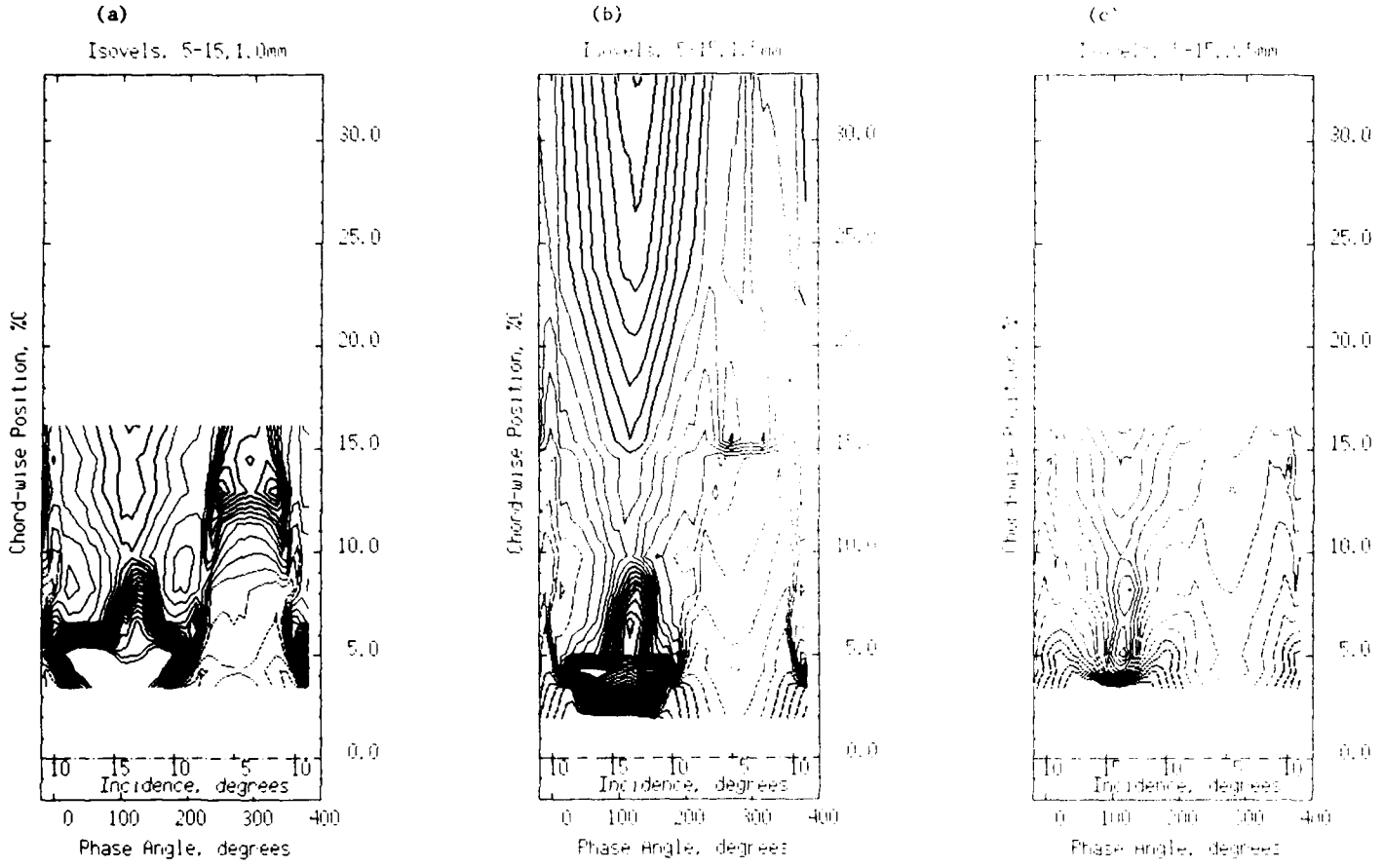

Figure 6.3 : Isovelocity Lines in space-time domain for Various Transverse Positions for 5-15 degrees Incidence
Color code: black 0-.29 ; navy blue .3-.59; blue .6-.88; red .89-1.17; orange 1.18-1.46; green 1.47-1.76; yellow 1.77-2.05

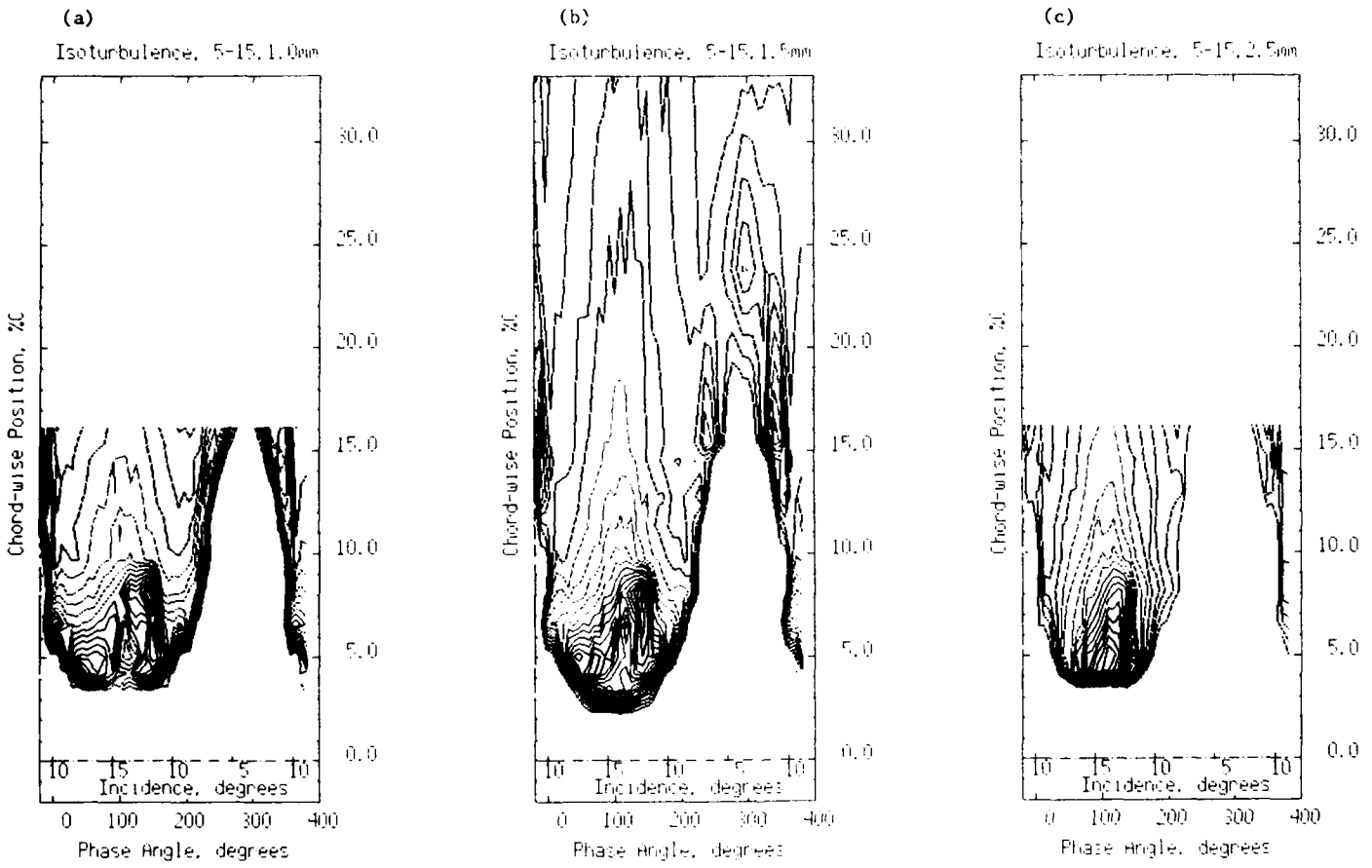

Figure 6.4 : Isoturbulence Lines in space time domain for Various Transverse Positions for 5-15 degrees Incidence
Color code: yellow .01-.07; green .08-.14 ; orange .15-.21; red .22-.28; blue .29-.35 ; navy blue .36-.42; black .43-.49

6.2 Boundary Layer Experiments

The test case 5 to 15 degrees has been selected for a deeper analysis, since it is the limit before deep separation. Measurements have been made with the rotating hot wire at 23 stations from leading edge to near wake. These stations are listed in appendix 3. The minimum distance from the wall is 2 mm, which is outside of the bubble. Overall results and results obtained near leading edge are shown in the figures 6.5 to 6.17. This series contains some relevant time steps amongst the 181 available ones. In all these figures (6.5 to 6.20) the overall velocity field is shown in (a), chordwise turbulence intensity is shown in (b) and Reynolds shear stress is shown in (c), with two stations deleted near leading edge and two stations deleted near the trailing edge, for more clarity. In conjunction, the velocities and turbulence intensities obtained with the fixed wire are shown in (d) and (e) respectively. The figures (f) and (g) show the corresponding chordwise turbulence intensity and Reynolds shear stresses respectively at all the stations near the leading edge.

The series of figures starts at increasing angle of attack (6.5), when the transition is found around 13% chord from leading edge (6.5 d, f). As the angle of attack increases (6.6 and 6.7), a low speed area can be observed close to the wall near 12% chord from the leading edge from fixed wire measurements (6.6 e and 6.7 e). A high turbulence level in the shear layer above this low velocity region is observed (6.6 and 6.7). The decrease in velocity in the inner layer could not be reached by the rotating wire. There may be a bubble close to the wall, as discussed in section 6.1. The maximum values of turbulence intensity and shear stress in figures 6.6 and 6.7 appear near the leading edge rather than in the wake, which was opposite at lower incidence (6.5). Downstream of 25% chord the boundary layer recovers rapidly. The low speed area disappears and another one appears around 5% chord at 9 degrees angle of attack (6.8). At 10 degrees (6.9) this low speed area is increasing, with a very thin but highly turbulent shear layer above it. Unfortunately the rotating wire reaches only the outer part of this layer and only a small portion of the corresponding stress is observed. The increasing incidence makes the separation bubble thicker and it was possible to detect the turbulent quantities by the rotating wire in more of the upstream stations. At 9 degrees incidence (6.8) the fixed wire measurement shows 10% turbulence near 7% chord, the rotating wire measurement also shows an increase in turbulence intensity and Reynolds shear at the station near 8% chordwise position.

This upstream movement of the transition point near the leading edge (d, f and g) is evident in all the figures starting from 6.5 to 6.15, after which the transition point gradually moves downstream. At 10 degrees incidence (6.9) small values of Reynolds shear stress are measured at 5.7% chord position. Around the same incidence the fixed wire at 1 mm from the surface at 4% chord shows the presence of the leading edge separation bubble (6.3 a). Therefore, the rotating wire is measuring the turbulence quantities in the free shear layer when it is just becoming turbulent. Rapid increase in Reynolds shear stress as well as chordwise turbulence intensity with the increasing incidence at 5.7% chord could be observed till maximum incidence time (6.9 to 6.14). The Reynolds shear stress at the stations downstream of 10% chord for the same figures does not increase considerably. However, growth of the turbulent layer is evident in all the stations downstream of 5% chord. This growth can be attributed to the large coherent structures present at the reattachment of the separation bubble. The large values of Reynolds shear stress are the effect of the large velocity gradients in the free shear layer over the separation bubble.

When the incidence decreases from the maximum value of 15 degrees a tendency towards bubble burst was observed (figure 6.3). In the corresponding figure (figure 6.15, between 5% to 10% chord) the rotating wire detects a decrease of allthe turbulent quantities towards the wall. This region roughly coincides with the elongated dark portion in figure 6.3 b. The Reynolds shear stress measured at 5.7% chord nearest to the surface (2 mm) even shows a negative value as in figure 6.15 g (note that the values plotted are minus the Reynolds stresses). The situation at this point is very close to separation (bubble bursting). The negative Reynolds stresses observed from the rotating wire data, indicate a negative turbulence production : although the reliability of this result is poor in such extreme situations, it is systematically observed at separation in the earlier experiments of De Ruyck and Hirsch [5,6] and it may be an indication of stall onset. At this time it can be seen that the trailing edge flow is separated up to about 80% chord, which is too far to cause the leading edge bubble to burst, hence the leading edge stall onset is not affected by trailing edge separation in this particular case.

Further decrease in incidence below 13 degrees reduces this tendency of bubble bursting and typical transition behaviour is again observed (figures 6.16 to 6.20). Apart from slight phase lag, the reducing angle of incidence brings about the same series of events in the reverse of what was seen during the increasing incidence. The turbulent boundary layer becomes

thinner, the turbulent quantities gradually reduce in value and become zero station after station starting with 5.7% chord station. At the lowest incidence (5 degrees) the turbulent transition can be seen only at stations downstream of 15% chord.

For comparison, the results just presented can be compared with similar data from De Ruyck and Hirsch [5,6] (figures 6.21 and 6.22). The results reproduced were obtained from the same airfoil, but with a tripping wire and without end-plates. During these experiments it was observed that in case of deep stall (from 7 to 17 degrees, not shown) the leading edge separation grows and separates. At angles of attack just below the dynamic stall limit, this leading edge vortex may be present, but it disappears after some time.

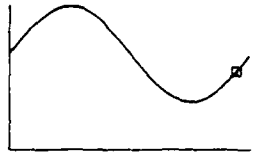

i= 8.14 degr. f=338.12 degr.

(a)

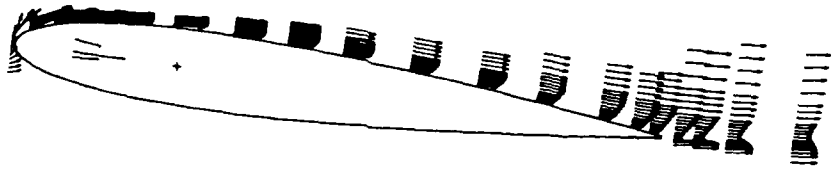

(b)

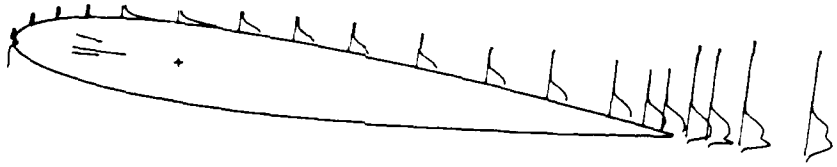

(c)

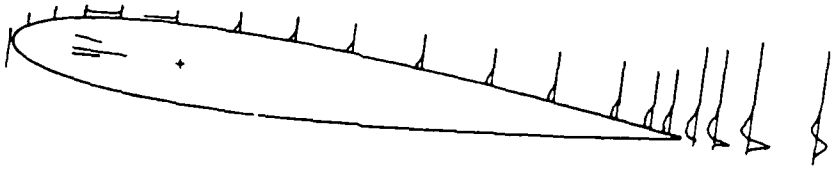

Figure 6.5 : 5° to 15° incidence, k = 0.3

(a) velocity vectors scale : — Q

(b) chordwise fluctuations $\sqrt{u'^2}/Q$ scale : — 10% Q

(c) - Reynolds stress $\overline{u'v'}/Q^2$ scale : — 1% Q^2

i= 7.36 degr. f=328.18 degr.

(d)

(e)

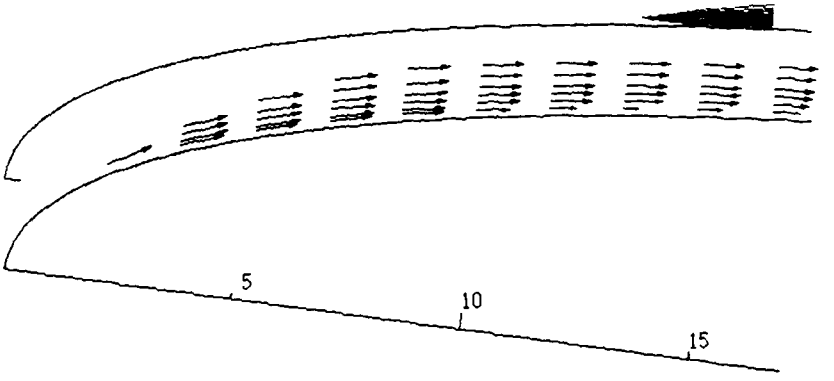

(f)

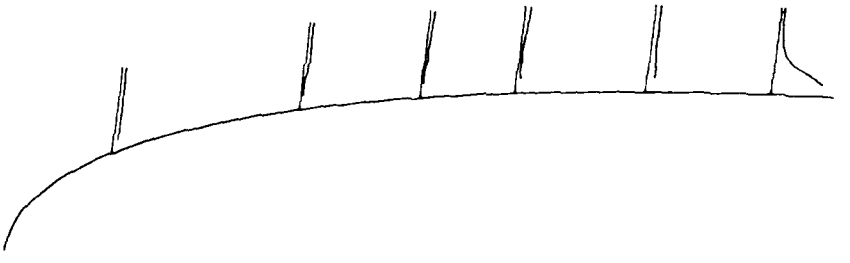

(g)

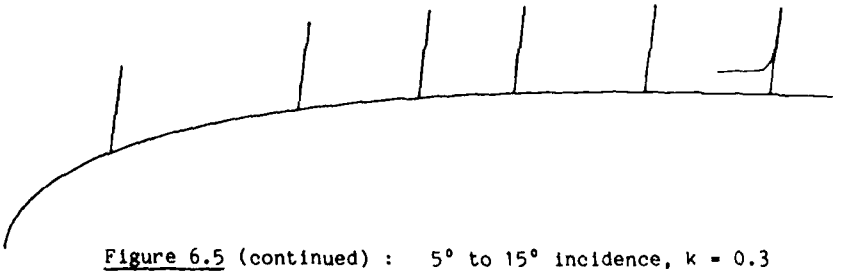

Figure 6.5 (continued) : 5° to 15° incidence, k = 0.3

(d) isoturbulence

(f) chordwise fluctuations $\sqrt{u'^2}/Q$ scale : —— 10% Q

(g) - Reynolds stress $\overline{u'v'}/Q^2$ scale : —— 1% Q^2

i= 7.36 degr. f=328.18 degr.

(a)

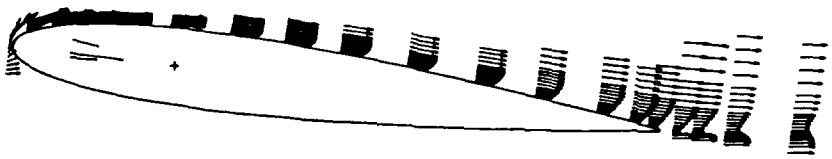

(b)

(c)

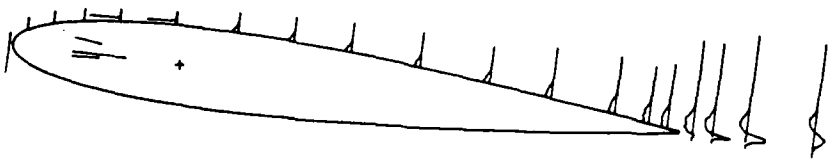

Figure 6.6 : 5° to 15° incidence, k = 0.3

(a) velocity vectors scale : — Q

(b) chordwise fluctuations $\sqrt{u'^2}/Q$ scale : — 10% Q

(c) - Reynolds stress $\overline{u'v'}/Q^2$ scale : — 1% Q^2

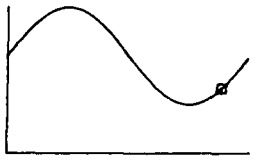

i= 6.67 degr. f=318.23 degr.

(d)

(e)

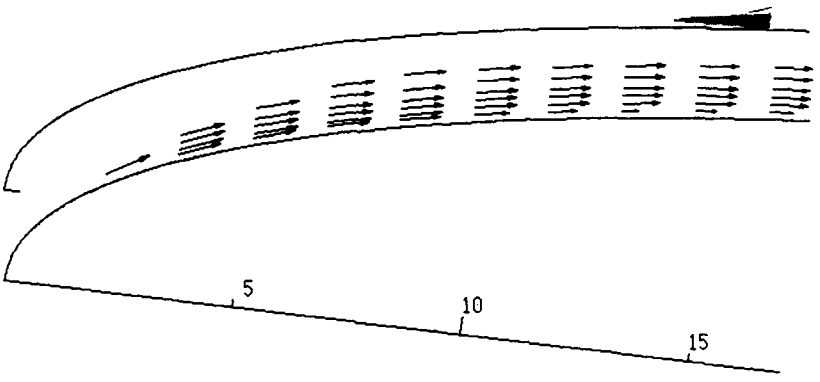

(f)

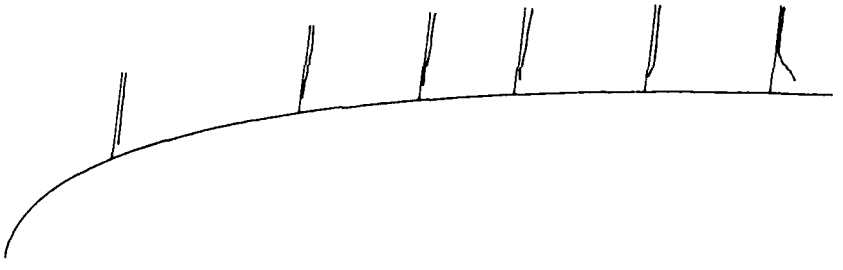

(g)

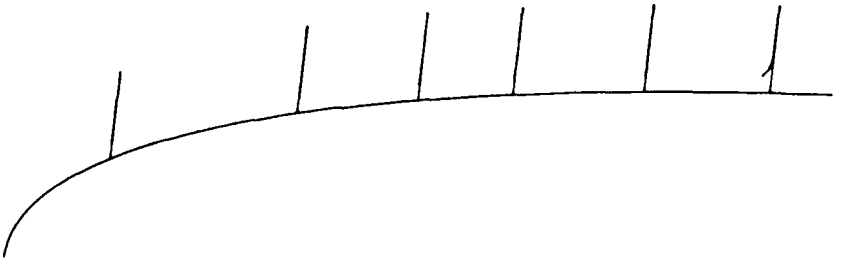

Figure 6.6 (continued) : 5° to 15° incidence, k = 0.3

(d) isoturbulence

(f) chordwise fluctuations $\sqrt{u'^2}/Q$ scale : —— 10% Q

(g) - Reynolds stress $\overline{u'v'}/Q^2$ scale : —— 1% Q^2

i= 6.67 degr. f=318.23 degr.

(a)

(b)

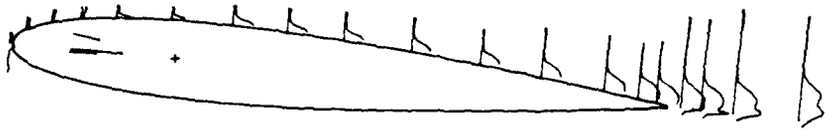

(c)

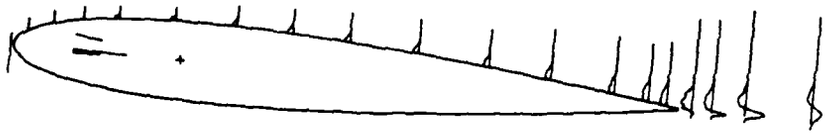

Figure 6.7 : 5° to 15° incidence, k = 0.3

(a) velocity vectors scale : — Q

(b) chordwise fluctuations $\sqrt{u'^2}/Q$ scale : — 10% Q

(c) - Reynolds stress $\overline{u'v'}/Q^2$ scale : — 1% Q^2

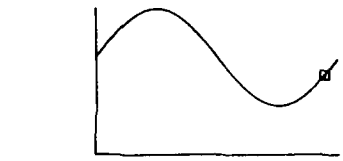

i= 8.14 degr. f=338.12 degr.

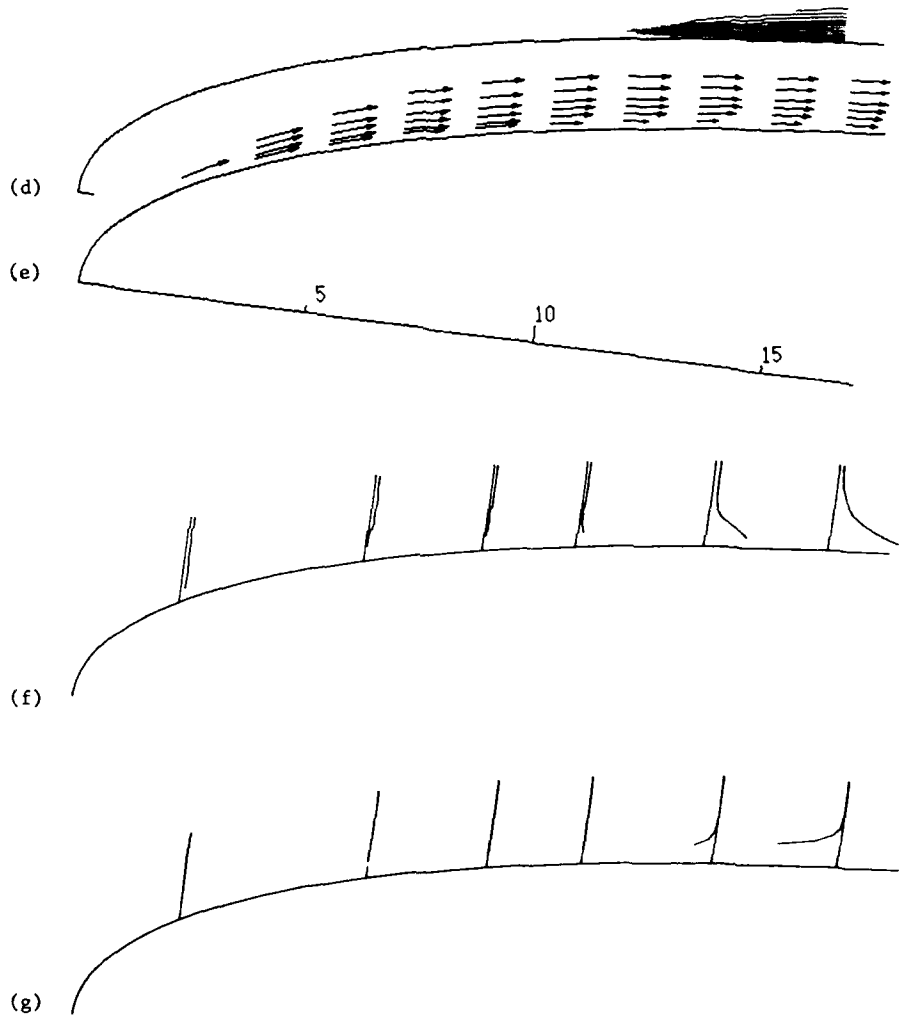

Figure 6.7 (continued) : 5° to 15° incidence, k = 0.3

(d) isoturbulence

(f) chordwise fluctuations $\sqrt{\overline{u'^2}}/Q$ scale : —— 10% Q

(g) - Reynolds stress $\overline{u'v'}/Q^2$ scale : —— 1% Q^2

i= 8.97 degr. f=348.07 degr.

(a)

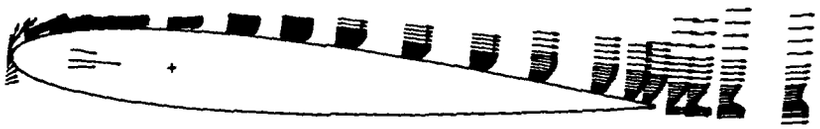

(b)

(c)

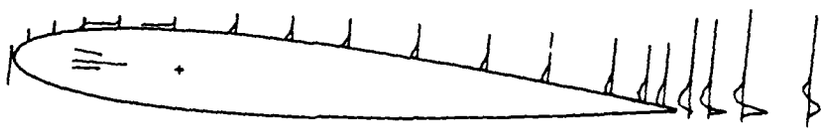

Figure 6.8 : 5° to 15° incidence, k = 0.3

(a) velocity vectors scale : — Q

(b) chordwise fluctuations $\sqrt{u'^2}/Q$ scale : — 10% Q

(c) - Reynolds stress $\overline{u'v'}/Q^2$ scale : — 1% Q^2

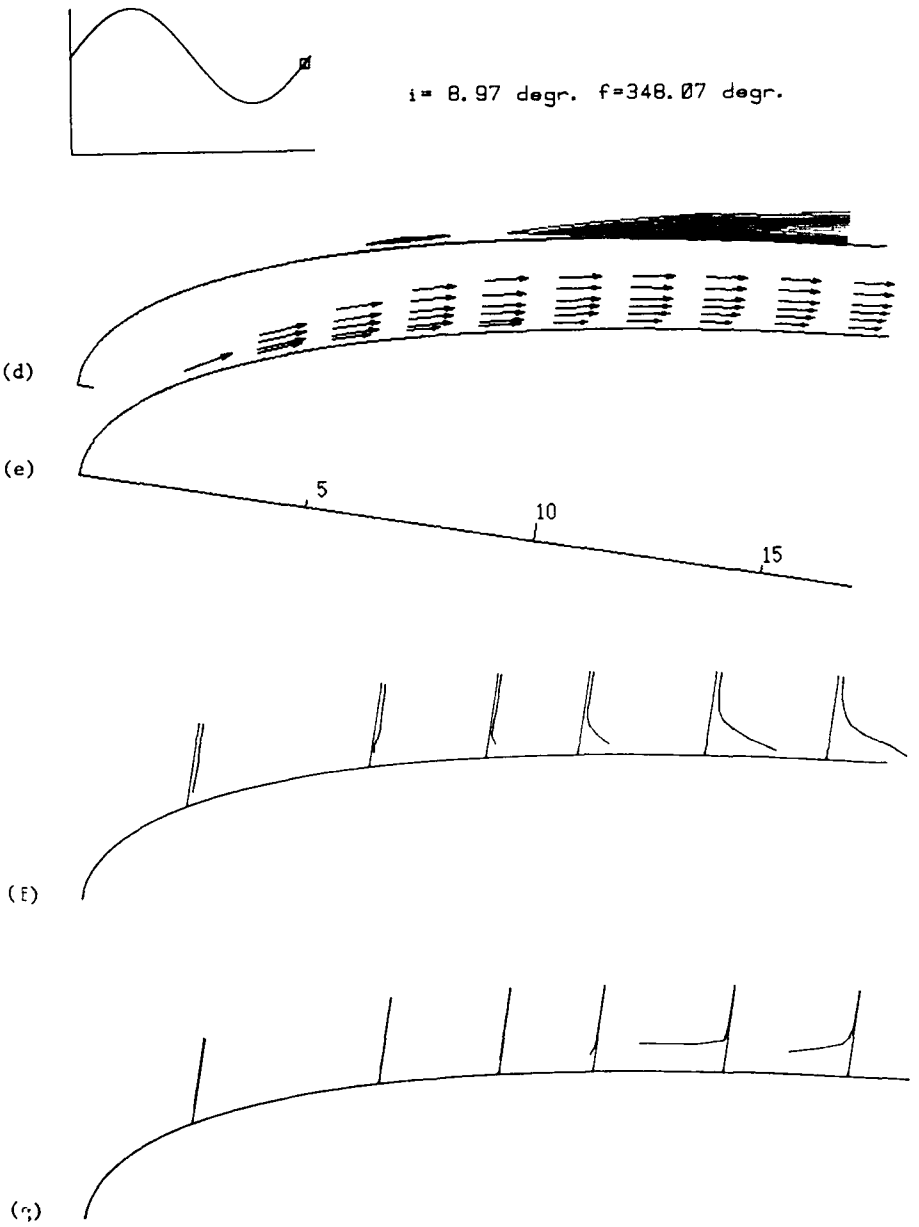

Figure 6.8 (continued) : 5° to 15° incidence, k = 0.3

(d) isoturbulence

(f) chordwise fluctuations $\sqrt{u'^2}/Q$ scale : —— 10% Q

(g) - Reynolds stress $\overline{u'v'}/Q^2$ scale : —— 1% Q^2

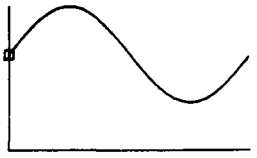

i=10.00 degr. f= 0.00 degr.

(a)

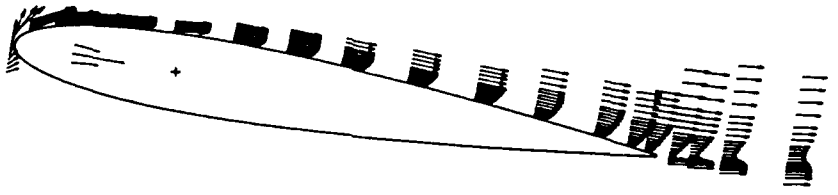

(b)

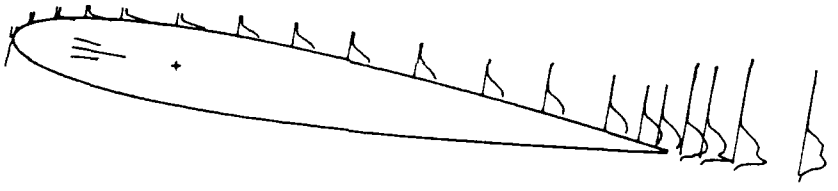

(c)

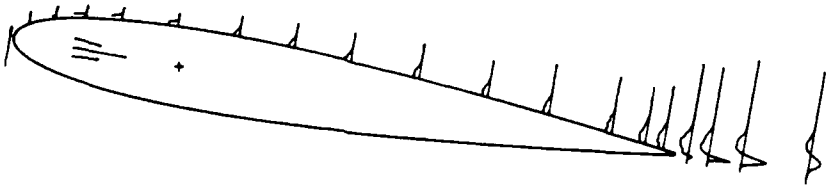

Figure 6.9 : 5° to 15° incidence, k = 0.3

(a) velocity vectors scale : — Q

(b) chordwise fluctuations $\sqrt{u'^2}/Q$ scale : — 10% Q

(c) - Reynolds stress $\overline{u'v'}/Q^2$ scale : — 1% Q^2

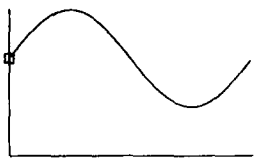

i=10.00 degr. f= 0.00 degr.

(d)

(e)

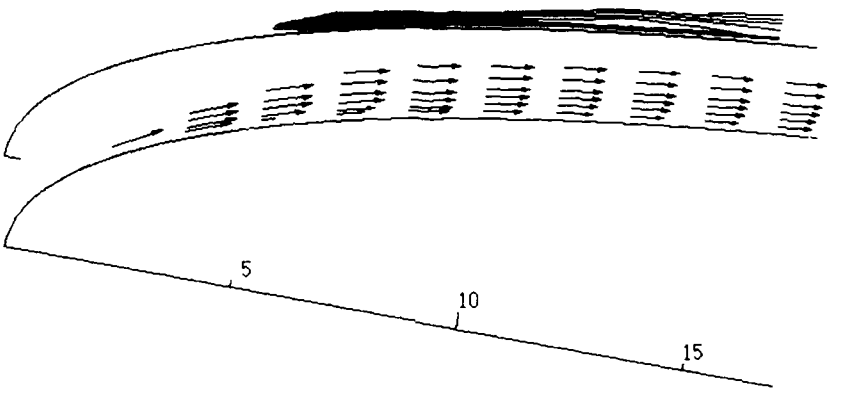

(f)

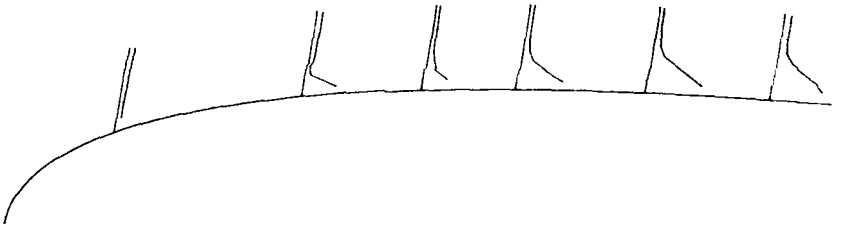

(g)

Figure 6.9 (continued) : 5° to 15° incidence, k = 0.3

(d) isoturbulence

(f) chordwise fluctuations $\sqrt{u'^2}/Q$ scale : —— 10% Q

(g) - Reynolds stress $\overline{u'v'}/Q^2$ scale : —— 1% Q^2

i=10.86 degr. f= 9.94 degr.

(a)

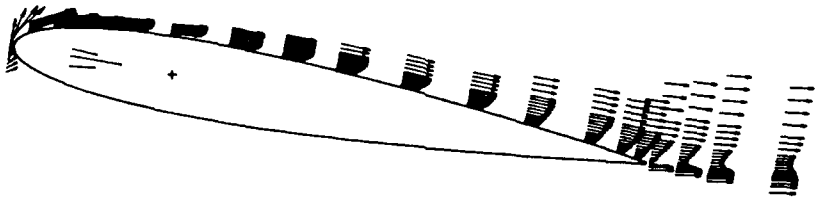

(b)

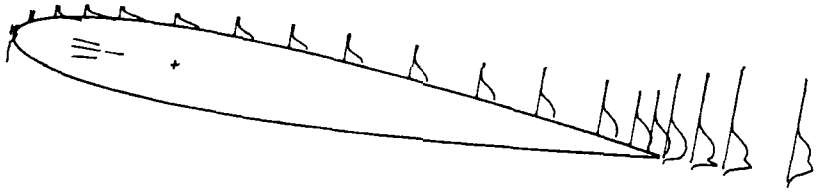

(c)

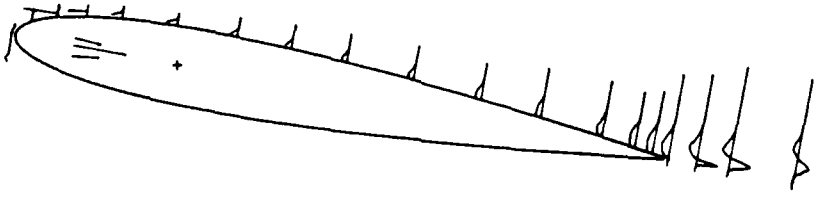

Figure 6.10 : 5° to 15° incidence, k = 0.3

(a) velocity vectors scale : — Q

(b) chordwise fluctuations $\sqrt{u'^2}/Q$ scale : — 10% Q

(c) - Reynolds stress $\overline{u'v'}/Q^2$ scale : — 1% Q^2

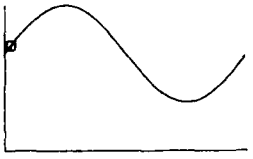

i=10.86 degr. f= 9.94 degr.

(d)

(e)

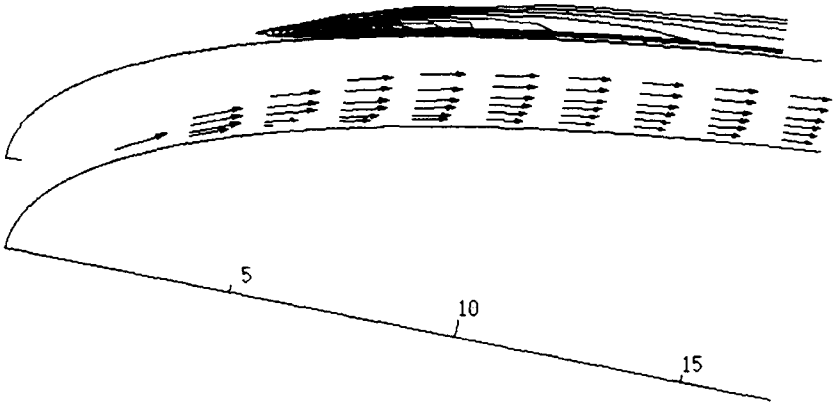

(f)

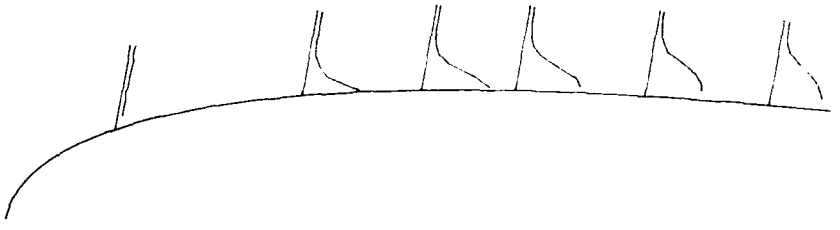

(g)

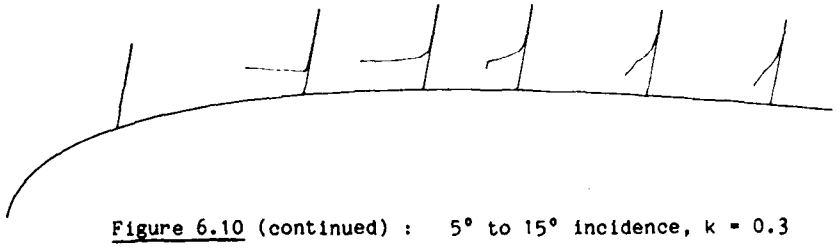

Figure 6.10 (continued) : 5° to 15° incidence, k = 0.3

(d) isoturbulence

(f) chordwise fluctuations $\sqrt{u'^2}/Q$ scale : —— 10% Q

(g) - Reynolds stress $\overline{u'v'}/Q^2$ scale : —— 1% Q^2

i=11.70 degr. f= 19.89 degr.

(a)

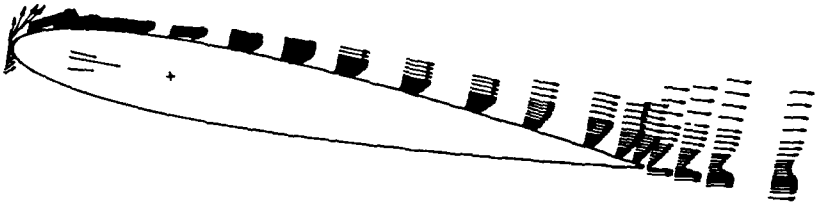

(b)

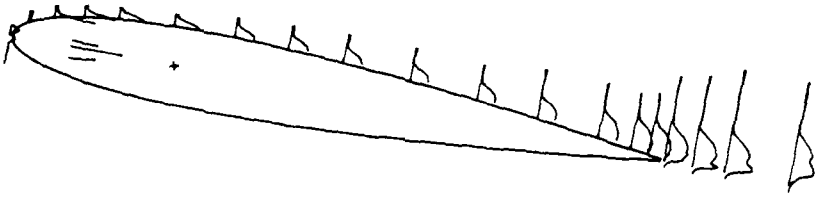

(c)

Figure 6.11 : 5° to 15° incidence, k = 0.3

(a) velocity vectors scale : — Q

(b) chordwise fluctuations $\sqrt{u'^2}/Q$ scale : — 10% Q

(c) - Reynolds stress $\overline{u'v'}/Q^2$ scale : — 1% Q^2

i=11.70 degr. f= 19.89 degr.

(d)

(e)

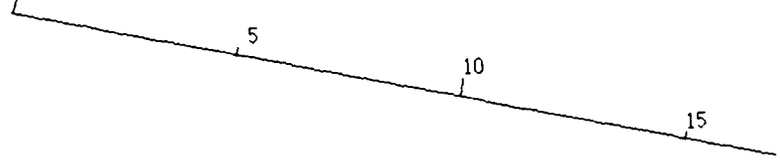

(f)

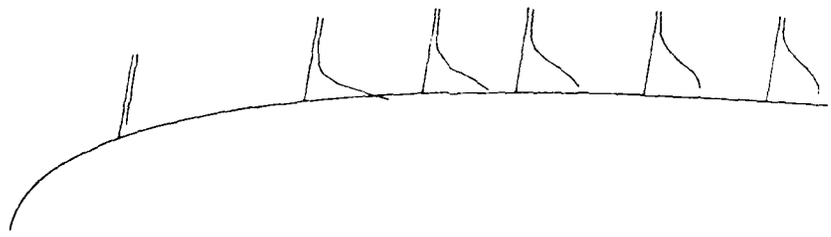

(g)

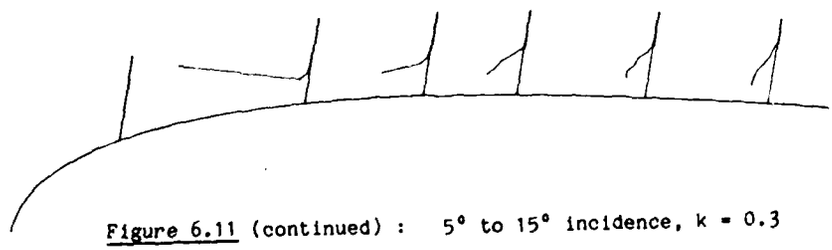

Figure 6.11 (continued) : 5° to 15° incidence, k = 0.3

(d) isoturbulence

(f) chordwise fluctuations $\sqrt{u'^2}/Q$ scale : —— 10% Q

(g) - Reynolds stress $\overline{u'v'}/Q^2$ scale : —— 1% Q^2

i=13.20 degr. f= 39.78 degr.

(a)

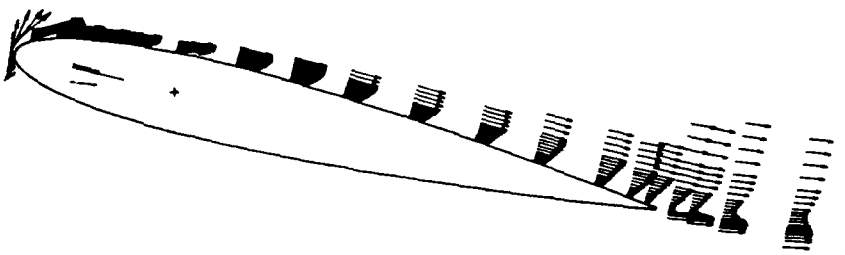

(b)

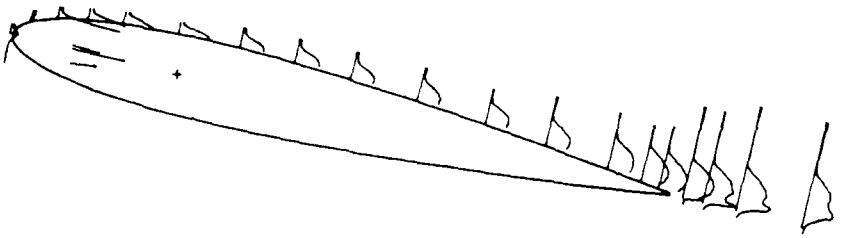

(c)

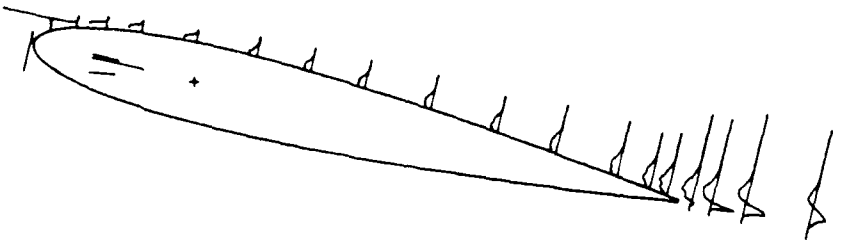

Figure 6.12 : 5° to 15° incidence, k = 0.3

(a) velocity vectors scale : — Q

(b) chordwise fluctuations $\sqrt{u'^2}/Q$ scale : — 10% Q

(c) - Reynolds stress $\overline{u'v'}/Q^2$ scale : — 1% Q^2

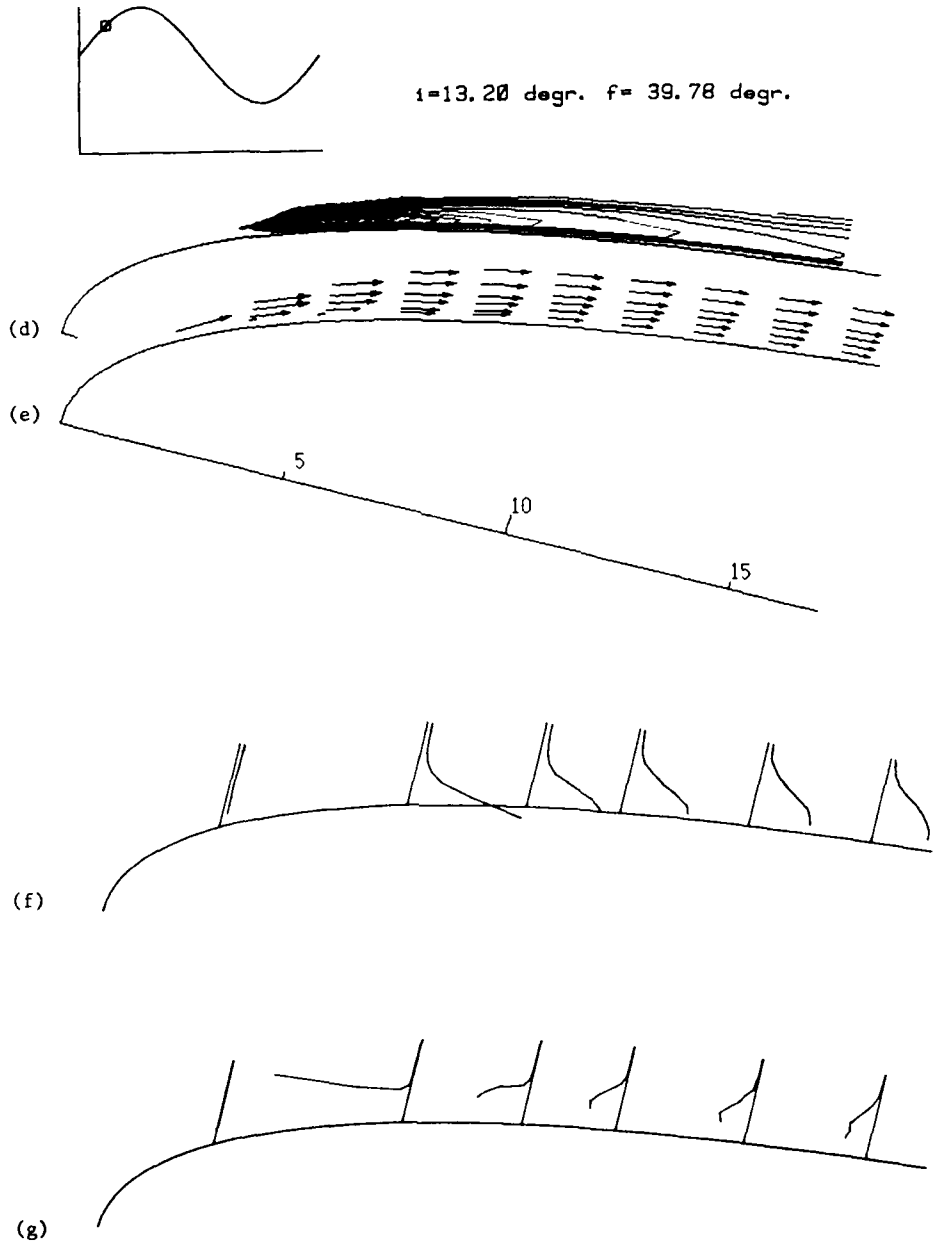

Figure 6.12 (continued) : 5° to 15° incidence, k = 0.3

(d) isoturbulence

(f) chordwise fluctuations $\sqrt{u'^2}/Q$ scale : —— 10% Q

(g) - Reynolds stress $\overline{u'v'}/Q^2$ scale : —— 1% Q^2

i=14.32 degr. f= 59.67 degr.

(a)

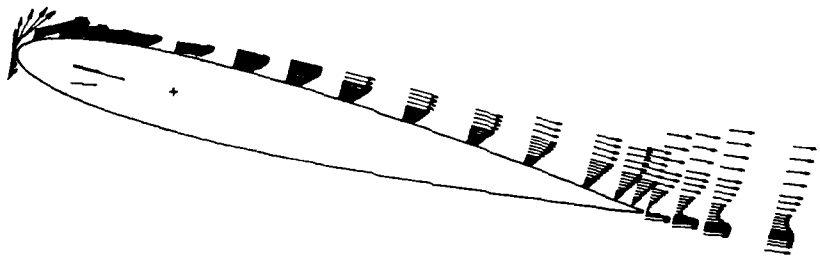

(b)

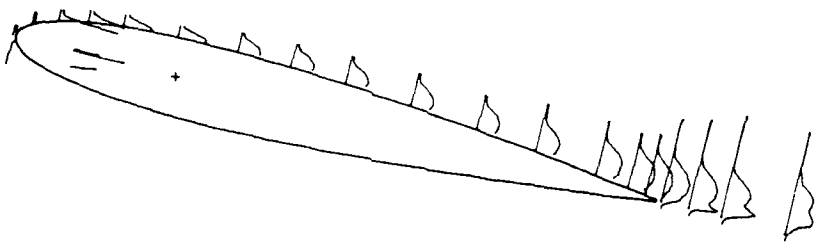

(c)

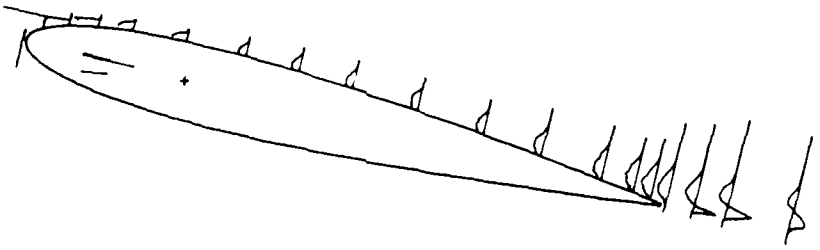

Figure 6.13 : 5° to 15° incidence, k = 0.3

(a) velocity vectors scale : — Q

(b) chordwise fluctuations $\sqrt{u'^2}/Q$ scale : — 10% Q

(c) - Reynolds stress $\overline{u'v'}/Q^2$ scale : — 1% Q^2

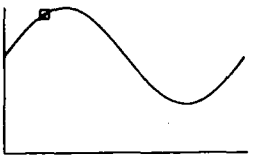

i=14.32 degr. f= 59.67 degr.

(d)

(e)

5

10

15

(f)

(g)

Figure 6.13 (continued) : 5° to 15° incidence, k = 0.3

(d) isoturbulence

(f) chordwise fluctuations $\sqrt{u'^2}/Q$ scale : —— 10% Q

(g) - Reynolds stress $\overline{u'v'}/Q^2$ scale : —— 1% Q^2

i=15.00 degr. f= 89.50 degr.

(a)

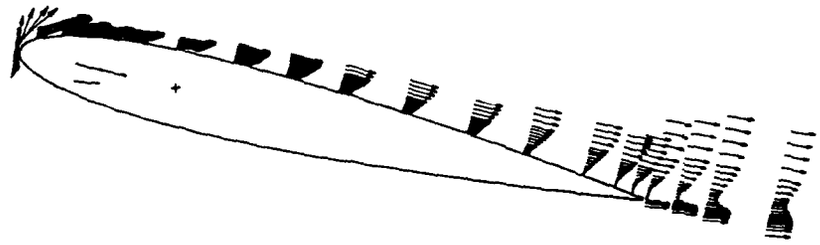

(b)

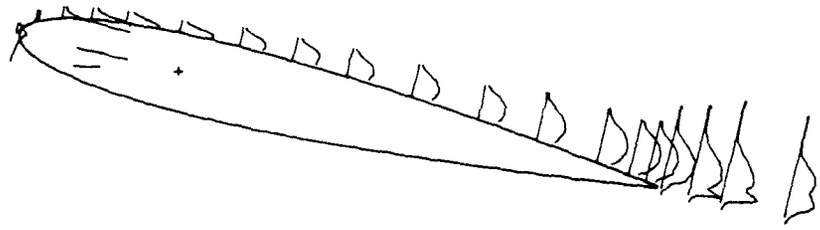

(c)

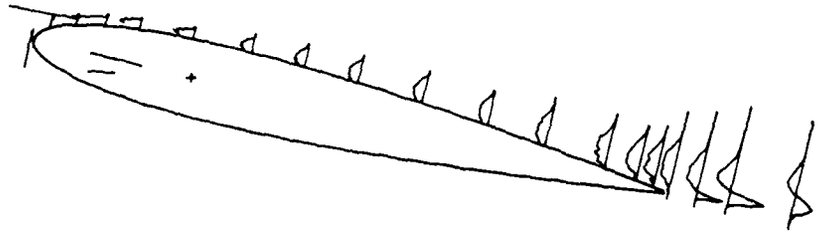

Figure 6.14 : 5° to 15° incidence, k = 0.3

(a) velocity vectors scale : — Q

(b) chordwise fluctuations $\sqrt{u'^2}/Q$ scale : — 10% Q

(c) - Reynolds stress $\overline{u'v'}/Q^2$ scale : — 1% Q^2

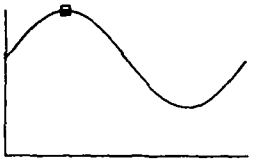

i=15.00 degr. f= 89.50 degr.

(d)

(e)

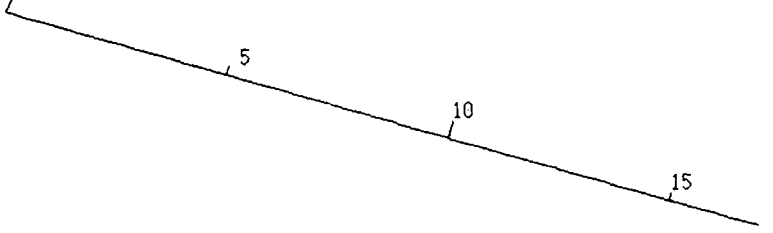

(f)

(g)

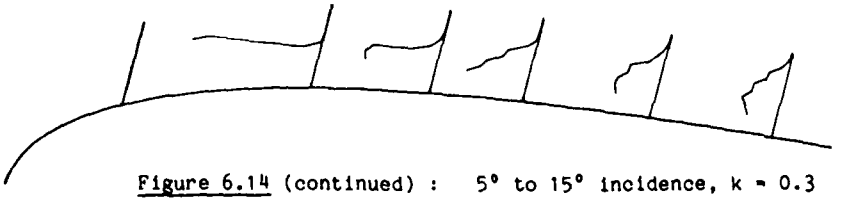

Figure 6.14 (continued) : 5° to 15° incidence, k = 0.3

(d) isoturbulence

(f) chordwise fluctuations $\sqrt{u'^2}/Q$ scale : —— 10% Q

(g) - Reynolds stress $\overline{u'v'}/Q^2$ scale : —— 1% Q^2

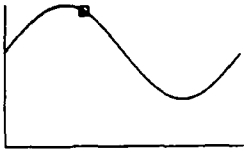

i=14.36 degr. f=119.34 degr.

(a)

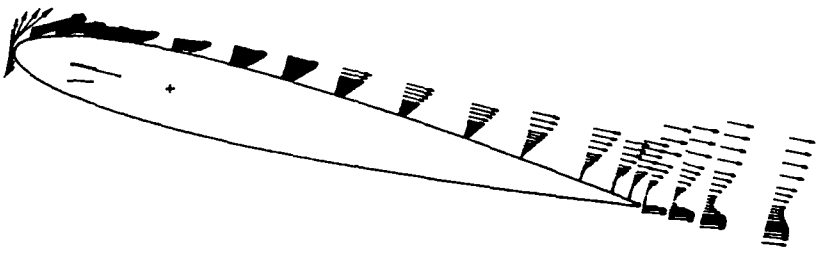

(b)

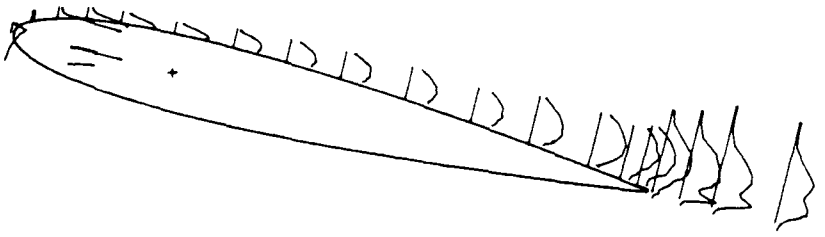

(c)

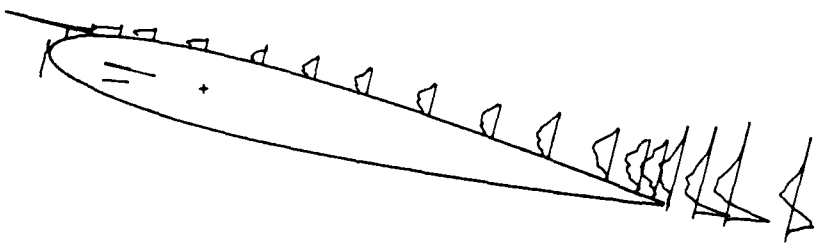

Figure 6.15 : 5° to 15° incidence, k = 0.3

(a) velocity vectors scale : — Q

(b) chordwise fluctuations $\sqrt{u'^2}/Q$ scale : — 10% Q

(c) - Reynolds stress $\overline{u'v'}/Q^2$ scale : — 1% Q^2

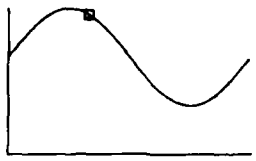

i=14.36 degr. f=119.34 degr.

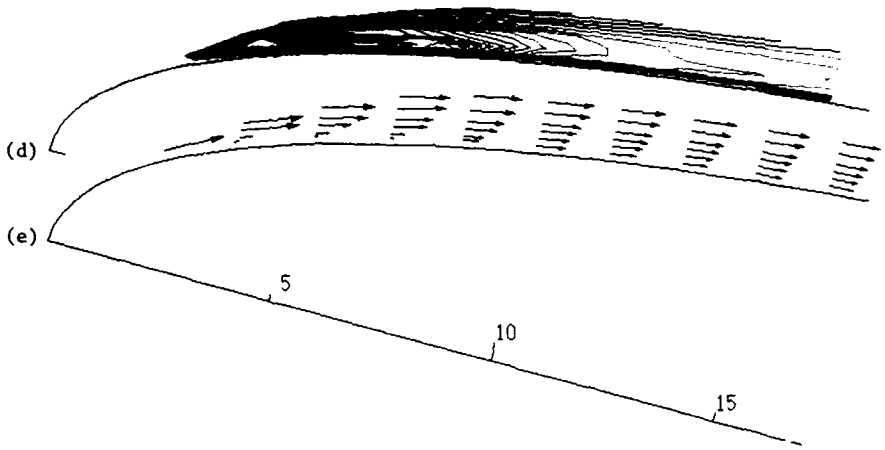

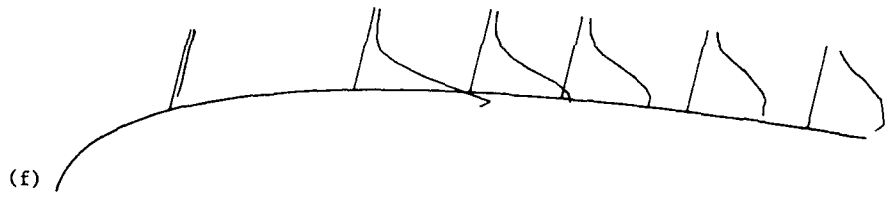

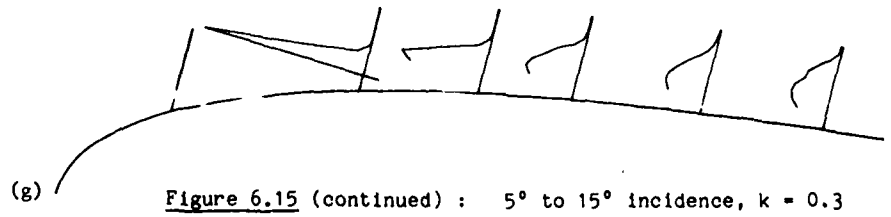

Figure 6.15 (continued) : 5° to 15° incidence, k = 0.3

(d) isoturbulence

(f) chordwise fluctuations $\sqrt{\overline{u'^2}}/Q$ scale : —— 10% Q

(g) - Reynolds stress $\overline{u'v'}/Q^2$ scale : —— 1% Q^2

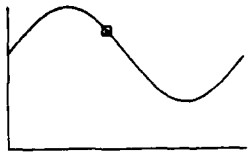

i=12.56 degr. f=149.17 degr.

(a)

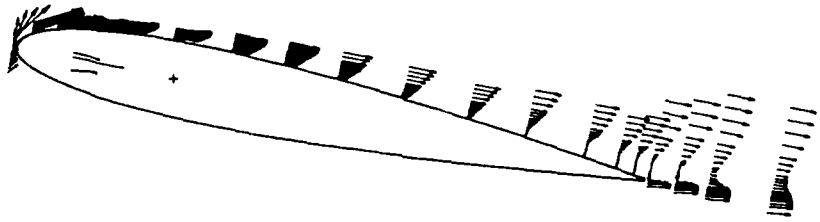

(b)

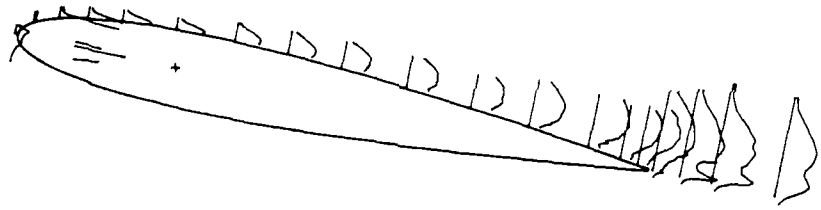

(c)

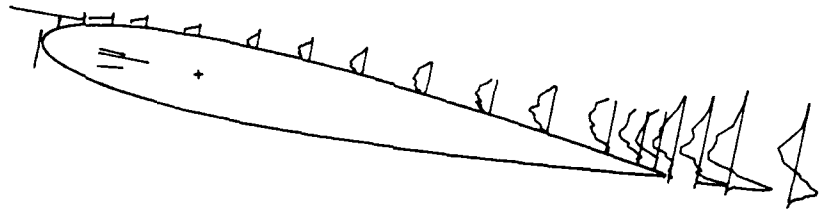

Figure 6.16 : 5° to 15° incidence, k = 0.3

(a) velocity vectors scale : — Q

(b) chordwise fluctuations $\sqrt{u'^2}/Q$ scale : — 10% Q

(c) - Reynolds stress $\overline{u'v'}/Q^2$ scale : — 1% Q^2

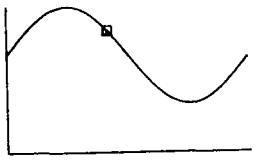

i=12.56 degr. f=149.17 degr.

(d)

(e)

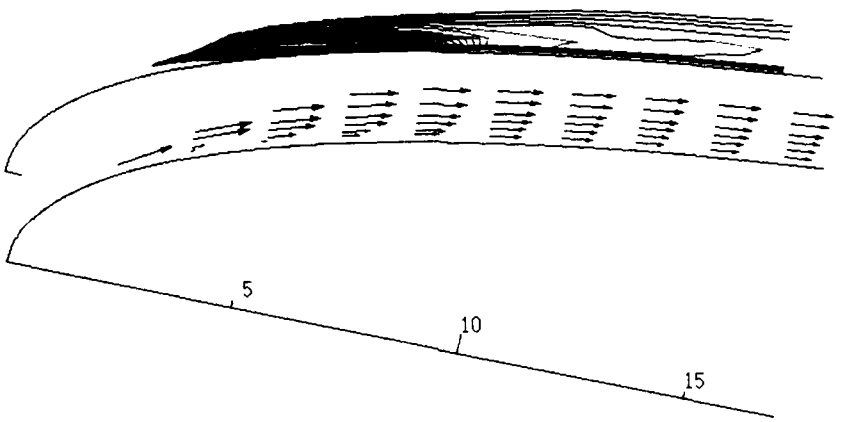

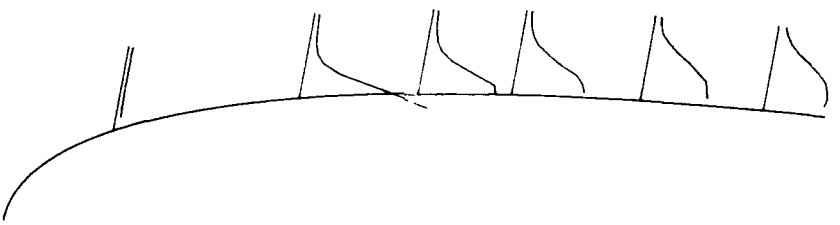

(f)

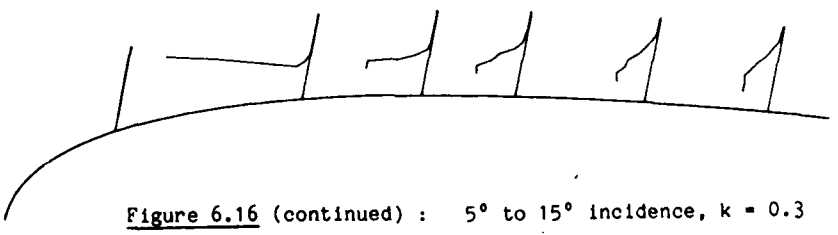

(g)

Figure 6.16 (continued) : 5° to 15° incidence, k = 0.3

(d) isoturbulence

(f) chordwise fluctuations $\sqrt{\overline{u'^2}}/Q$ scale : —— 10% Q

(g) - Reynolds stress $\overline{u'v'}/Q^2$ scale : —— 1% Q^2

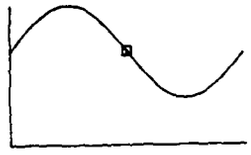

i=10.09 degr. f=179.01 degr.

(a)

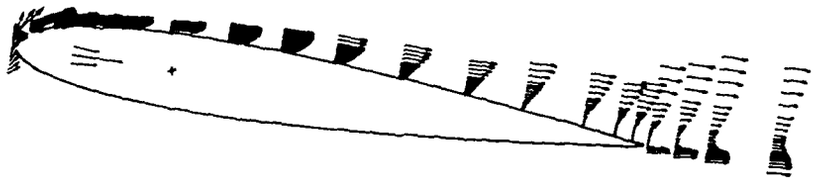

(b)

(c)

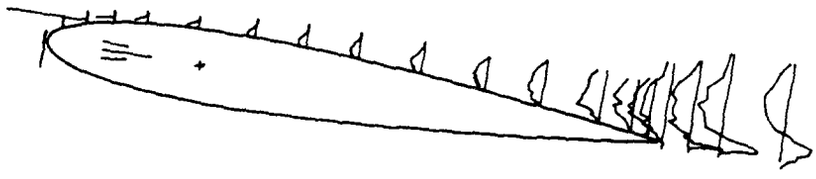

Figure 6.17 : 5° to 15° incidence, k = 0.3

(a) velocity vectors scale : — Q

(b) chordwise fluctuations $\sqrt{u'^2}/Q$ scale : — 10% Q

(c) - Reynolds stress $\overline{u'v'}/Q^2$ scale : — 1% Q^2

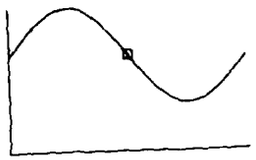

i=10.09 degr. f=179.01 degr.

(d)

(e)

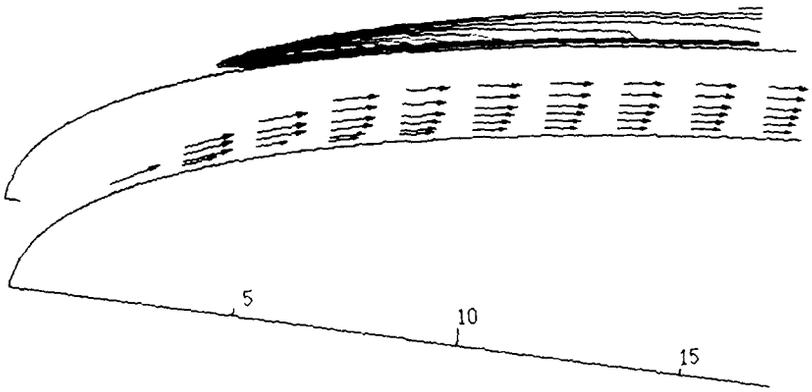

(f)

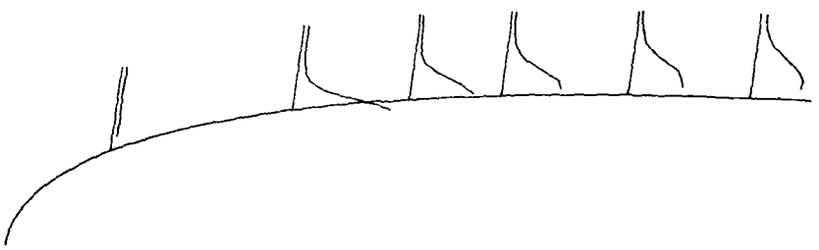

(g)

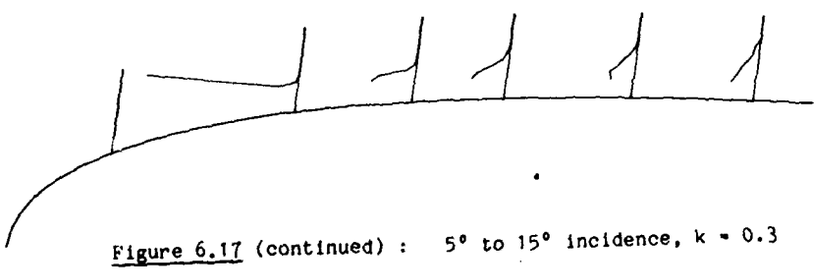

Figure 6.17 (continued) : 5° to 15° incidence, k = 0.3

(d) isoturbulence

(f) chordwise fluctuations $\sqrt{u'^2}/Q$ scale : —— 10% Q

(g) - Reynolds stress $\overline{u'v'}/Q^2$ scale : —— 1% Q^2

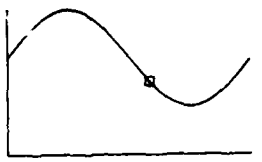

i= 7.59 degr. f=208.84 degr.

(a)

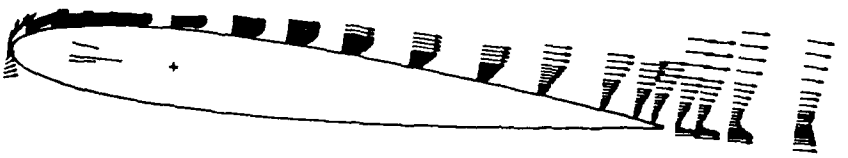

(b)

(c)

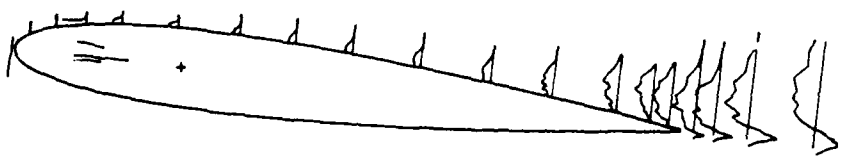

Figure 6.18 : 5° to 15° incidence, k = 0.3

(a) velocity vectors scale : — Q

(b) chordwise fluctuations $\sqrt{u'^2}/Q$ scale : — 10% Q

(c) - Reynolds stress $\overline{u'v'}/Q^2$ scale : — 1% Q^2

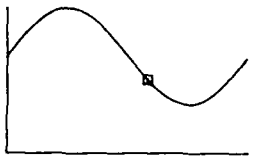

i= 7.59 degr. f=208.84 degr.

(d)

(e)

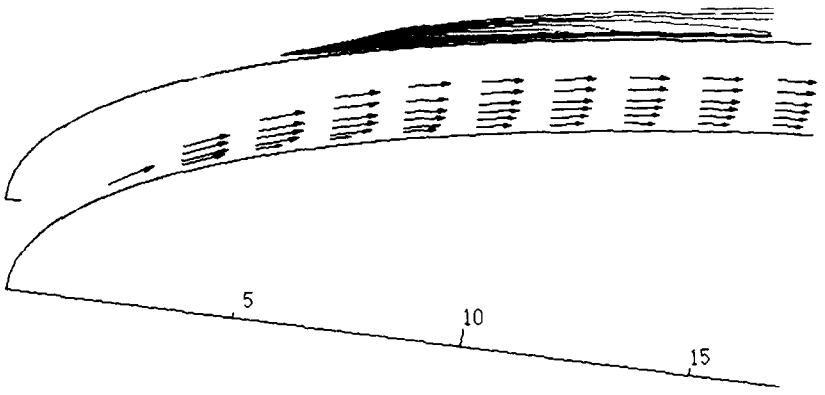

(f)

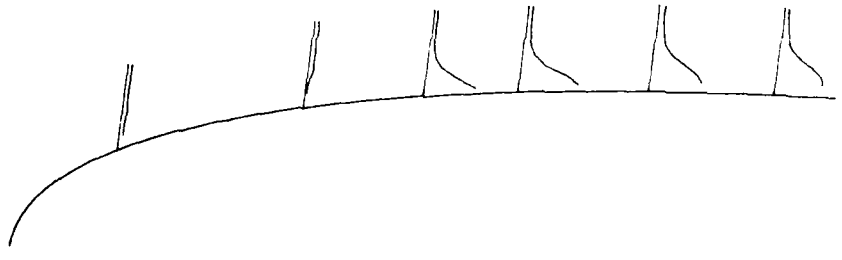

(g)

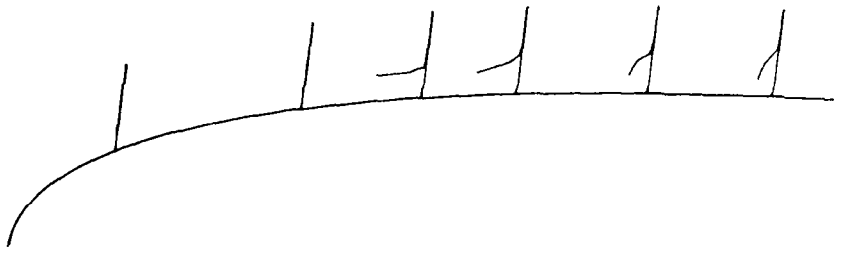

Figure 6.18 (continued) : 5° to 15° incidence, k = 0.3

(d) isoturbulence

(f) chordwise fluctuations $\sqrt{\overline{u'^2}}/Q$ scale . —— 10% Q

(g) - Reynolds stress $\overline{u'v'}/Q^2$ scale : —— 1% Q^2

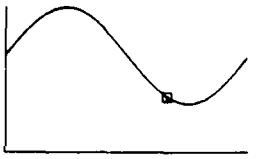

i= 5.73 degr. f=238.67 degr.

(a)

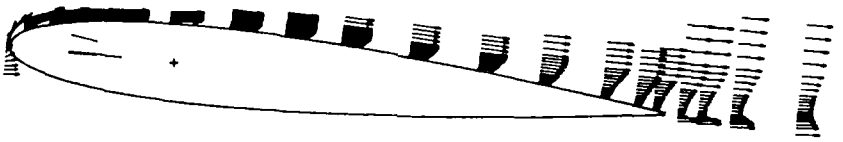

(b)

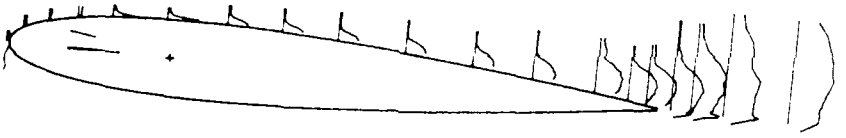

(c)

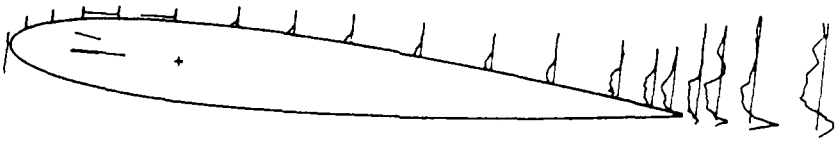

Figure 6.19 : 5° to 15° incidence, k = 0.3

(a) velocity vectors scale : — Q

(b) chordwise fluctuations $\sqrt{\overline{u'^2}}/Q$ scale : — 10% Q

(c) - Reynolds stress $\overline{u'v'}/Q^2$ scale : — 1% Q^2

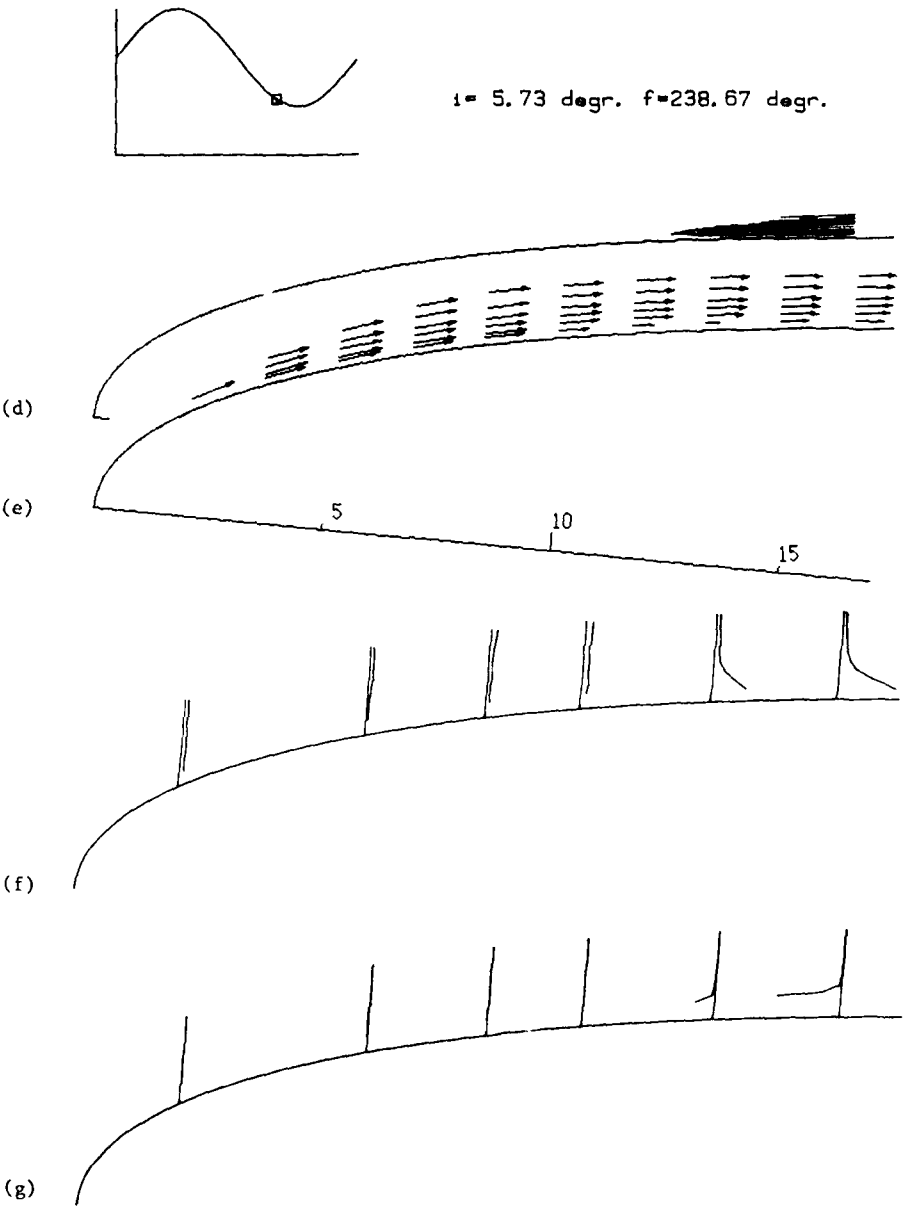

Figure 6.19 (continued) : 5° to 15° incidence, k = 0.3

(d) isoturbulence

(f) chordwise fluctuations $\sqrt{u'^2}/Q$ scale : —— 10% Q

(g) - Reynolds stress $\overline{u'v'}/Q^2$ scale : —— 1% Q^2

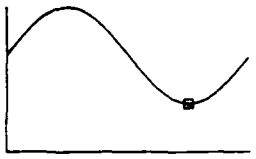

i= 5.00 degr. f=268.51 degr.

(a)

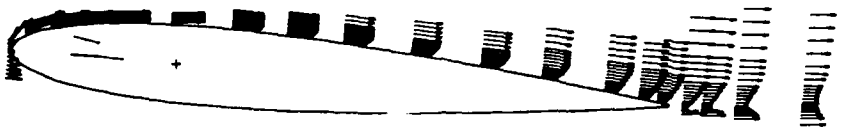

(b)

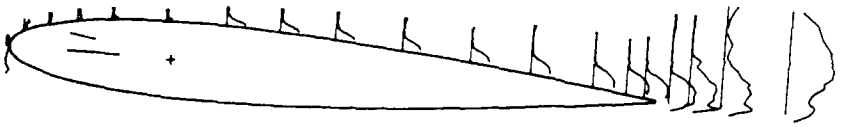

(c)

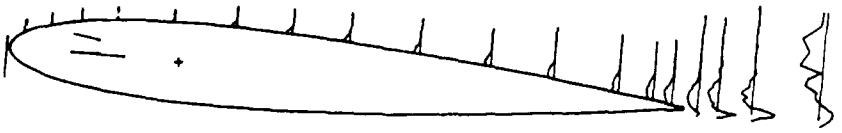

Figure 6.20 : 5° to 15° incidence, k = 0.3

(a) velocity vectors scale : — Q

(b) chordwise fluctuations $\sqrt{u'^2}/Q$ scale : — 10% Q

(c) - Reynolds stress $\overline{u'v'}/Q^2$ scale : — 1% Q^2

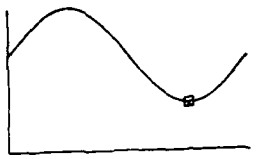

i= 5.00 degr. f=268.51 degr.

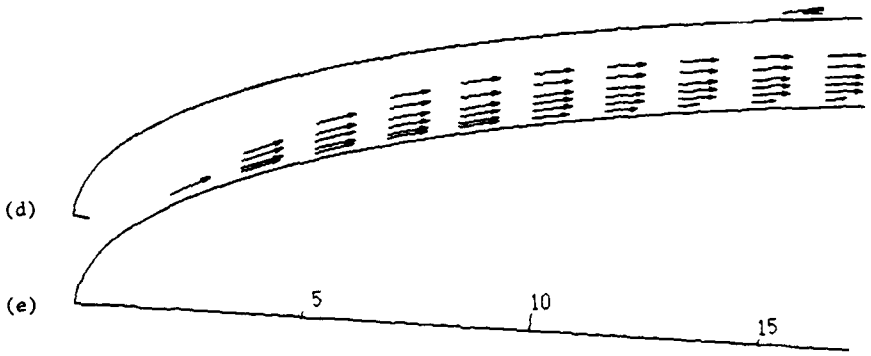

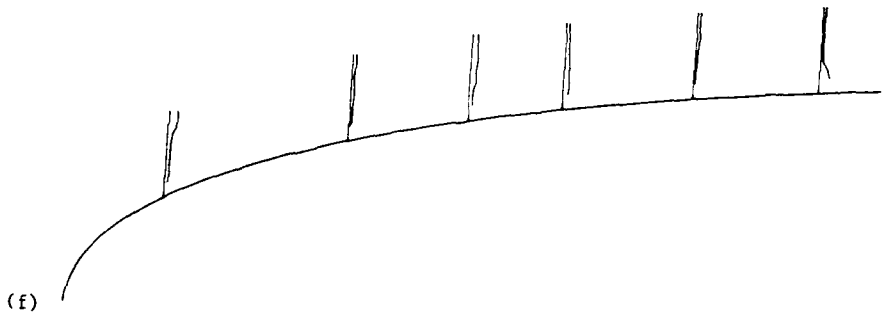

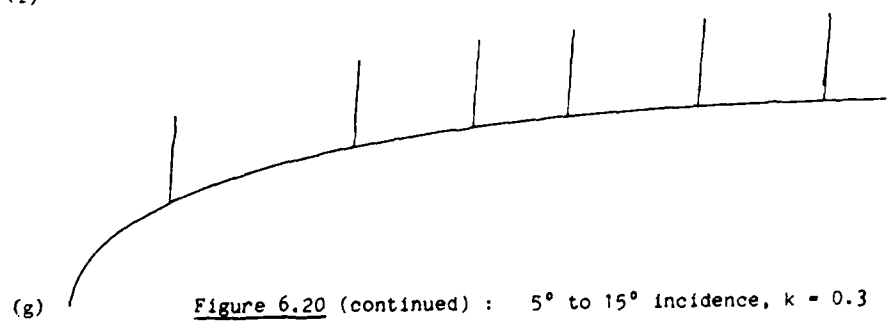

Figure 6.20 (continued) : 5° to 15° incidence, k = 0.3

(d) isoturbulence

(f) chordwise fluctuations $\sqrt{\overline{u'^2}}/Q$ scale : —— 10% Q

(g) - Reynolds stress $\overline{u'v'}/Q^2$ scale : —— 1% Q^2

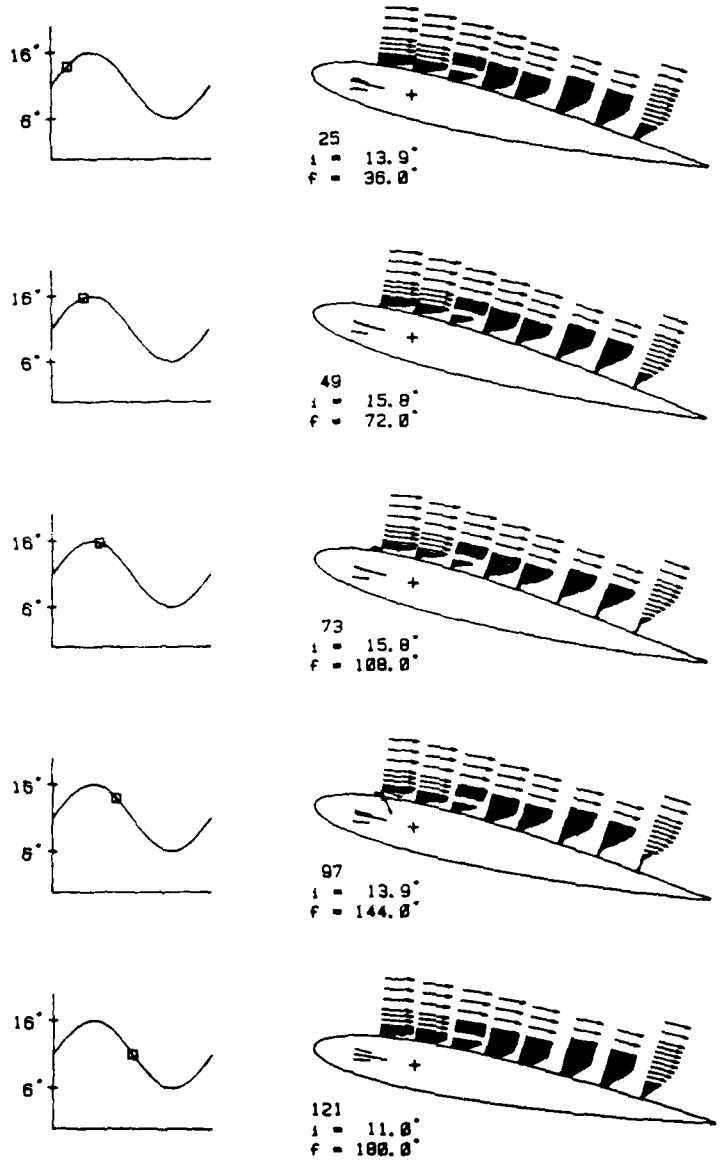

Figure 6.21 : from De Ruyck and Hirsch [5]
6 to 16 degrees, frequency coefficient = 0.3, no end-plates

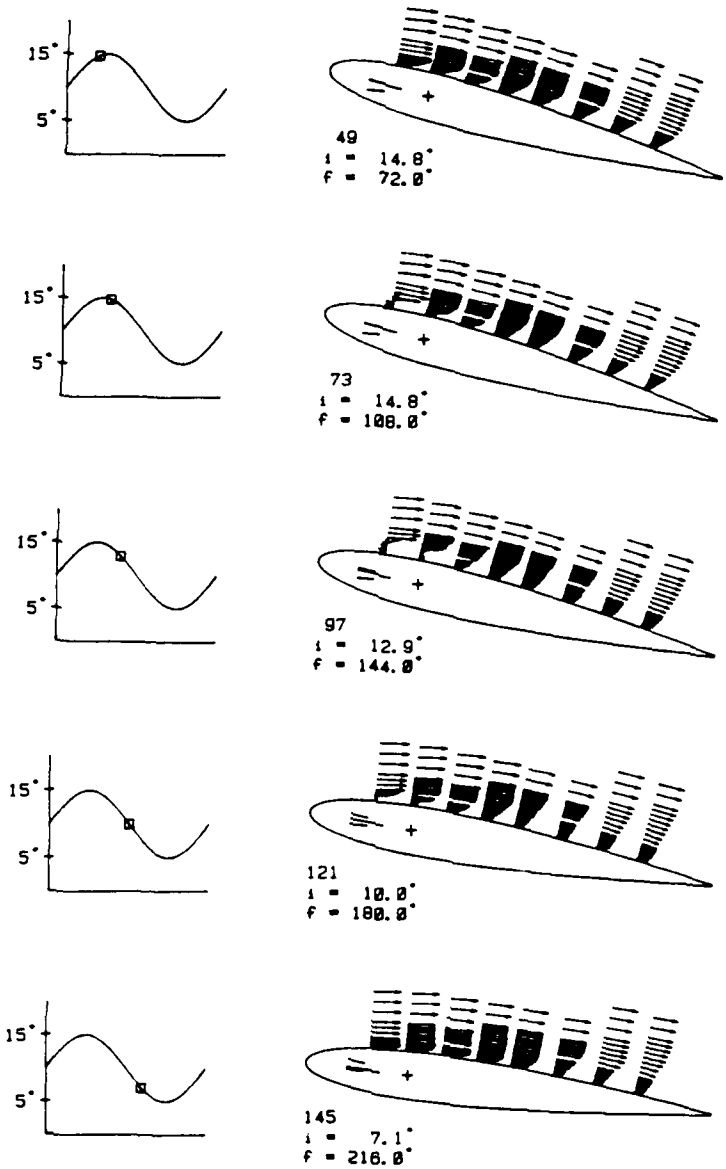

Figure 6.22 : from De Ruyck and Hirsch [5]
5 to 15 degrees, frequency coefficient = 0.48, no end-plates).

6.3. Flow Near the Trailing Edge and in the Near Wake:

The experiments around the trailing edge have been made at 5 to 15 degrees incidence without any boundary layer tripping and at 8 to 18 degrees incidence with the same tripping wires as in [6,7].

The development of the flow near the trailing edge and in the near wake at 5 to 15 degrees incidence can be seen in figures 6.5 to 6.20 in a, b and c. Two relevant and different trailing edge flows are shown on an enlarged scale in figures 6.23 and 6.24. The figures a, b and c in these cases show velocity vector, chordwise turbulence intensity and Reynolds shear stress, respectively. The gradual growth of boundary layer towards the trailing edge can be easily recognized in all the figures (6.5 to 6.20).

If the flow near the leading edge separation bubble is excluded from this part of the discussion, the maximum value of the chordwise turbulence intensity and the Reynolds shear stress invariably occurs between 5% to 10% chord downstream of the trailing edge in the pressure side of the wake in all the figures (6.5 to 6.20 and 6.23 and 6.24). Downstream of 10% chord from the trailing edge the values of the turbulence quantities reduce as it should in the far wake. Without further analysis of the data it is not possible to say at what distance the wake becomes self preserving and what is the effect of unsteadiness and trailing edge separation on it. However, the wake behaviour is close to e steaty state wake behaviour. From the figures it is observed that :

(i) the turbulence intensity is relatively smaller near the centreline of the wake,

(ii) the Reynolds shear stress is zero close to the centreline

(iii) the turbulence intensity as well as the Reynolds shear stress reach a peak in the side where half-wake width is small (large transverse gradients in velocity).

In the near wake from 5% to 10% chord downstream of the trailing edge, peaks are observed at the pressure side, and these peaks do not coincide with the maximum values of velocity gradients. These peaks may be due to the effect of streamwise curvature in the flow, which is known to introduce "surprisingly large changes in the turbulence structure of shear layers"[29]. According to Bradshaw[29], "These changes are usually an order of magnitude more important than normal pressure gradients and other explicit terms appearing in the mean-motion equations for curved flows".

The trailing edge separation is detected soon after the incidence exceeds 13 degrees (6.13 a). At the onset of trailing edge separation the chordwise

turbulence intensity close to the surface remains unchanged but the Reynolds shear stresses drop to near zero values. With the increase of incidence the separation point moves upstream (6.13, 6.14). The separated portion over the airfoil near trailing edge keeps growing even after the incidence reduces after the maximum value (6.15, 6.16). More than 20% of the airfoil is separated when the incidence is 12.56 degrees (6.16). The activity in this separated portion of the airfoil is relatively quiet as can be seen in 6.24. The velocity is reversed but the magnitude is very small: same order of magnitude as the turbulence intensity. The chordwise turbulence intensity falls to less than 25% of the maximum value measured at the same chordwise station (which is detected around the separation line). The Reynolds shear stress in this region is scattered around zero indicating a very small correlation between u and v. The results obtained are comparable with the wake results obtained by De Ruyck and Hirsch in [2].

A qualitative analysis of the velocity vectors near the trailing edge confirms that during increasing incidence the velocity vector at the trailing edge is tangential to the pressure surface. This is in accordance with the Geising and Maskell trailing edge condition.

Figures 6.25 to 6.39 show the results of the measurements near the trailing edge for 8 to 18 degees incidence and with the tripping wire present at 10% chord. In the figures a) shows the velocity vectors, b) shows the chordwise turbulence intensities and c) shows the Reynolds shear stress. For a better understanding of the strong interaction between leading edge vortex and the flow at the trailing edge, the corresponding figures of the mean flow field are reproduced from [5,6] in figures d), wherever possible. It is remembered that these early experiments were performed without end-plates.

The general observations at 5 to 15 degrees incidence can also be made in this case: the maximum value of the turbulent intensity as well as the Reynolds shear stress occur near 5% chord downstream of the trailing edge in the pressure side of the wake. Severe flow turning may be the cause as can be seen in figures 6.32 to 6.34.

This series of figures starts with 17 degrees and increasing incidence (6.25). The trailing edge separation point in the present case has moved up to 80% chord (6.25 a). The separated region again is a low activity region : with lower chordwise turbulence intensity (6.25 b), near zero Reynolds shear stress (6.25 c) and the reverse flow velocity of the same order of magnitude as the turbulent intensity (6.25 a). In 6.25 d it can be seen

that the leading edge vortex has just started forming at the first measuring station (15% chord). From figure 6.1 d it can be seen that this roughly coincides with the incidence at which the reattachment point of the leading edge separation bubble has reached 15% chord on its way to complete separation. In the early experiments without end plates the trailing edge separation point has moved upstream of 60% chord position, instead of 80% in the present case. Due to the leakages at the blade tips, the opposite behaviour would normally be expected (more downwash should delay the separation), which means that the tip leakages affect the flow in a way which is more significant than just a downwash velocity. In general the earlier separation causes a general phase shift between the complete flow behaviour of the experiments with and without end-plates.

At higher incidence the separation point has moved upstream of the 80% chord and the reversed flow velocity has noticeably increased (6.26 a, 6.27 a). The chordwise turbulence intensity also slightly increases, however the Reynolds shear stresses show considerable scatter without any noticeable increase in the mean value. The scatter indicates that under these circumstances the ensemble averaging of 100 data points is not sufficient.

The rolling down of the leading edge vortex (6.28 d) sweeps the trailing edge separation point downstream of 80% chord as the incidence reduces from the maximum value (6.28, 6.29, 6.30). Upstream of this vortex front a strong reversed flow is build up (6.31). The leading edge vortex itself is already away from the chord line once it leaves the trailing edge and a strong vortex of opposite vorticity forms in the near wake (figures 6.32, 6.33, 6.34). Large peak values of chordwise turbulence intensity and Reynolds shear stresses are observed during this process. After the passage of this trailing edge vortex the flow near the trailing edge and the near wake breaks down completely (figures 6.35).

In the fixed wire measurement (section 6.1) it was observed that the cycle to cycle variation of the movement of this separation point was quite large. The scatter in the velocity vector as well as in the turbulence quantities in 6.36, 6.37 and .38 is a result of this non-periodicities. The figure 6.39 completes the cycle showing the steps leading to the sequence in 6.25. In this experiment, the flow just downstream of the trailing edge was generally found to be parallel to the non-separated side of the trailing edge.

Although there is a complete breakdown of the flow in the suction side and formation of a number of large vortices close to the airfoil, the Geising and Maskell trailing edge condition can be considered as valid close

to the trailing edge, since in general the velocity at the trailing edge remains tangent to the pressure side of the blade. Downstream of the trailing edge however, the separating streamline is strongly distorted by the trailing edge vortices and a complete analysis of the data including the leading edge and trailing edge vortices will be necessary. In the analysis, the indication suggested by Polling and Telionis [24] about non-zero loading in the trailing edge and in the near wake should be taken in to account.

6.4 Comparison with previous work

The differences between the present experimental set up and the early experiments of De Ruyck and Hirsch [1 to 6] are the presence of end-plates and the absence of a tripping wire in the 5° to 15° test case.

When comparing the data for the 5° to 15° case the observed differences are not relevant, although a significant downwash could be expected in the absence of end plates in the early experiments. This can be explained by the small size of the gaps between the blade ends and the tunnel walls (3% chord). The tripping wire was placed at 10% chord distance from the leading edge, whereas the laminar region is observed up to 15% chord, which gives not much difference.

More difference is observed at 8° to 18° angle of attack. The gaps at the blade ends enhance the separation, which may be due to an overall non-two dimensional (but still symmetric) suction side flow. The earlier separation causes an overall phase shift. Stronger return flows are also observed when using end-plates.

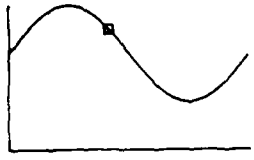

i=12.56 degr. f=149.17 degr.

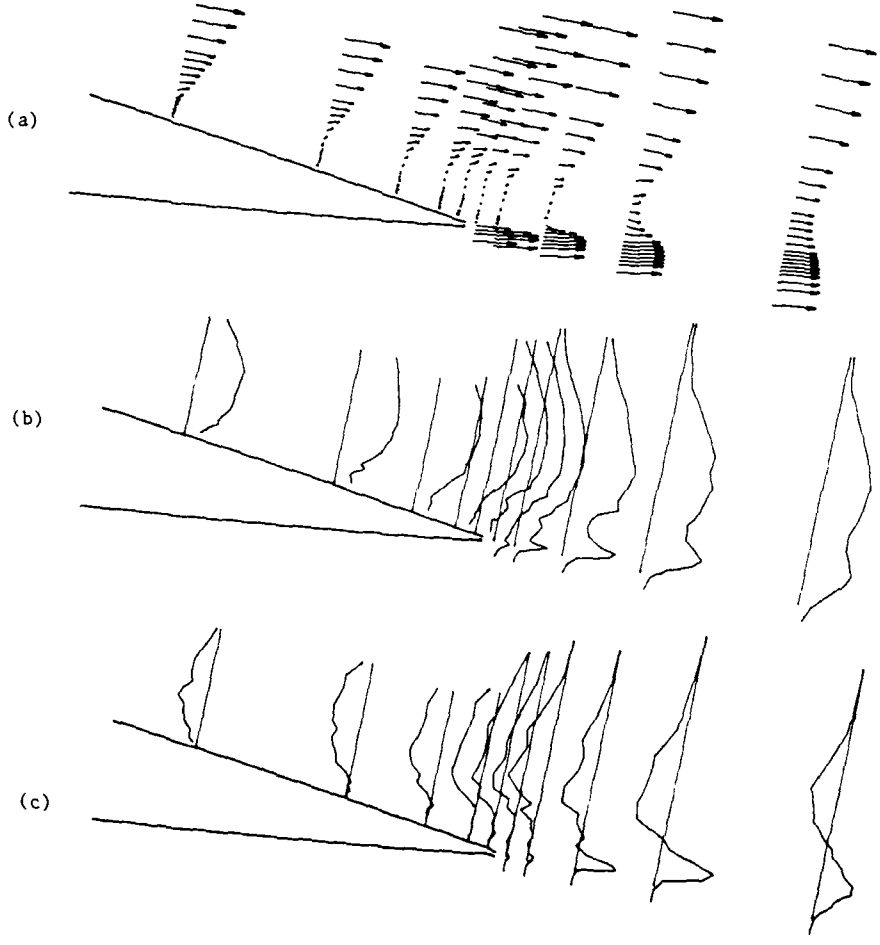

Figure 6.23 : 5° to 15° incidence, k = 0.3

(a) velocity vectors scale : — 40% Q

(b) chordwise fluctuations $\sqrt{u'^2}/Q$ scale : — 4% Q

(c) - Reynolds stress $\overline{u'v'}/Q^2$ scale : — .04% Q^2

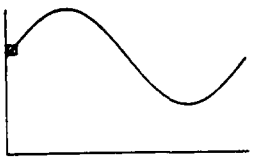

i=10.86 degr. f= 9.94 degr.

(a)

(b)

(c)

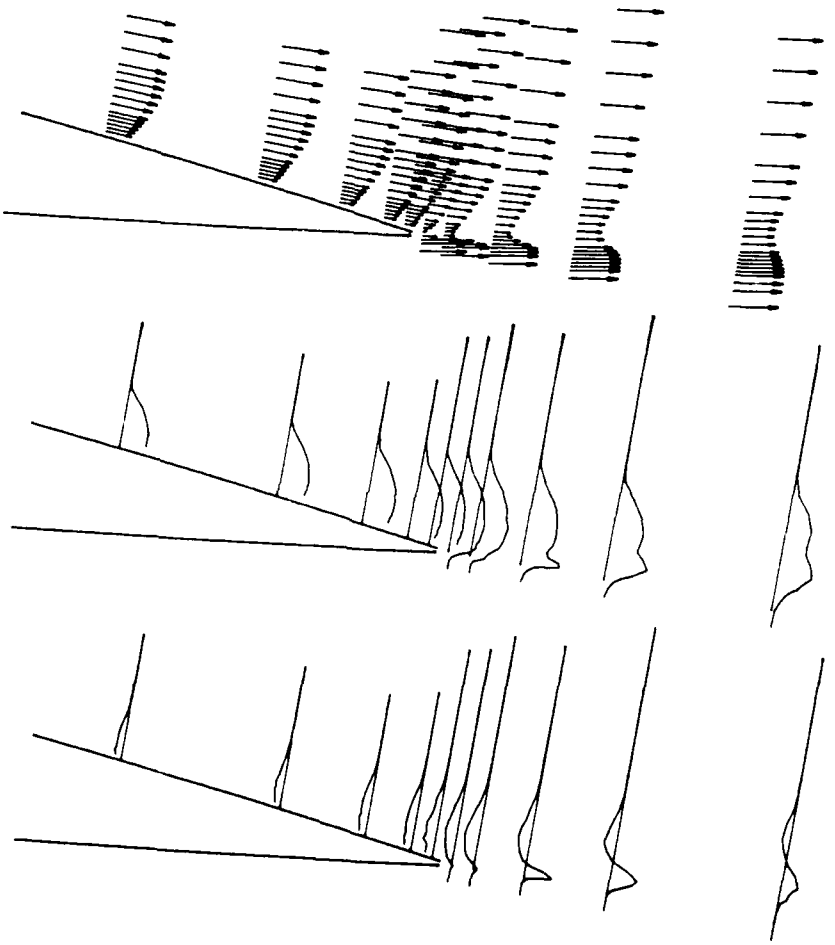

Figure 6.24 : 5° to 15° incidence, k = 0.3

(a) velocity vectors scale : — 40% Q

(b) chordwise fluctuations $\sqrt{u'^2}/Q$ scale : — 4% Q

(c) - Reynolds stress $\overline{u'v'}/Q^2$ scale : — .04% Q^2

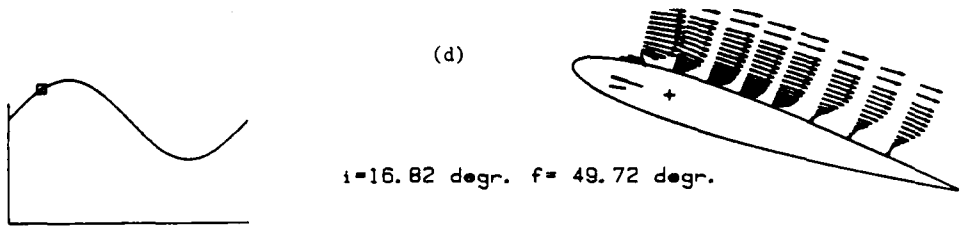

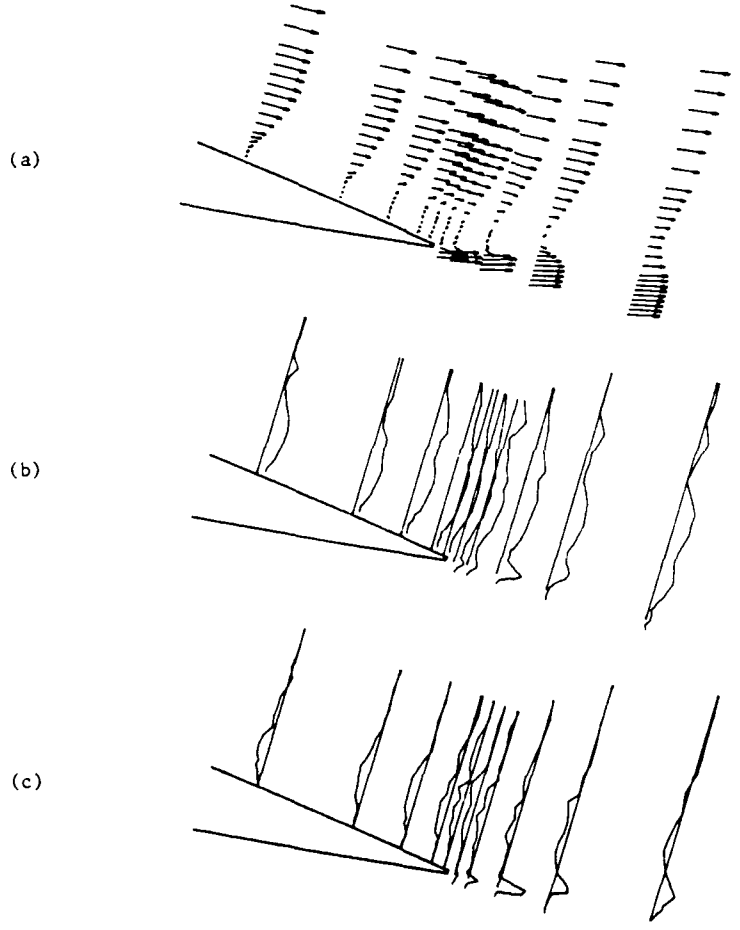

Figure 6.25 : 8° to 18° incidence, k = 0.3

(a) velocity vectors scale : — 60% Q

(b) chordwise fluctuations $\sqrt{u'^2}/Q$ scale : — 20% Q

(c) - Reynolds stress $\overline{u'v'}/Q^2$ scale : — .2% Q^2

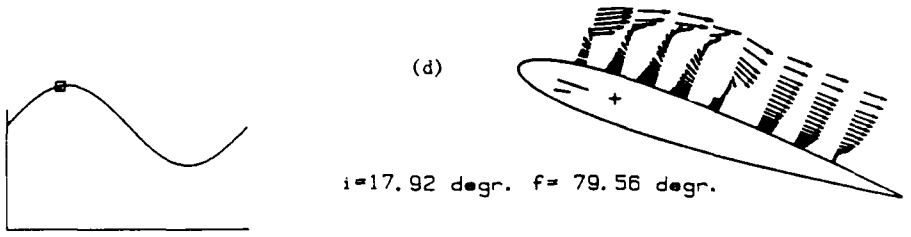

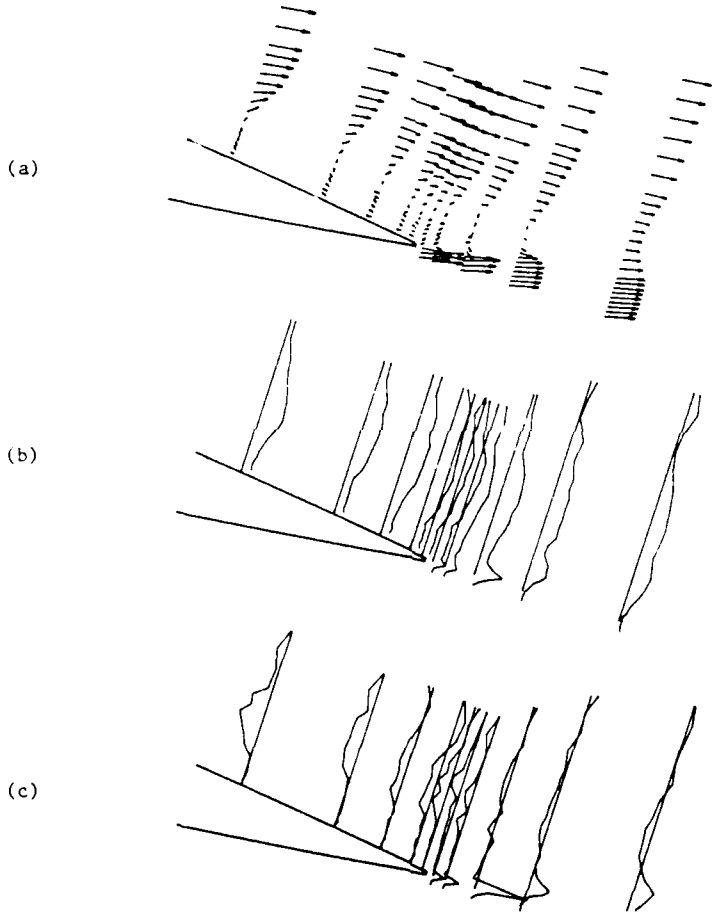

Figure 6.26 : 8° to 18° incidence, k = 0.3

(a) velocity vectors scale : — 60% Q

(b) chordwise fluctuations $\sqrt{u'^2}/Q$ scale : — 20% Q

(c) - Reynolds stress $\overline{u'v'}/Q^2$ scale : — .2% Q^2

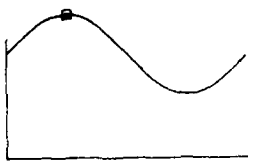

(d)

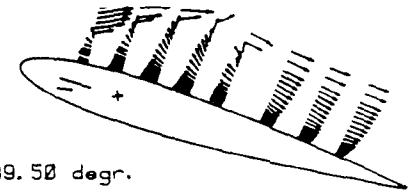

i=18.00 degr. f= 89.50 degr.

(a)

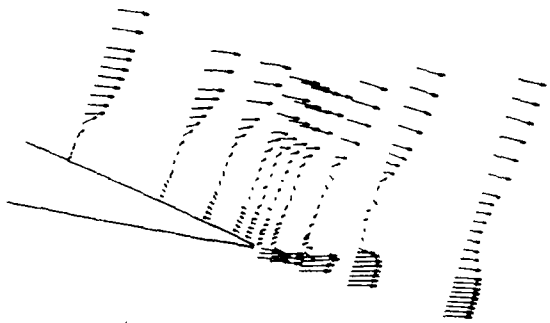

(b)

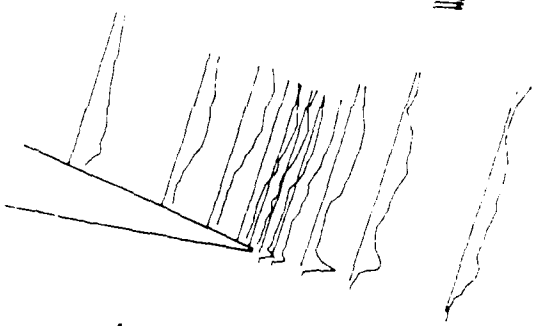

(c)

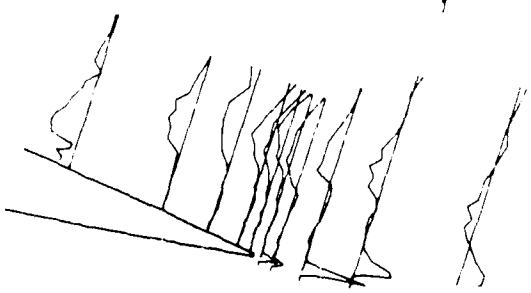

Figure 6.27 : 8° to 18° incidence, k = 0.3

(a) velocity vectors scale : — 60% Q

(b) chordwise fluctuations $\sqrt{u'^2}/Q$ scale : — 20% Q

(c) - Reynolds stress $\overline{u'v'}/Q^2$ scale : — .2% Q^2

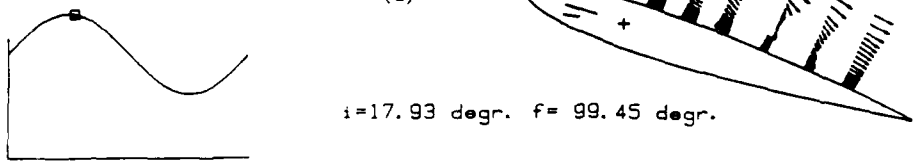

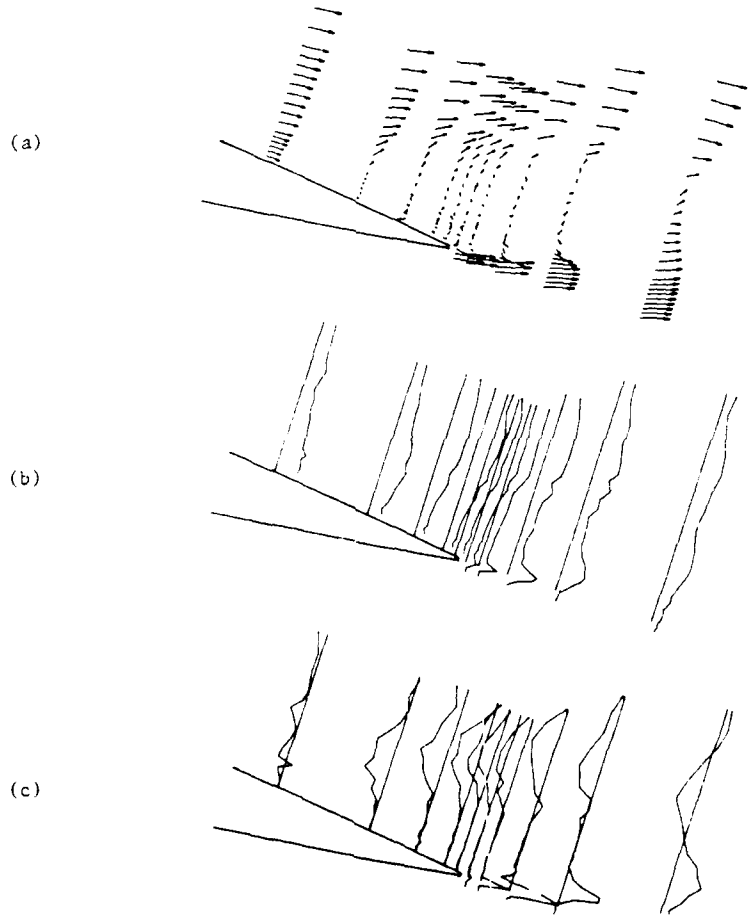

Figure 6.28 : 8° to 18° incidence, k = 0.3

(a) velocity vectors scale : — 60% Q

(b) chordwise fluctuations $\sqrt{u'^2}/Q$ scale : — 20% Q

(c) - Reynolds stress $\overline{u'v'}/Q^2$ scale : — .2% Q^2

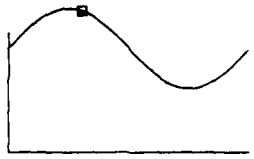

(d)

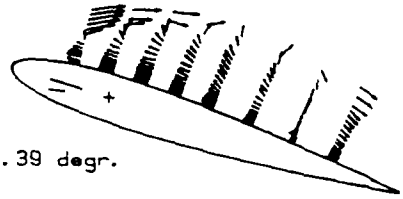

i=17.72 degr. f=109.39 degr.

(a)

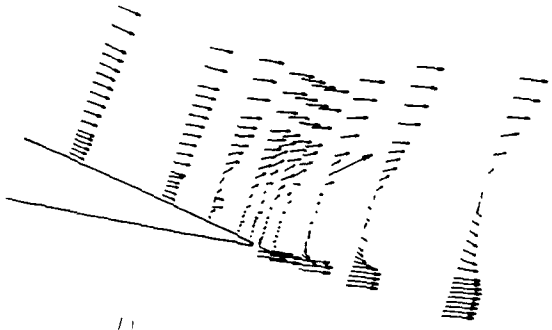

(b)

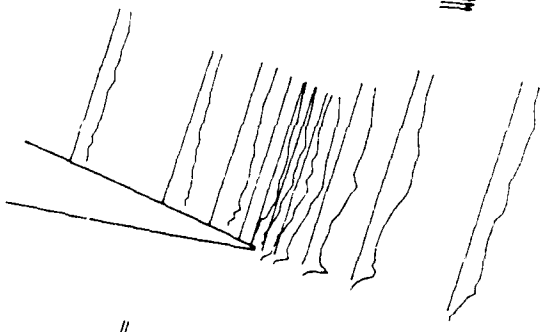

(c)

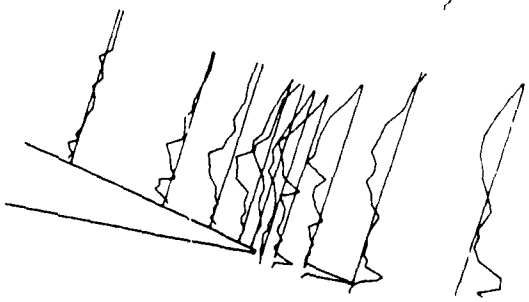

Figure 6.29 : 8° to 18° incidence, k = 0.3

(a) velocity vectors scale : — 60% Q

(b) chordwise fluctuations $\sqrt{u'^2}/Q$ scale : — 20% Q

(c) - Reynolds stress $\overline{u'v'}/Q^2$ scale : — .2% Q^2

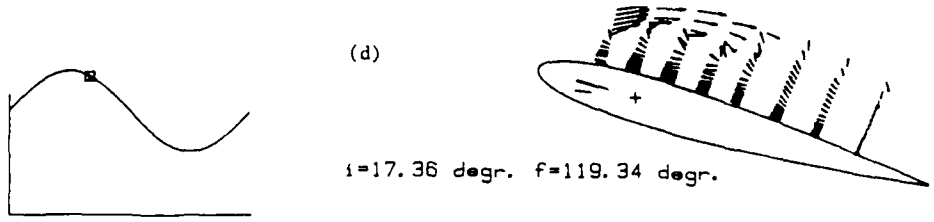

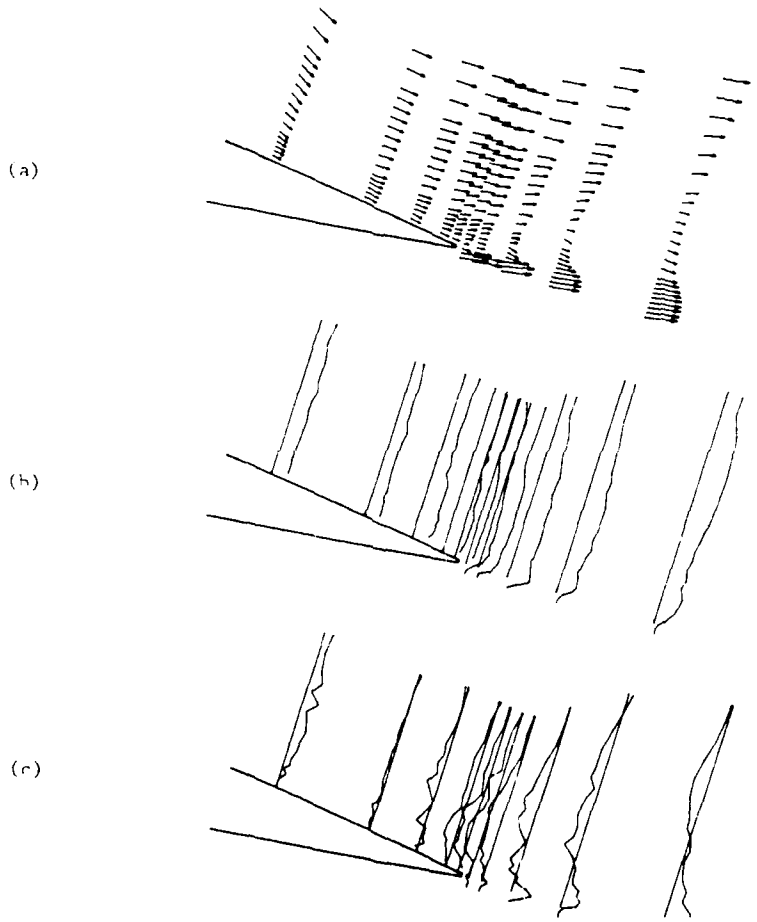

Figure 6.30 : 8° to 18° incidence, k = 0.3

(a) velocity vectors scale : — 60% Q

(b) chordwise fluctuations $\sqrt{u'^2}/Q$ scale : — 20% Q

(c) - Reynolds stress $\overline{u'v'}/Q^2$ scale : — .2% Q^2

(d)

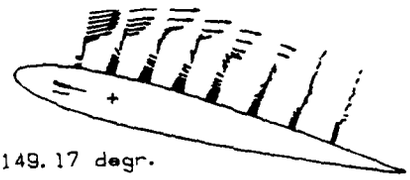

i=15.56 degr. f=149.17 degr.

(a)

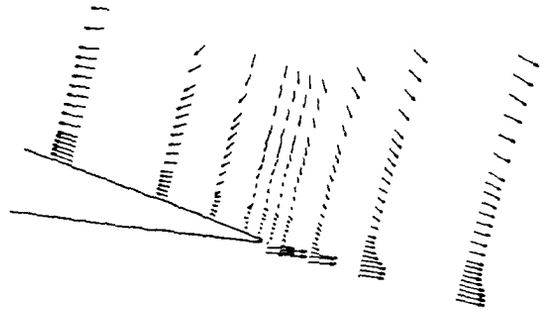

(b)

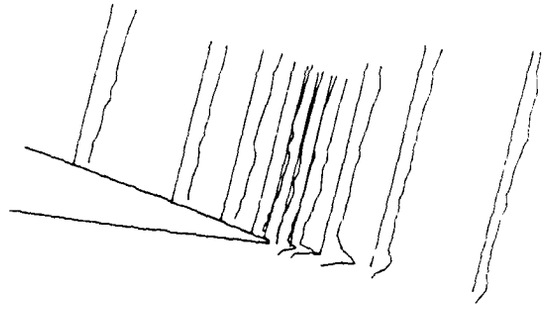

(c)

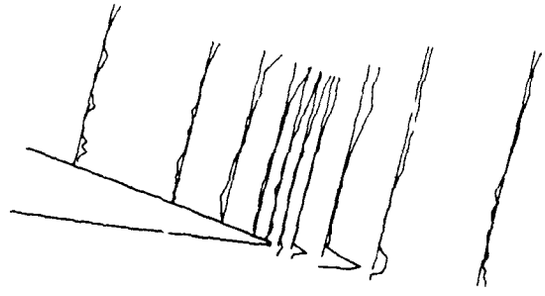

Figure 6.31 : 8° to 18° incidence, k = 0.3

(a) velocity vectors scale : — 60% Q

(b) chordwise fluctuations $\sqrt{u'^2}/Q$ scale : — 20% Q

(c) - Reynolds stress $\overline{u'v'}/Q^2$ scale : — .2% Q^2

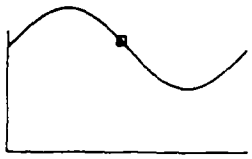

i=13.95 degr. f=169.06 degr.

(a)

(b)

(c)

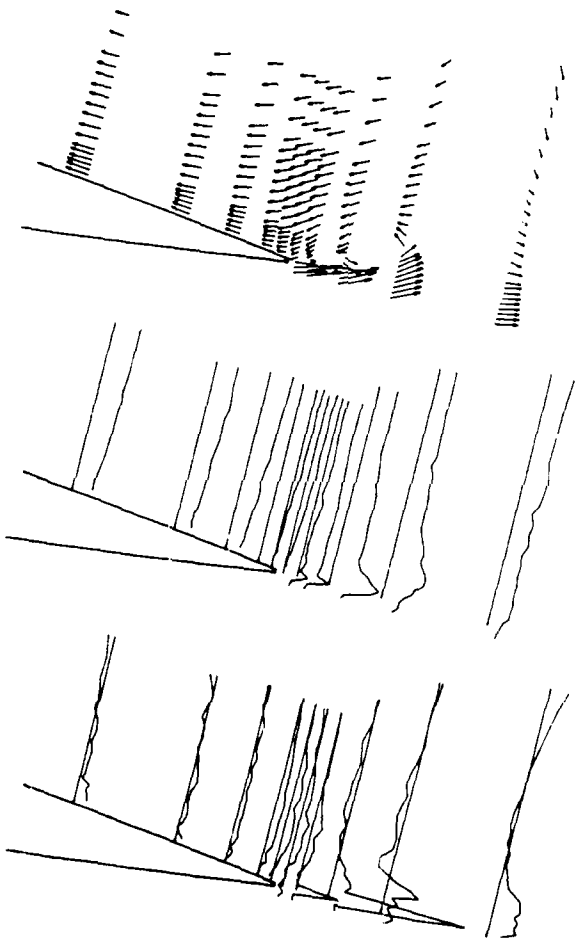

Figure 6.32 : 8° to 18° incidence, k = 0.3

(a) velocity vectors scale : — 60% Q

(b) chordwise fluctuations $\sqrt{u'^2}/Q$ scale : — 20% Q

(c) - Reynolds stress $\overline{u'v'}/Q^2$ scale : — .2% Q^2

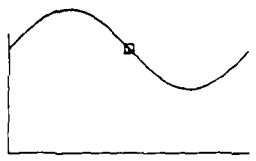

(d)

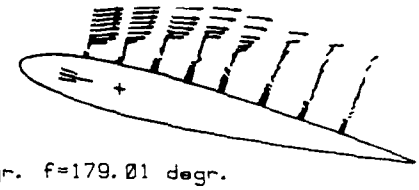

i=13.Ø9 degr. f=179.Ø1 degr.

(a)

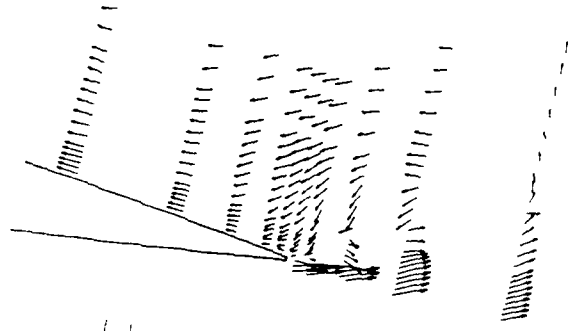

(b)

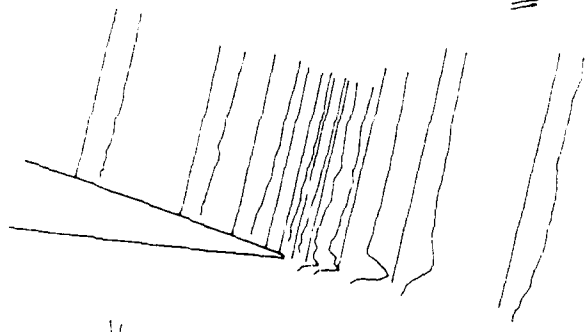

(c)

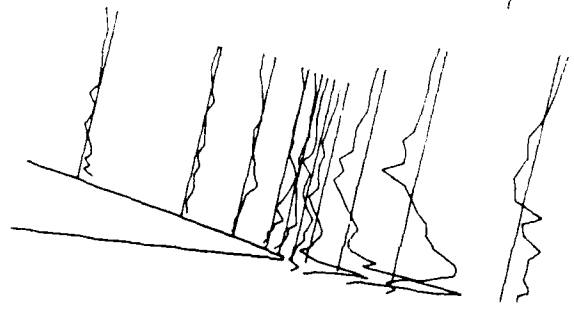

Figure 6.33 : 8° to 18° incidence, k = 0.3

(a) velocity vectors scale : — 60% Q

(b) chordwise fluctuations $\sqrt{u'^2}/Q$ scale : — 20% Q

(c) - Reynolds stress $\overline{u'v'}/Q^2$ scale : — .2% Q^2

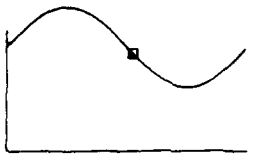

i=12.22 degr. f=188.95 degr.

(a)

(b)

(c)

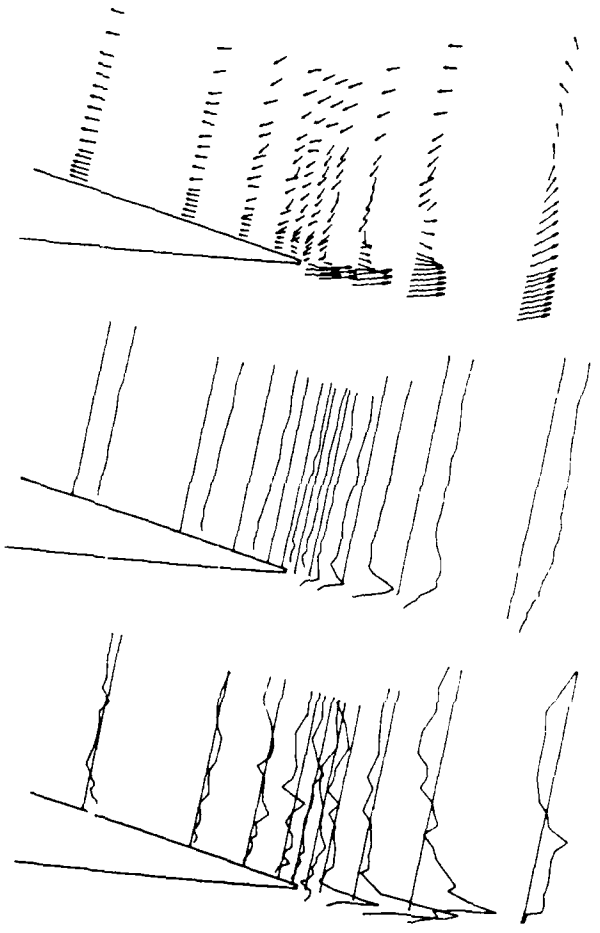

Figure 6.34 : 8° to 18° incidence, k = 0.3

(a) velocity vectors scale : — 60% Q

(b) chordwise fluctuations $\sqrt{u'^2}/Q$ scale : — 20% Q

(c) - Reynolds stress $\overline{u'v'}/Q^2$ scale : — .2% Q^2

i= 9.87 degr. f=218.78 degr.

(a)

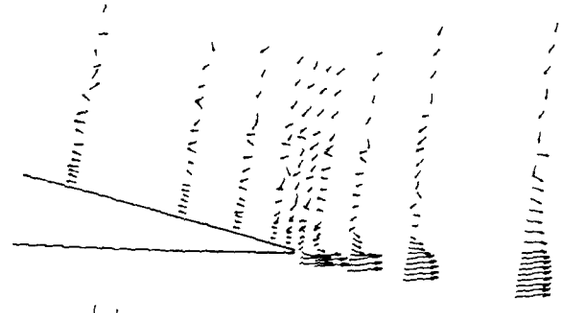

(b)

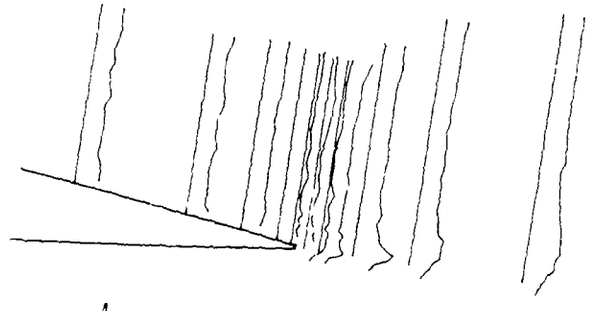

(c)

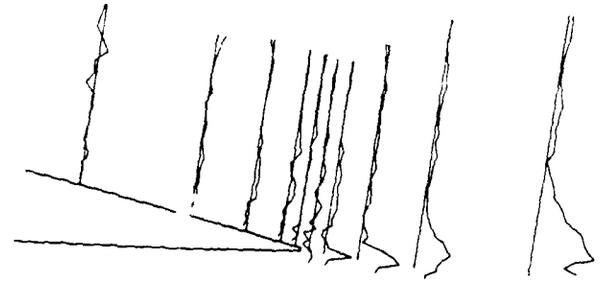

Figure 6.35 : 8° to 18° incidence, k = 0.3

(a) velocity vectors scale : — 60% Q

(b) chordwise fluctuations $\sqrt{u'^2}/Q$ scale : — 20% Q

(c) - Reynolds stress $\overline{u'v'}/Q^2$ scale : — .2% Q^2

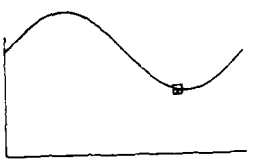

(d)

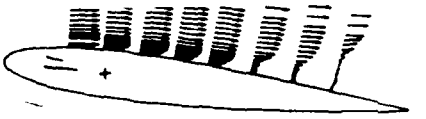

i= 8.10 degr. f=258.56 degr.

(a)

(b)

(c)

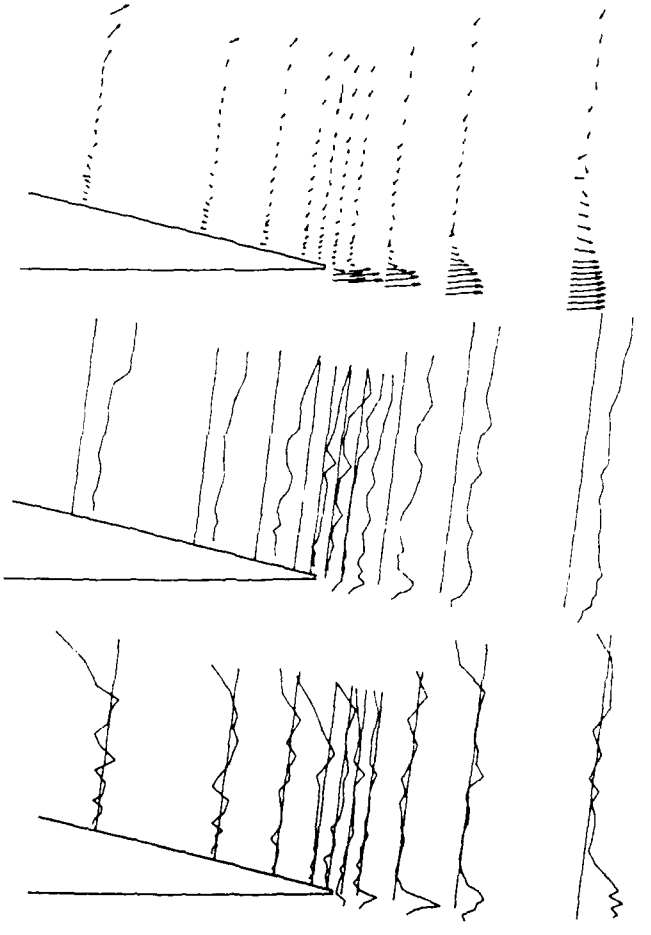

Figure 6.36 : 8° to 18° incidence, k = 0.3

(a) velocity vectors scale : — 60% Q

(b) chordwise fluctuations $\sqrt{u'^2}/Q$ scale : — 20% Q

(c) - Reynolds stress $\overline{u'v'}/Q^2$ scale : — .2% Q^2

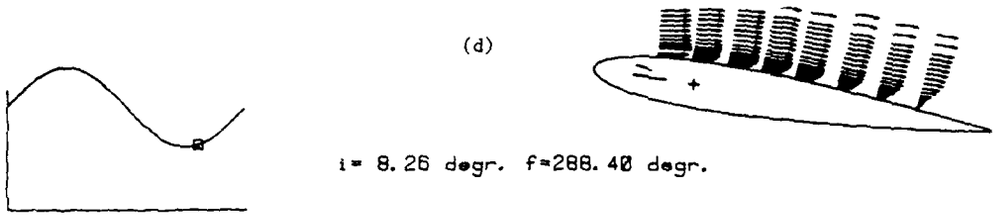

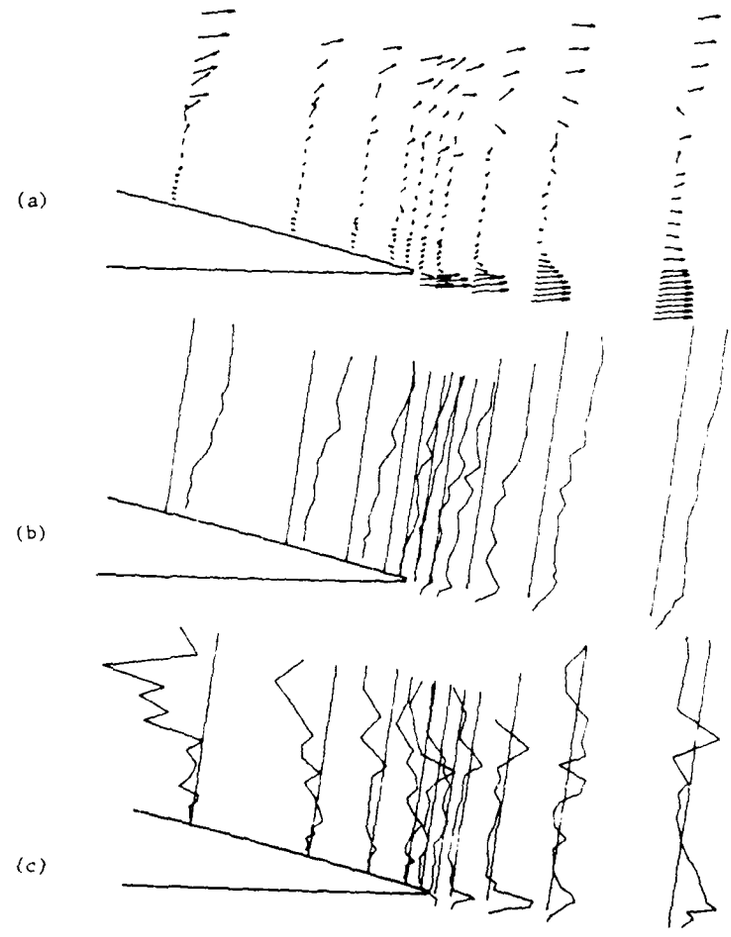

Figure 6.37 : 8° to 18° incidence, k = 0.3

(a) velocity vectors . scale : — 60% Q

(b) chordwise fluctuations $\sqrt{u'^2}/Q$ scale : — 20% Q

(c) - Reynolds stress $\overline{u'v'}/Q^2$ scale : — .2% Q^2

i= 9.67 degr. f=318.23 degr.

(a)

(b)

(c)

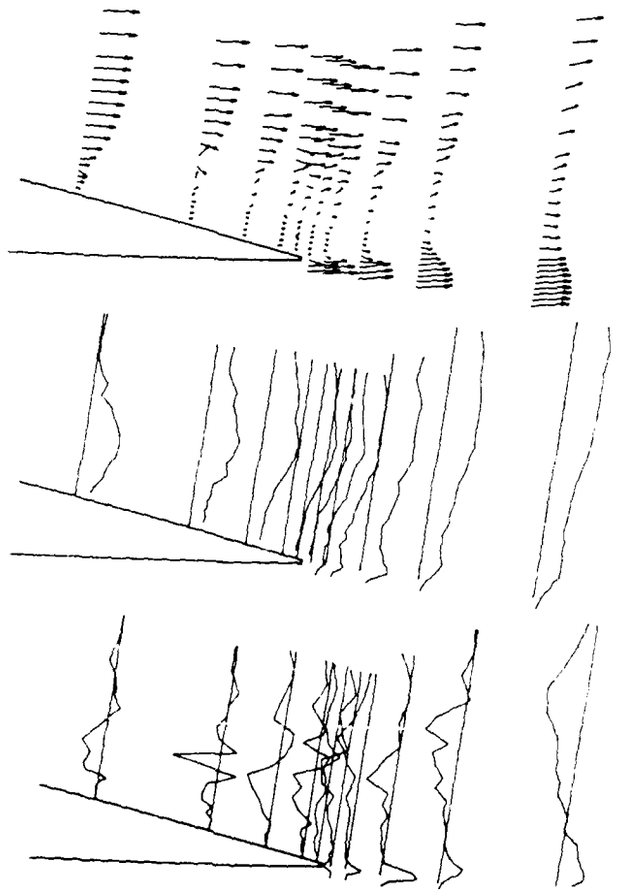

Figure 6.38 : 8° to 18° incidence, k = 0.3

(a) velocity vectors scale : — 60% Q

(b) chordwise fluctuations $\sqrt{u'^2}/Q$ scale : — 20% Q

(c) - Reynolds stress $\overline{u'v'}/Q^2$ scale : — .2% Q^2

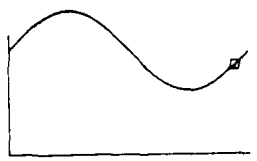

(d)

i=11.14 degr. f=338.12 degr.

(a)

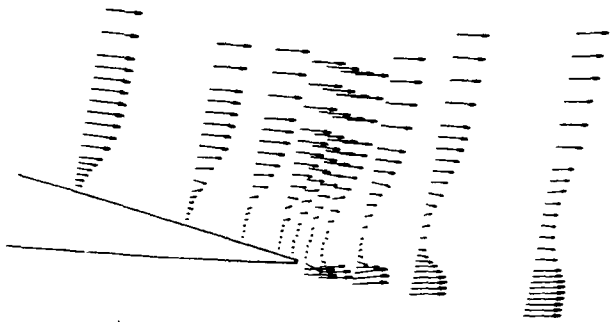

(b)

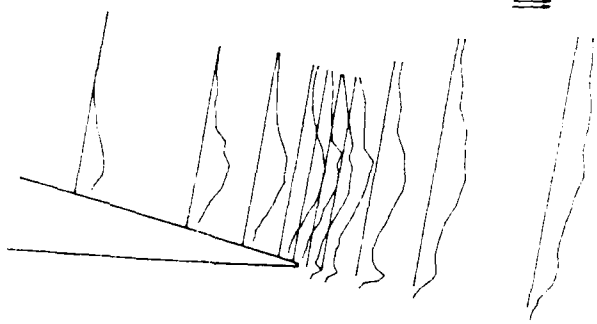

(c)

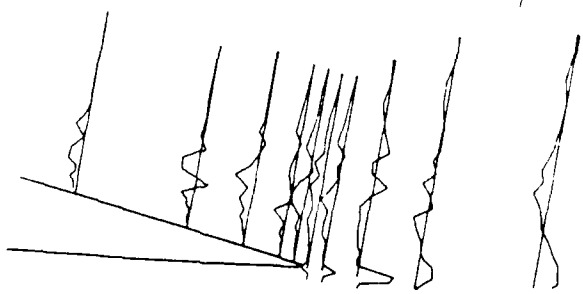

Figure 6.39 : 8° to 18° incidence, k = 0.3

(a) velocity vectors scale : — 60% Q

(b) chordwise fluctuations $\sqrt{u'^2}/Q$ scale : — 20% Q

(c) - Reynolds stress $\overline{u'v'}/Q^2$ scale : — .2% Q^2

7. CONCLUSIONS

In the present work experimental data are obtained about leading edge and trailing separations. The formation of a leading edge bubble has been observed, with laminar separation, transition and turbulent reattachment. The bubble is very thin and the exact separation point is to be found by measurements very close to the wall, preferably with flush mounted sensors. Leading edge stall is found to be triggered by the bursting of the leading edge bubble, soon after the static stall limit is exceeded. No interaction with the trailing edge separation is observed. Strong turbulence is observed in the shear layer above the bubble.

The trailing edge separation is a low speed, low turbulence event, with near zero Reynolds shear stresses. A weak vortex can be formed at high angles of attack. The passage of the leading edge vortex disturbs the trailing edge pattern into a high energy area with strong turbulence. The Geising and Maskell trailing edge condition is valid in all cases, as far as the flow close to the trailing edge is considered.

When compared to the early experiments of De Ruyck and Hirsch [1 to 6], it is found that the presence of gaps at the blade ends, and the presence of a tripping wire at 10% chord distance of the leading edge has no significant effects of the overall flow behaviour in unstalled conditions. At higher angles of attack, differences are observed due to three dimensional effects of the uncovered blade ends in the early experiments, where the separation occurs sooner and less return flow is observed.

The test case 5° to 15° degrees delivers a complete set of data from leading edge to near wake, including data about the leading edge bubble.

Future work should be directed at an extensive analysis of the obtained data, eventually complemented by similar data at the other incidences. This should be done in connection with numerical solutions.

REFERENCES

[1] DE RUYCK J., HIRSCH C., 1981, "Turbulence Structure in the Wake of an Oscillating Airfoil", Report Vub-Str-12, Vrije Universiteit Brussel, Dept of Fluid Mech., 1981

[2] DE RUYCK J., HIRSCH C., 1982, "Instantaneous Turbulence Profiles in the Wake of an Oscillating Airfoil", AIAA Paper 82-0353, 1982

[3] DE RUYCK J., HIRSCH C., 1983, "Turbulence Structure in the Boundary Layer an Oscillating Airfoil", Report VUB-STR-14, Vrije Universiteit Brussel, Dept. Fluid Mech., 1983

[4] DE RUYCK J., HIRSCH C., 1984, "Instantaneous Flow Field Measurements of Stalled Regions on an Oscillating Airfoil", AIAA Paper 84-1565, 1984

[5] DE RUYCK J., HIRSCH C., 1984, "Turbulence Structure in the Boundary Layers of an Oscillating Airfoil", Report Vub-Str-13, Vrije Universiteit Brussel, Dept of Fluid Mechanics, 1984

[6] DE RUYCK J., HIRSCH C., 1985 "Velocity and Turbulence Measurements in Dynamically Stalled Boundary Layers on an Oscillating Airfoil", AGARD conference proceedings CP386 on Unsteady Aerodynamics, pp 4-1, 4-13

[7] MC CROSKEY W.J., 1977, "Some Current Research in Unsteady Fluid Dynamics", Trans. ASME, Journal of Fluid Engineering Vol. 99, pp. 8-39, 1977

[8] MARTIN J.M., EMPEY R.W., MC CROSKEY W.J., CARADONNA F.X., 1973, "An Experimental Analysis of Dynamic Stall on an Oscillating Airfoil", presented at the 29th Annual National Forum of the American Helicopter Society, May 1973.

[9] MC CROSKEY W.J., CARR L.W., MC ALISTER K.W., 1976, "Dynamic Stall Experiments on Oscillating Airfoils" AIAA Journal, vol. 14, No. 1, January 1976, pp. 57-63.

[10] MC ALISTER K.W., CARR L.W., "Water-Tunnel Experiments on an Oscillating Airfoil at Re = 21,000", NASA TM 78446, 1978

[11] MC CROSKEY W.J., MC ALISTER K.W., CARR L.W., PUCCI S.L., LAMBERT O., INDERGRAND R.F., 1980, "Dynamic Stall on Advanced Airfoil Sections" presented at the 36th Annual National Forum of the American Helicopter Society, May 1980 - Journal of the American Helicopter Society, July 1981.

[12] MC CROSKEY W.J., PUCCI S.L., 1981, "Viscous-Inviscid Interaction on Oscillating Airfoils" AIAA Paper no 81-0051, 1981

[13] BASS R.L.,JOHNSON J.F. and UNRUH J.F.,1982, "Correlation of Lift and Boundary-Layer Activity on an Oscillating Lifting Surface", AIAA

Journal, vol. 20, No. 8, August 1982, pp. 1051-1056

[14] MEHTA U.B., 1978, "Dynamic Stall of an Oscillating Airfoil" Agard cp 227, Unsteady Aerodynamics, p 23-1,1978

[15] BRENDEL M. and MUELLER T. J., 1988 "Boundary Layer Measurements on an Airfoil at a Low Reynolds Number in an Oscillating Freestream",AIAA Journal, vol. 23,No. 6, March 1981, pp. 257 -263

[16] EATON J.K. and JOHNSTON J.P.,1981 "A Review of Research on Subsonic Turbulent Flow Reattachment" AIAA Journal, vol. 19,No. 9, September 1981, pp. 1093-1100

[17] SERPA J. M., LESSMANN R. C. and HAGIST W. M., 1987 "Turbulent Separated and Reattached Flow Over Curved Surface", Journal of Fluids Engineering, December 1987, Vol. 109, pp 403 - 409

[18] SIMPSON R. L., CHEW Y.-T. and SHIVAPRASAD B. G.,1981 "The Structure of a Separating Turbulent Boundary Layer. Part 1. Mean Flow and Reynolds stresses",Journal of Fluid Mechanics, 1981, Vol. 113, pp 23 - 51

[19] SIMPSON R. L., CHEW Y.-T. and SHIVAPRASAD B. G.,1981 "The Structure of a Separating Turbulent Boundary Layer. Part 2. Higher - Order Turbulence Results",Journal of Fluid Mechanics, 1981, Vol. 113, pp 53 - 73

[20] SHILOH K., SHIVAPRASAD B. G. and SIMPSON R. L.,1981 "The Structure of a Separating Turbulent Boundary Layer. Part 3. Transverse Velocity Measurements",Journal of Fluid Mechanics, 1981, Vol. 113, pp 75 - 90

[21] SIMPSON R. L.,SHIVAPRASAD B. G. and CHEW Y.-T.,1983 "The Structure of a Separating Turbulent Boundary Layer. Part 4. Periodic Free Stream Unsteadyness",Journal of Fluid Mechanics, 1983, Vol. 127, pp 219 - 261

[22] SATYANARAYANA B., DAVIS S., 1978 "Experimental Studies of Unsteady Trailing-Edge Conditions", AIAA Journal, vol. 16,No. 2, February 1978, pp. 125-129

[23] BASU B. C. and HANCOCK J. H., 1978 "The Unsteady Motion of a Two-dimensional Aerofoil in Incompressible Inviscid Flow", Journal of Fluid Mechanics, 1978, Vol. 87, Part 1, pp 159-178

[24] Poling D. R. and Telionis D. P., 1986 "The Response of Airfoils to Periodic Disturbances - The Unsteady Kutta Condition", AIAA Journal, vol. 24, No. 2, August 1986, pp 193 -199

[25] Poling D. R. and Telionis D. P., 1987 "The Trailing Edge of a Pitching Airfoil at High Reduced Frequencies", Journal of Fluids Engineering, December 1987, Vol. 109, pp 410 - 414

[26] HO C.M., CHEN S.H., 1980 "Unsteady Wake of a Plunging Airfoil", AIAA Paper nr 80-1446, 1980

[27] HO C.M., CHEN S.H., 1981 "Unsteady Kutta Condition of a Plunging Airfoil", IUTAM Symposium Toulouse, France, 1981; "Unsteady Turbulent Shear Flows", pp 197 - 206, Springer Verlag.

[28] HILLIER R. and DULAI B.S.,1985 "Pressure Fluctuation in a Turbulent Separated Flow", Fifth Symposium on Turbulent Shear Flows, Cornell University, August 1985, pp. 5.13 - 5.18

[29] BRADSHAW P., 1973 "Effect of Streamline Curvature on Turbulent Flow", AGARD-AG-169, August 1973.

Appendix 1

Profile Shape of the Leading Edge

X mm	Y mm (Modified)	Y mm (With tripping)
0	0	0
1	4.2	4.3
2	5.9	6.0
3	7.4	7.2
4	8.5	8.2
5	9.5	9.1
6	10.3	9.8
7	11.1	10.6
8	11.8	11.2
9	12.4	11.9
10	13.1	12.5
11	13.7	12.5
12	14.3	13.5
13	14.8	14.0
14	15.2	14.6
15	15.7	15.0
16	16.1	15.5
17	16.1	15.5
18	17.0	16.3
19	17.4	16.7
20	17.8	17.0
25	19.7	18.9
30	21.4	20.4
35	22.9	21.8
40	24.2	23.1
45	25.4	24.4
50	26.5	25.5
55	27.4	-

Appendix 2

Stations Near the Leading Edge

Position	Distance from L.E. along the surface in mm	x in mm	x/c %
1(p)	19	11.7	1.94
2	29	20.9	3.46
3	34	25.6	4.24
4	39	30.4	5.03
5(p)	43	34.4	5.7
6	49	39.9	6.61
7(p)	59	49.2	8.15
8	69	58.8	9.74
9(p)	71	61.0	10.1
10	79	68.4	11.32
11(p)	88	77.3	12.8
12	89	78.0	12.91
13	99	87.7	14.52
14(p)	104	93.0	15.4
15	109	97.4	16.13
16(p)	155	143.8	23.8
17(p)	211	199.9	33.1

Appendix 3

Stations for Rotating Wire Measurements

Position	x/c %
1	-0.5
2	1.94
3	5.7
4	8.15
5	10.1
6	12.8
7	15.4
8	23.8
9	33.1
10	41.5
11	50.1
12	60.5
13	71.1
14	80.5
15	90.2
16	95.4
17	98.2
18	99.5
19	100.7
20	102.0
21	105.0
22	110.0
23	120.0